Institute of Physics
Polish Academy of Sciences

Andrei Avdonin

Properties of ZnMnTe alloy doped with oxygen and chromium

Ph. D. Thesis

Supervisor:
prof. dr hab. R. R. Gałązka

Warsaw 2010

Contents

List of Tables

List of Figures

Abbreviations

AFM - Atomic force microscopy.
BAC - Band anticrossing.
DLTS - Deep level transient spectroscopy.
DMS - Diluted magnetic semiconductor.
EDX - Energy dispersive X-ray analysis.
FC - Field cooling.
HMA - Highly missmatched alloy.
PL - Photo luminescence.
PLM - Pulsed laser melting.
PR - Photo-modulated reflection.
RTA - Rapid thermal annealing.
SMS - Semimagnetic semiconductor.
XRD - X-ray diffraction.
MBE - Molecular beam epitaxy.
MCD - Magnetic circular dichroism.
MFM - Magnetic force microscopy.
SEM - Scanning electron microscopy.
SIMS - Secondary ion mass spectrometry.
ZFC - Zero field cooling.

1 Introduction

This work is an experimental study of semimagnetic semiconductors (SMS)[1] based on $ZnMnTe$. An overview on SMS and $ZnMnTe$ in particular can be found in [25, 35, 81]. The $ZnMnTe$ is a relatively well studied compound of the group $II-VI$ materials, which is usually considered as a material for application in spintronics.

Despite the fact that a series of promising effects were observed in SMS and in $ZnMnTe$ in particular, there are very few examples of their real applications. Among these effects are the giant band splitting, resulting from $sp-d$ hybridization, or the ferromagnetic phase transition. Observation of these effects usually requires low temperatures and strong magnetic fields[2]. Since the majority of useful effects depend on sample magnetization, the synthesis of a material with inherent room temperature ferromagnetism is a key requirement for successful application of SMS.

One of the possible approaches is to take an existing known material and modify its properties by additional doping. In this work an attempt was made to dope $ZnMnTe$ separately with oxygen and chromium. The motivation of such choice including the expected benefits of the new materials will be presented in the corresponding overview sections.

The main problem in this direction is the low solubility of both doping agents. This fact and also the fact that several doping agents are introduced simultaneously increases the probability of appearance of new phase precipitations. Since such precipitations exist in the investigated samples, a part of this work is devoted to their study.

The study of precipitations is receiving more attention, at least in the field of SMS. Since the appearance of precipitations often cannot be avoided, their study can help to turn the disadvantage into an advantage and find some of their useful properties. There are examples of materials (e.g. $ZnCrTe$) in which ferromagnetism produced by nonuniform doping results in good semimagnetic semiconductor. It is manifested for example in the Zeeman splitting of electron bands in the absence of external magnetic field.

Apart from possible spintroncs applications the studied materials can also find applications in other areas, where non-magnetic properties of such materials would be of use. There are reports, where $ZnMnTe:O$ or similar material is considered as a material for the x-ray imaging applications [22], photovoltaic [21] or even thermoelectric applications [82]. The $ZnMnTe:Cr$ is considered as a good candidate for solid state infrared lasers [75]. Thus a study of such materials may be justified from both fundamental and application point of view.

Instead of concentrating on some particular phenomena this work represents a general characterization of the studied materials, which includes

[1] or Diluted Magnetic Semiconductors (DMS)

[2] in case of $ZnMnTe$ the temperatures below or close to liquid helium temperature are required

investigation of structural, electrical, magnetic and optical properties. This is why the work raises more questions then it answers. However, it might be considered as a starting point for those who will be interested in these materials in the future, as it draws the attention to problems related with synthesis and new properties which require a closer look.

The thesis is organized as two independent parts devoted to two studied compounds, $ZnMnTe:O$ and $ZnMnTe:Cr$. Each part in turn is divided in two sections. The first section contains an overview of reports related to studied materials. The second section contains the experimental data and the discussion.

The results presented in this work were published in three articles:

- A. Avdonin, Le Van Khoi, W. Pacuski, V. Domukhowski, R.R. Gałązka, "Preparation and Optical Properties of $Zn_{1-x}Mn_xTe_{1-y}O_y$ Highly Mismatched Alloy", Acta Physica Polonica A, **112**, 407-414 (2007).

- A. Avdonin, W. Knoff, R.R. Gałązka,
"Magnetic Properties of $Zn_{1-x}Mn_xTe_{1-y}O_y$ Alloys", Acta Physica Polonica A, **116**, 916-917 (2009).

- A. Avdonin, Le Van Khoi, W. Knoff, R.R. Gałązka,
"Magnetic properties of $(Zn,Mn)Te$" Semimagnetic Alloy co-Doped with Chromium, Acta Physica Polonica A, **116**, 974-975 (2009).

In the end, the author would like to thank persons who helped to carry out this work. In particular the author would like to thank the supervisor prof. dr hab. R.R. Gałązka and dr. Le Van Khoi, with whom author spent most of the time, for the possibility to make this work, guidance and helpful discussions, prof. dr hab. A. Mycielski and mgr. B. Witkowska for the pure materials used for synthesis, prof. dr hab. W.D. Dobrowolski for possibility to make magnetization and Hall effect measurements and continuous urging during the last month of writing, prof. dr hab. T. Story for the possibility to use the SQUID magnetometer, which was of much help, mgr. W. Knoff for help with magnetization measurements, mgr. V. Domuchowski for x-ray diffraction measurements, doc. dr hab. B. Kowalski and mgr. A. Reszka for electron microscopy investigation, dr. R. Jakiela for SIMS and electron microprobe measurements, dr. M. Aleszkiewicz for STM and MFM measurements, prof. dr hab. T. Wosiński and dr T. Tsarova for DLTS measurements, and all others whom author unintentionally forgot to mention.

2 ZnTe doped with oxygen

2.1 Review of material-specific properties

2.1.1 Oxygen at impurity concentrations

Oxygen and tellurium belong to the same (VI-th) group of the periodic table and thus the oxygen is an isoelectronic impurity in ZnTe. Isoelectronic impurities have the same number of valence electrons, however they disturb the potential of the crystalline lattice node where they substitute the host atom. Usually when the disturbance is relatively small, the isoelectronic impurities create so called resonant energy levels which fall into the bands of allowed energy states, and very rarely manifest themselves in electrical or optical phenomena.

In some special cases, when the disturbance of the lattice potential is large enough they create localized states inside the band gap. The situation is similar with the appearance of localized states inside a quantum well with a finite depth. If the depth of the well is less then a certain critical value the localized state inside the quantum well will not appear.

Among all elements of the group VI, oxygen and tellurium have the most different properties. As an example a comparison of covalent radii, electronegativities (Pauling scale) and the first ionization potentials of group VI elements is presented in Table 1 [1].

Table 1: Properties of group VI elements.

element	Covalent radius (Å)	Electro-negati-vity	Ioniz. energy (eV)
O	0.66	3.44	13.62
S	1.04	2.58	10.36
Se	1.17	2.55	9.75
Te	1.37	2.10	9.01

Thus of all group VI elements oxygen substituting tellurium (O_{Te}) is more probable to create a localized state inside the band gap. Such state was observed in ZnTe doped with oxygen. It should be noticed that substitution of tellurium with oxygen in II-VI compounds does not necessarily result in a localized state inside the band gap. For example in CdTe:O the substitutional O_{Te} defect creates a resonance level inside the conduction band [2, 3].

First report on oxygen-related energy level in the band gap of ZnTe

dates from 1962 [4]. Although authors did not associated it with substitutional oxygen, they nevertheless very precisely described its electronic structure. They observed that in some ZnTe crystals grown from vapour phase appears a characteristic wide band (Fig. 1) centered at about 1.9 eV. The band almost entirely consists of phonon replicas[3] of a weak zero-phonon line. The zero phonon line is centered at 1.986 eV at 20 K. As a proof it was demonstrated that photoluminescence (PL) and absorption spectra are mirror images of each other about the single zero-phonon line (Fig. 1).

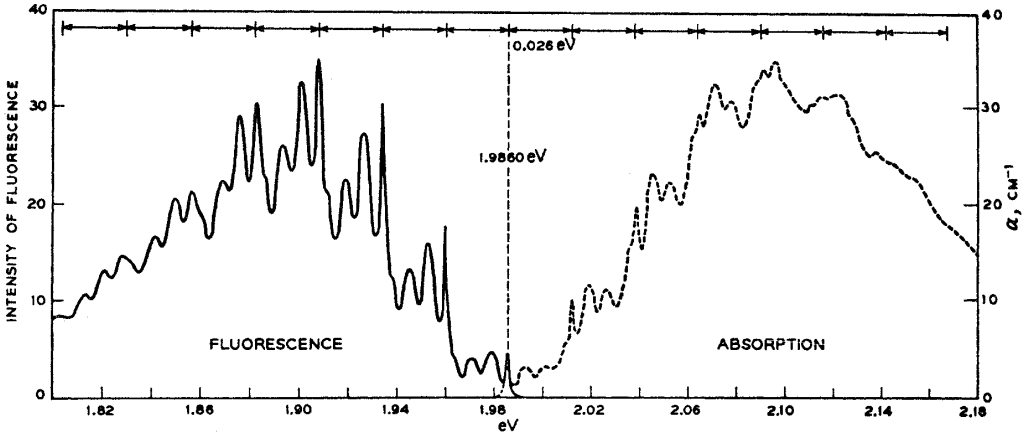

Figure 1: The photoluminescence and absorption of O_{Te} center in $ZnTe$. The no-phonon line is common to both spectra. The LO phonon energy is indicated by arrows on the top of the figure. Two broad peaks in each repeated interval arise from transverse and longitudinal acoustic phonons [4].

Authors of [4] also observed that at low temperatures appears a second no-phonon line shifted by 1.7 meV to lower energies with respect to the line at 1.986 eV. In the following reports those lines were marked as B- and A-line respectively (Fig. 2a,b). Considering the behaviour of A and B lines authors concluded that recombination center must involve an electron and a hole bound to an impurity.

The reasoning is as follows: The B-line appears only at very low temperatures, accompanied by a decrease and disappearance[4] of the A-line. The relaxation time of the PL at 1.6 K (B-line) is about 1 μs, at least 10 times longer than at 20 K (A-line). Thus it is concluded that B-line corresponds to a forbidden transition and the A-line to an allowed transition. "Of all complexes involving three or fewer electrons and holes, only a complex containing one electron and one hole may give rise to state splitting with some optical transitions allowed and other forbidden. The splitting of the state must arise from the exchange interaction between the electron and the hole..." [4]. In ZnTe because of the j-j coupling between electron

[3]The assignment of all phonon replicas is made in [12].

[4]Line A disappears at T<2 K when thermal energy is smaller then the separation between A and B lines.

(j_e=1/2) and hole (j_h=3/2) the excited state of such center will be splitted into states with J=(j_h-j_e)=1 and J=(j_h+j_e)=2. The allowed transition (A) corresponds to J=1, and the forbidden transition (B) to J=2 state (Fig. 2c).

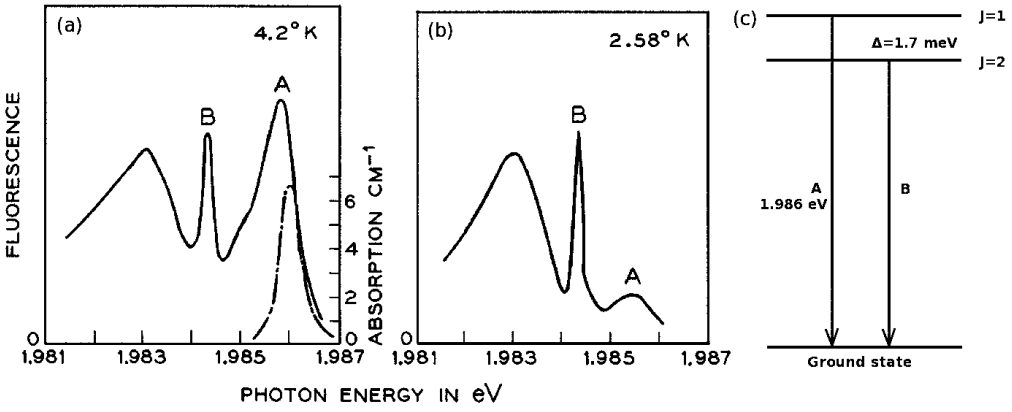

Figure 2: The photoluminescence (solid line) and absorption (dashed) of no-phonon lines of O_{Te} center in $ZnTe$ at 4.2 K (a) and 2.58 K (b). Energy diagram of the excited states of O_{Te} center in $ZnTe$ (c) [4].

This model was confirmed by investigation of the splitting of the A and B lines in the external magnetic field. In accord with the model, B-line (with J=2) splits in five components [4, 5]. The A-line should split in three components. However the splitting of the A-line (J=1) in magnetic field was not observed because it has a smaller g-factor and it is much wider then the B-line [5].

The fact that the oxygen is responsible for red PL in ZnTe was demonstrated in [6]. Authors showed that red PL increases in samples intentionally doped with oxygen[5]. An additional confirmation was brought in [5]. An isotope shift of the no-phonon PL line of about 0.45 meV was observed in samples doped with oxygen isotope O^{18}. The isotope shift is more evident for the narrow B-line.

Absence of the fine structure of lines A and B suggests that the PL center involves a simple point defect. An attempt to observe splitting due to crystal field was made in [5], however the results were inconclusive. Thus it is believed, that the oxygen related center in ZnTe is formed by an oxygen impurity substituting tellurium atom in the anion sub-lattice. There is no experimental proof that oxygen is indeed a substitutional impurity. However numerical calculations [3] confirm such model.

The electronic structure of the radiative center was proposed in [6]. Previously it was demonstrated that radiative center involves an electron and a hole. Thus, according to the model, substitutional O_{Te} center is an

[5]It is not very reliable demonstration since annealing of ZnTe in 1 atm. of zinc vapour at 1000 °C, followed by rapid quenching [5], also increases the intensity of the red PL. The effect is reversible.

electron trap. And a hole is weakly bound to it by a long-range Coulomb potential (Fig. 3a) in "an acceptor-like wave function" [6]. Such bound exciton state is called an isoelectronic acceptor, or exciton bound to neutral O_{Te} impurity[6].

The hypothesis that O_{Te} is an electron trap[7] (i.e. it first binds an electron) is based on comparison of electronegativity and ionization potential of oxygen and tellurium (see Table 1). Some evidences that O_{Te} center is an electron trap are reported in [6, 8].

In [6] authors base their arguments on the fact that electron-phonon coupling depends chiefly on the particle which is strongly attached to the local potential. The wave functions of the trapped electron and trapped hole have different types of symmetry. Authors predict that if isoelectronic center tightly binds an electron (isoelectronic acceptor), due to the symmetry of lattice distortions, the lattice can not distinguish different electron and hole spin states. Hence the entire phonon-spectra of A and B line should have the same shape (with B line shifted to lower energies by the A-B splitting) as it is the case in ZnTe:O. In case of isoelectronic hole trap the shapes of the A and B lines should be different.

A more direct confirmation is reported in [8]. Authors measured photoluminescence decay time of the excitons bound to isoelectronic O_{Te} center[8] (Fig. 3c). One can see that at $T < 3\ K$ the decay time (τ) is constant and equal to the decay time of the line B ($\tau = \tau_B = 318\ ns$). At $T < 20\ K$, τ is affected by both A and B lines. In this region τ decreases since $\tau_A < \tau_B$ ($\tau_A = 9\ ns$). The dashed line on the Fig. 3c is obtained by fitting the experimental data with an analytical expression and using τ_A and τ_B as fitting parameters.

In the temperature range $20\ K < T < 300\ K$ the decay time τ deviates from the analytical curve and increases. Such increase is explained by the thermal release of weakly bound holes from the O_{Te} center. With increasing temperature there is a greater probability of thermal release and thus holes spend longer time away from the electron trapped on oxygen impurity. Such increase confirms that the **released particles are the holes**. Indeed, the holes are the majority carriers in ZnTe and thus thermal release does not quench the PL but only delays it. The overall PL efficiency does not change. If the released particles would be the electrons, they would recombine through other channels surrounded by free holes. The activation energy obtained from the temperature dependence of the decay time was

[6] Usually an exciton bound to a neutral (not isoelectronic) impurity is a system of three particles. In this case, however, the center involves only two particles, an electron and a hole.

[7] There are also opposite opinions [7]. From the empirical pseudopotential analysis of group VI elements it is concluded that oxygen is much less attractive to electrons than sulphur, selenium and tellurium. Thus in II-VI semiconductors substitutional oxygen impurity is attractive to holes and repulsive to electrons. This result is probably wrong, since there are evidences that O_{Te} is an electron trap.

[8] Reports on luminescence kinetics were also made in [9, 10].

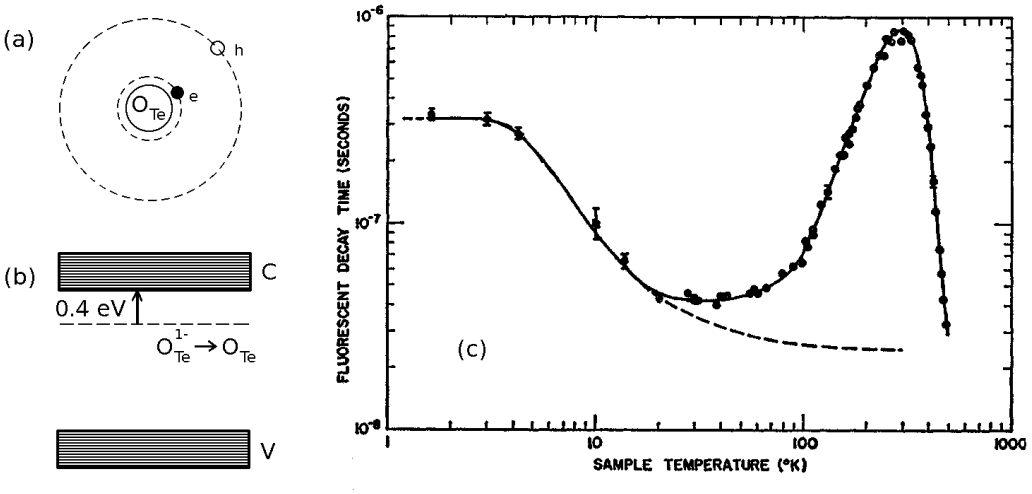

Figure 3: (a) A schematic diagram of an exciton bound to isovalent oxygen impurity in ZnTe. (b) The position of the oxygen-related state inside the band gap of ZnTe. (c) The dependence of the oxygen-bound exciton decay time on temperature in ZnTe:O. Dashed curve represents a fitted analytical dependence.

5.7 meV. This value is probably of the order of the binding energy of the hole to the center.

Above 300 K the decay time and PL intensity both rapidly fall. This phenomenon is explained by the thermal release of the electrons tightly bound to the O_{Te} center. Since the released electrons are the minority carriers in ZnTe, they recombine with holes through some other (possible non-radiative) channels, and thus the intensity of the PL decreases. The decay time decreases with activation energy of $\sim 0.4\ eV$. At low temperatures the A line of the exciton bound to O_{Te} is 0.394 eV below the ground state of the free exciton in ZnTe. Since these two values are very close it is concluded that O_{Te} creates an energy state inside the band gap, $\sim 0.4\ eV$ below the conduction band minimum (Fig. 3b). This energy level corresponds to transition $O_{Te}^{1-} \rightarrow O_{Te}$. The position of this level was also confirmed by numerical calculations [3, 11].

A series of weaker lines were observed [12] in the PL spectrum of ZnTe:O, excited with light which energy was below the energy of the line A. The structure and behaviour of the new lines (located $12 - 44\ meV$ below the line A) is very similar with the behavior of lines A and B. They also contain A-like and B-like lines corresponding to allowed and forbidden transitions and sidebands of phonon replicas. Authors distinguish four such structures (marked as OO_1, OO_2, OO_3, OO_4) and assign them to excitons bound to close pairs of substitutional oxygen impurity. Thus the OO_1 emission, wich has the lowest energy is assigned to pairs with smallest O-O separation. The model is confirmed by the convergence of the OO_n series to the line A emission at larger O-O separation.

2.1.2 Oxygen at alloying concentrations.

The term "alloying" here defines such concentrations at which the impurity not just introduces localized states to the band diagram of the host crystal, but also considerably modifies its band structure. In this concentration range the crystal may be considered as an alloy of two semiconductors (e.g. $ZnTe$ and ZnO), in which both components play an important role.

Band bowing

One of the effects observed in $ZnTeO$ alloy is a strong band bowing effect. The band bowing effect is manifested in a nonlinear dependence of the alloy band gap as a function of the alloy composition. In simple cases the band gap of the two-component alloy changes linearly with the increasing content of the second component. However if the components of the alloy differ much in size or electronegativity the dependence of the band gap on the alloy composition becomes nonlinear.

When the non-linearity is small the bowing is described by an empirical formula

$$E_g = E_{g1}(1-x) + E_{g2}x - bx(1-x), \tag{1}$$

where E_g, E_{g1}, E_{g2} are the band gaps of the alloy, component 1 and component 2, x is the content of the component 2 in the alloy. Constant b characterizes the magnitude of the bowing and it is called "bowing coefficient". Coefficient b is considered constant only if the non-linearity is small. When the non-linearity is not small, b is not necessarily constant and may depend on x.

In alloys like $ZnTeO$, were the difference in the size and the electronegativity is large (such alloys are often called Highly Mismatched Alloys or HMA), the bowing effect is particularly strong. The estimation made on the basis of numerical calculations [13] shows, that replacing 1% of tellurium atoms with oxygen would decrease the band gap of $ZnTeO$ by about 100 meV.

An estimation of the bowing coefficient may be derived from the experimental dependence presented on Fig. 4a [14]. The dependence of the bowing coefficient on the difference of anion radii in $Zn-group-VI$ alloys is very close to linear. The difference of anion radii for $ZnTeO$ alloy is the largest among $Zn-VI$ alloys (it is indicated on Fig. 4a by an arrow). Thus the value of the bowing coefficient in $ZnTeO$ alloy should be around 8.5 eV. This value should be considered only as an estimation, since it will be shown below that this value does not take into account the composition dependence of the bowing coefficient.

Composition dependence of the bowing coefficient

The numerical calculation [13] shows that the bowing coefficient in $ZnTeO$ is composition dependent (Table 2, Fig. 4b). It is strong and has a strong variation on the edges were x is close to 0 or 1, while in the middle part of the composition interval it is smaller and almost constant.

Experimental value of the bowing coefficient

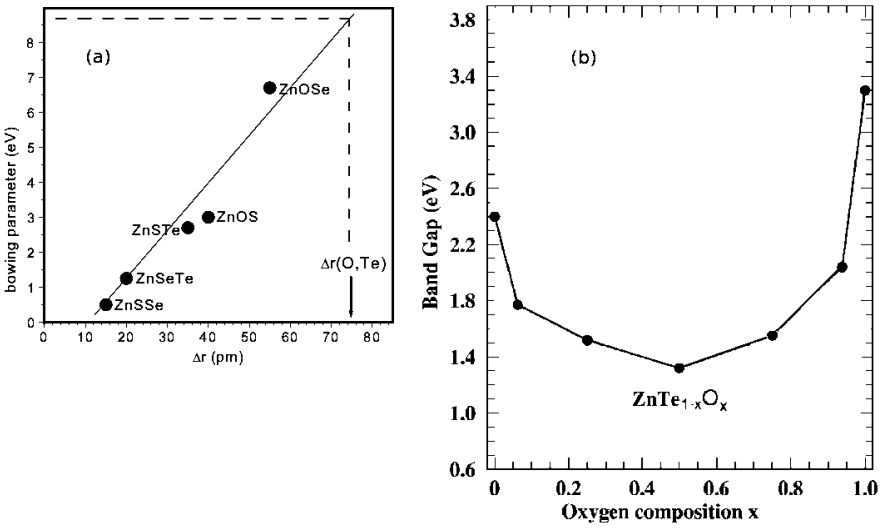

Figure 4: (a) Experimental dependence of the bowing coefficient of $Zn-VI$ alloys vs. difference of anion radii [14]. (b) Calculated dependence of the band gap on the composition of $ZnTe_{1-x}O_x$ alloy [13].

Table 2: Dependence of the bowing coefficient on composition of $ZnTe_{1-x}O_x$ alloy [13].

x	0.0625	0.25	0.5	0.75	0.9375
b (eV)	11.65	5.9	6.10	8.12	20.52

The question of experimental value of the bowing coefficient in $ZnTeO$ alloy is still open. Probably the only experimental report on the value of the bowing coefficient in $ZnTeO$ was made in [14]. The reported value is $b = 2.7\ eV$. Authors suggest that this value should be considered as the lower limit of bowing coefficient value, since the concentration of the oxygen incorporated into ZnTe matrix was probably overestimated. The discussed samples were prepared by sputter deposition on a substrate at room temperature, and the oxygen concentration was measured by the EDX technique. Thus probably a lot of oxygen was present in form of zinc oxide and was not incorporated into $ZnTe$ lattice. The decrease of the band gap measured on these samples by absorption spectroscopy reached 300 meV and occasionally 400 meV.

Origin of the band bowing

The reason of similar large bowing effect in III-V alloys was addressed numerically in [15]. Authors distinguish two mechanisms which influence the bowing coefficient, (i) the charge exchange and (ii) structural relaxation.

The charge exchange is manifested in appearance of localized states

which form conduction band minimum and valence band maximum. Numerical calculations show that the states of the conduction band minimum are localized on the anions with higher electronegativity (i.e. on oxygen atoms in ZnTeO). In binary semiconductors the states of the conduction band minimum are localized on cations. However in HMA those states are almost completely localized on the anions with higher electronegativity. At the same time valence band maximum states are localize on anions with lower electronegativity (i.e. on tellurium).

The structural relaxation in mixed-anion alloys is manifested in the motion of cations surrounding the replaced anion. Cation displacement leads to a strong intraband coupling within conduction band and separately within the valence band. This coupling lowers the conduction band minimum and raises the valence band maximum, thus reduces the band gap.[9]

The reason why the bowing coefficient in $ZnTeO$ alloy is composition dependent is based on the fact, that in this compound the isovalent impurity state is very deep and very localized. It stays localized even at high impurity concentration. When, due to the decrease of the band gap, the state becomes covered by the continuum of the band sates, the bowing coefficient becomes smaller and almost constant, like in ordinary alloys.

Impurity band

Usually as the concentration of an impurity in semiconductors increases, the energy states introduced by the impurity are described by impurity band of delocalized states. Delocalized states (and impurity band) start to appear when the wave functions of individual impurities start to overlap. According to Mott criterion the critical concentration at which the impurity band starts to appear is given by $a_B n_{crit}^{1/3} = 0.25$, were a_B is Bohr radius of a hydrogen-like state, n_{crit} is the critical concentration.

It is believed that in HMA [16] the isovalent impurity states, located in the band gap, are very localized and do not interact sufficiently so as to form an impurity band. Instead the energy of localized states remains relatively constant, while the shifting states of semiconductor's bands move into the fundamental band gap and overtake those localized states before they form an impurity band. This is a theoretical model produced for III-V alloys, however the same model should be applied for II-VI HMA. For now no experimental data on oxygen impurity band is available.

Band anticrossing model

The band bowing effect and also a number of other effects which appear in HMA may be successfully described by band anticrossing (BAC) model. For the first time the model was proposed in [17] to explain the pressure behaviour of the band gap energy in $GaInNAs$ HMA (see Fig. 5a). Authors suggested that the non-linearity and saturation of band gap energy

[9] In the case of mixed-cation alloys, were lattice relaxation is manifested in anion movement, the interband coupling between the conduction and valence band becomes dominant. Thus the band gap increases.

at high external pressure is a manifestation of an anticrossing behaviour of two strongly interacting energy levels with distinctly different pressure dependence. In $GaInAs$ the dependence of the band gap on pressure is linear. Thus it is concluded that the anticrossing is caused by the appearance of nitrogen-related localized states inside the band gap.

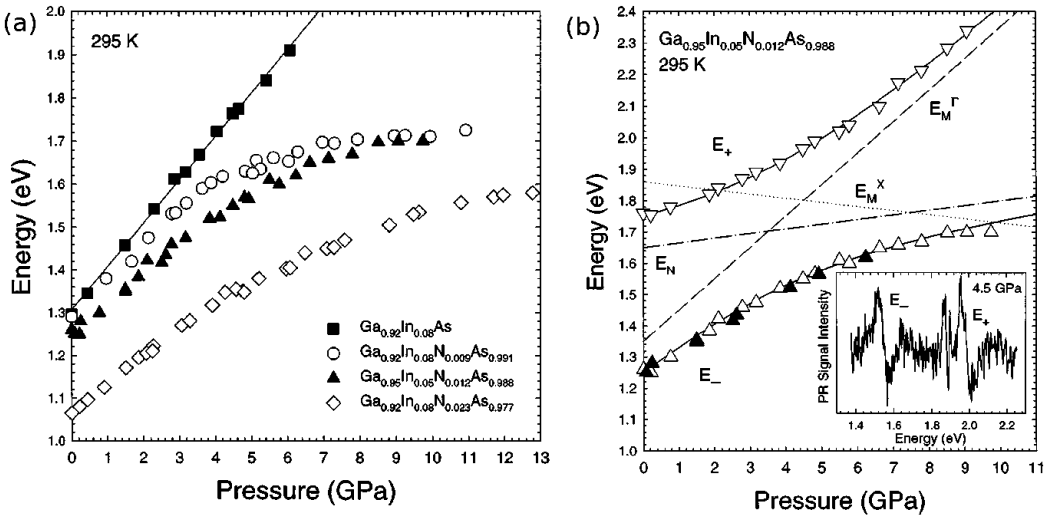

Figure 5: (a) Change of the fundamental band gaps of different $Ga_{1-x}In_xN_yAs_{1-y}$ samples as a function of hydrostatic pressure. The solid line is the linear fit to $Ga_{0.92}In_{0.08}As$ sample. (b) Change of the E_- and E_+ transition energies of $Ga_{0.95}In_{0.05}N_{0.012}As_{0.988}$ as a function of applied pressure. The open triangles are PR data, and the filled triangles are phototransmission data. E_M^Γ is the pressure dependence of the conduction band edge of $Ga_{0.95}In_{0.05}As$. E_N is the pressure dependence of the N-level. Solid lines are calculated using equations (3). The inset shows a PR spectrum taken at 4.5 GPa [17].

In this simple analytical model authors [17] consider two interacting energy levels, (i) one associated with the extended states of the GaInAs matrix, and (ii) another associated with the localized nitrogen states. The interaction between the two levels is considered as a perturbation, and following standard procedure of the perturbation theory the solution is derived from the following eigenvalue problem

$$\begin{vmatrix} E - E_M & V_{ML} \\ V_{ML} & E - E_L \end{vmatrix} = 0. \tag{2}$$

Here E_M and E_L are the energy of the matrix conduction band minimum and the energy of the nitrogen localized state respectively, relative to the top of the valence band. V_{ML} is a matrix element describing interaction between those two levels.

Solution of the (2) provides two dispersion curves

$$E_{\pm} = \frac{1}{2}(E_L + E_M \pm [(E_L - E_M)^2 + 4V_{ML}^2]^{\frac{1}{2}}), \quad (3)$$

which correspond to two energy subbands, marked as E_+ and E_-. The existence of these two bands was confirmed experimentally by photo-modulated reflection (PR) measurement [17] (see Fig. 5b, inset). As it is expected the bands appear in PR spectra above and below the single band which exists in $GaInAs$. The variation of E_+ and E_- with both pressure and nitrogen concentration could be fitted (Fig. 5b) to equations (3).

The energies of the E_+ and E_- bands depend on external pressure via parameter E_M. Experiment show that the band gap of the $GaInAs$ (E_M) increases linearly with pressure and the energy of the localized nitrogen state was found to be almost constant.

The dependence of the E_+ and E_- on nitrogen concentration is described by parameter V_{ML}^2. It was found that V_{ML}^2 increases linearly with nitrogen concentration x ($V_{ML}^2 = C_{LM}^2 x$). One can see that with increasing nitrogen concentration the E_+ band shifts up and the E_- shifts down. It is suggested that the downward shift of the E_- branch can account for the band bowing effect.

The fact that nitrogen greatly influences the *conduction* band and has negligible effect on valence band is confirmed by observation that the energy of spin-orbit splitting Δ_{SO} does not change with nitrogen concentration.

The sates of one of the E_+ and E_- bands have more localized character and the states of the other more extended character. According to BAC model if the energy of the localized impurity state is located above the conduction band minimum, the states associated with the lower E_- band retain delocalized character of the conduction band states, and those associated with E_+ band have more localized character of the impurity centers. As an example may serve $GaAsN$.

However if the localized state is located inside the band gap then the subbands switch their character. Such situation is observed for example in $ZnMnTeO$ (or $CdMnTeO$ with manganese content above 40%).

Band anticrossing in ZnMnTeO

Everything stated above is also applicable to II-VI HMA, including $ZnTeO$, for which the largest magnitude of BAC is expected. However BAC in $ZnTeO$ stil was not demonstrated experimentally[10]. Due to technological difficulties the fabrication of $ZnTeO$ with high enough concentration of substitutional oxygen was not achieved neither by equilibrium techniques no by non-equilibrium techniques.

It was found however [20, 21, 2], that addition of a reasonable amount of manganese to II-VI compounds increases the stability of substitutional oxygen. There are reports on successful implantation of several percent of oxygen into $CdMnTe$ [20, 2] and $ZnMnTe$ [21, 2].

[10] A numerical calculation, confirming the appearance of an intermediate oxygen-related band in $ZnTeO$ was reported in [18]

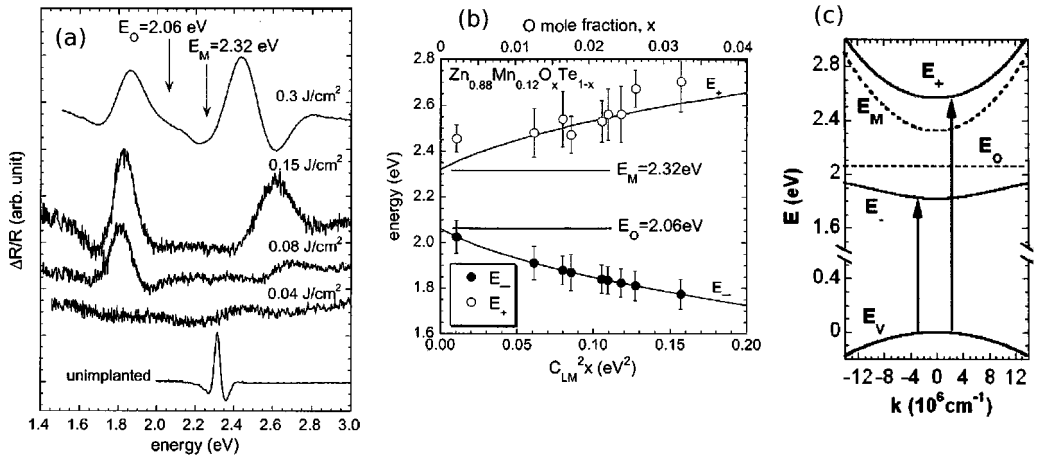

Figure 6: (a) PR spectra of the $Zn_{0.88}Mn_{0.12}Te$ implanted with 3.3% of oxygen, for different energy flows during pulsed laser melting. A spectrum of unimplanted $Zn_{0.88}Mn_{0.12}Te$ is also shown for comparison. (b) The energy of the E_+ and E_- for $Zn_{0.88}Mn_{0.12}O_xTe_{1-x}$ as a function of oxygen mole fraction x. Solid lines represent E_+ and E_- bands calculated according to BAC model [2]. (c) The calculated energy band structure for $Zn_{0.88}Mn_{0.12}O_xTe_{1-x}$ with $x = 0.01$ [21].

Band anticrossing effect was observed only in samples treated after the implantation by pulsed laser melting. Samples synthesized this way are not stable. Rapid thermal annealing at temperatures above 350 $°C$ decreases or completely eliminate the BAC effect. Such degradation is explained by the escape of oxygen atoms from the lattice nodes and creation of oxygen bubbles [21].

Band anticrossing effect in $ZnMnTeO$ was observed by means of photomodulated reflection (Fig. 6a) and absorption [21, 2] as a function of oxygen concentration (Fig. 6b) and applied pressure. The effect exists only in oxygen doped samples and is not observed in the undoped samples after a similar treatment. In accordance with the BAC model there are two bands in the PR spectra of $ZnMnTeO$ samples marked as E_+ and E_-. The separation between the bands increases with increasing oxygen concentration. The experimental data could be fitted to the equation (3). Because there is no method to determine reliably the concentration of substitutional oxygen or the interaction constant V_{ML}^2, the value of V_{ML}^2 is estimated to be 3.5 eV [21] or 2.2 eV [2]. The band structure of $ZnMnTeO$ calculated according to BAC model is shown on Fig. 6c.

In $ZnMnTeO$ the lower subband E_- has more localized O-like nature and the states of the upper E_+ subband have more extended character.

2.2 Review of the methods of synthesis

Equilibrium doping during growth. Oxygen solubility in ZnTe

The very first attempts on doping of $ZnTe$ with oxygen during the growth from both the vapour phase [8, 5] and melt [6], had demonstrated that the solubility of oxygen in $ZnTe$ is very low. The solubility of oxygen in $ZnTe$ was estimated [8] from the analysis of the oxygen-related absorption, and was found to be $3 \cdot 10^{17}\ cm^{-3}$. Hence in order to achieve a higher doping levels one should use a non-equilibrium process. Despite the fact that oxygen has a very low solubility in $ZnTe$, the crystals are often unintentionally doped with oxygen, especially the crystals grown from vapour phase inside the quartz ampules.

The reason of the low solubility is probably the large difference between properties of tellurium and oxygen, especially the difference of the covalent radius (see Table 1). Although the enthalpy of formation of ZnO is larger than that of $ZnTe$[11], the interatomic distance in ZnO is only 1.97 Å versus 2.64 Å in $ZnTe$. Thus the $ZnTe$ lattice is too wide for oxygen to form strong bonds with all four surrounding cations. Numerical calculations [3] show that due to relaxation of the surrounding cations the $Zn-O$ separation in $ZnTe:O$ is 2.10 Å. However since oxygen forms a *deep* isoelectronic trap in $ZnTe$, the difference between tellurium and substituting oxygen is very large and that makes the substitution energetically unfavorable. All known isoelectronic traps are substances of a limited solubility in the host [6].

Non-equilibrium doping. Powder and polycrystals

In order to increase the oxygen content the nonequilibrium techniques should be used. Concerning powder or polycrystalline samples two methods were reported, (i) ball milling in oxygen atmosphere [22] and (ii) synthesis by the radio frequency (RF) sputter process [14].

The ball milling was applied in a framework of investigation of phoshpors for X-ray imaging applications. The discussed $ZnTe:O$ powders were dry doped by ball milling the bulk $ZnTe$ crystals for 48 h in a ultra-high purity O_2 atmosphere. During ball milling occurs a mechanically stimulated ion implantation of active oxygen into the lattice. The implantation is possible due to large local electric fields, generated in the microcracks formed during crystal destruction. After the milling the powders were annealed and etched in a forming gas ($95\%N_2/5\%H_2$) atmosphere at 1000 °C for 1 h, in order to remove the tellurium oxides from the surface of the micro-crystals. Authors report only on luminescence measurements. Oxygen-related band was observed at $\sim 680\ mn$ ($\sim 1.82\ eV$). The lack of the phonon-structure suggests that the concentration of oxygen is higher than equilibrium concentration. However the exact oxygen content was not reported.

In RF-sputter process the $ZnTe$ target was used as a source material. Variable amounts of oxygen gas were added to the argon sputtering gas as a reactive component. The deposition was made on glass substrates at room temperature. The properties of the layers were controlled by photo absorp-

[11] $(-348)\frac{kJ}{mol}$ in ZnO vs $(-117)\frac{kJ}{mol}$ in $ZnTe$.

tion, X-ray diffraction and EDX analysis. Authors observed manifestations of increasing oxygen incorporation with the increase of oxygen pressure. For instance the band gap of the samples decreased by up to $300 - 400\ meV$. There was also a decrease of the lattice constant in highly oxygen-doped samples. However the crystalline quality of the layers decreased with increasing oxygen content. Additional annealing at $T > 300°C$ improved the crystalline qaulity, however the band gap of the annealed samples returned to the value of pure $ZnTe$. The concentration of oxygen in the samples was measured by EDX analysis and reached 30 $mole$ %. Authors suggest that measured concentration is probably overestimated, since EDX is sensitive to overall oxygen concentration. The concentration of oxygen incorporated into the $ZnTe$ lattice is probably much lower.

Non-equilibrium doping. MBE grown thin layers

The synthesis of $ZnTeO$ alloys by Molecular beam epitaxy (MBE) was reported in [23, 24]. The thin layers were grown on (001)-oriented $GaAs$ substrates at 300 $°C$. An RF plasma cell was used as oxygen source. The thickness of the grown samples varied between 600 nm and 1000 nm. The maximal oxygen concentration achieved was 5 $mole$ %. As it was with sputter-deposited $ZnTeO$ alloy the intensity of the XRD line decreases rapidly with the increasing oxygen concentration. However the observed dependence of the lattice constant is different.

It is reported that in the MBE-grown $ZnTeO$ alloy the lattice constant does not follow the Vegard's law. It first increases and reaches the maximum at about 0.7% of oxygen and then decreases. It is slightly below the value of pure $ZnTe$ at 5% of oxygen. The oxygen concentration was measured by secondary ion mass spectrometry (SIMS). It is reported that the concentration of oxygen in the samples increases with increasing oxygen flow rate, regardless of the anomaly in lattice constant behaviour.

Authors observed the oxygen-related smooth PL band at about 1.88 eV. The band is attributed to oxygen clusters, formed of coupled isolated oxygen atoms. Optical reflection experiments were carried out at room temperature. Based on the analysis of the reflection spectra, authors report that the band gap of the alloy increases with increasing oxygen content. Such behaviour is explained by BAC effect. However authors could not observe the lower subband and data of optical absorption were not presented.

Non-equilibrium doping. Thin layers made by ion implantation

It is probably the most effective method to create thin layers of $ZnTeO$ with high oxygen concentration. The reports on ion implantation of oxygen into II-VI semiconductors are presented in [20, 21, 2]. After the implantation, especially if the concentration of implanted atoms is high, the surface of the semiconductor is highly damaged. To repair the damaged surface and to "activate" the implanted oxygen atoms the samples are subjected to rapid thermal annealing[12] (RTA) or pulsed laser melting (PLM) or both.

[12] Annealing at temperatures ranging from 300 to 800 $°C$ for 10 s.

After RTA the activation efficiency[13] is only 5% [20].

A much better results are achieved by PLM. During the PLM the surface is melted for a very short period ($10^{-8}-10^{-6}$ s). After the laser pulse follows rapid epitaxial regrowth. It was shown that using the PLM method, the amorphous layers formed by high dose implantation can be regrown into nearly perfect single crystals, with electrical activities of dopants well above those achievable by furnace annealing [2].

After PLM $ZnTeO$ or $CdTeO$ demonstrate properties characteristic for highly mismatched alloys, however such alloys are not stable. RTA at temperatures above $300°C$ decreases or completely eliminates the manifestations of alloying with oxygen (for example the BAC effect).

A much better stability was found in $ZnMnTeO$ alloys [2]. Authors explain such higher stability by formation of relatively strong $Mn-O$ bonds. For an alloy with 12% of manganese a concentration of 3% of active oxygen was achieved, with activation efficiency of 50%.

For $ZnMnTeO$ samples only results of photo-modulated reflection as a function of composition and external pressure were reported. Thus the data on PL, structural and magnetic properties of $ZnMnTeO$ alloys is not available.

Summary: Methods of synthesis

- The solubility of oxygen in ZnTe is $3 \cdot 10^{17}$ cm^{-3}.
- High doping may be achieved only by nonequilibrium techniques (RF sputtering, MBE, ion implantation).
- $ZnTeO$ is not stable above 300 $°C$.
- Manganese increases solubility and stability of oxygen in $ZnTe$.
- The most reliable method for high oxygen doping is ion implantation of the $ZnMnTe$ followed by pulsed laser melting.
- The oxygen doping level achieved in MBE or ion implantation method is about 5 $mole$ %.

2.3 Technological part

Sample synthesis

In this work an attempt was made to prepare bulk $ZnTe$ samples simultaneously doped with manganese and oxygen. For this purpose was used a high temperature Bridgman furnace designed for growth of DMS like $ZnMnTe$. The synthesis was carried out in evacuated and sealed silica ampules. Usually to avoid interaction between manganese and the ampule walls, the ampule is covered from the inside with a thin graphite layer. In our case application of this method was not possible since oxygen present

[13] Part of active substitutional oxygen atoms.

in the charge reacted with the graphite layer, producing CO_2 gas at high pressure. Thus the contact between manganese and silica walls could not be avoided. In order to minimize the destruction of the ampule by manganese the samples were prepared by rapid cooling method. Another advantage of rapid cooling is the possibility to increase the oxygen content in the solid state by rapid freezing of the impurities which exist in the melt. Rapid cooling also limits the segregation of impurity, and thus the composition is uniform along the ingot. However, the samples prepared by rapid cooling are polycrystalline.

The synthesis was carried out in the sealed vacuumed silica ampules using ZnTe, MnTe and ZnO compounds as source materials. The ampules with the charge were heated up to 1350 °C and were held at that temperature for five hours to achieve better homogenization of the material. After that the ampules were rapidly cooled down by removing them from the hot region of the furnace. The whole process was carried out in the nitrogen gas atmosphere under the pressure of 5 Bar[14]. The external pressure was needed to compensate the pressure of the material vapor inside the ampules and to maintain the shape of the softened quartz glass. The resulting material has the form of polycrystalline ingots 10-14 mm in diameter and about 60 mm long.

Description of sample series

All samples were prepared in the same temperature conditions. The only parameters that were changed are the concentrations of manganese and oxygen in the charge. A summary of al $ZnMnTe : O$ samples is presented in Table 3.

Two sets of samples were made to find the optimal conditions for oxygen doping. In the first set the manganese concentration was kept constant and the oxygen concentration was varied. In the second set the oxygen concentration was constant and the manganese concentration was varied. The third set (Table 3) contains samples that do not fit the first two.

Before proceeding to samples characterization the main conclusions concerning the effectiveness of oxygen doping will be presented. The conclusions are based on the results of EDX, X-ray diffraction, and exciton reflectivity measurements. Such measurements provide information about manganese content, behaviour of the lattice constant and the band gap in the samples. The results of the measurements are summarized in Table 3.

The main conclusions concerning the effectiveness of oxygen doping are:

- The solubility of oxygen in ZnTe is very low (not observable by mentioned measurements, see sample 4487). This is in agreement with [8], where the estimated solubility was $3 \cdot 10^{17}\ cm^{-3}$.
- Manganese indeed considerably increases the solubility of oxygen in ZnTe.

[14]Pressure at room temperature.

Table 3: Summary of sample series.

Nr.	Sample ID	Initial Mn fraction	Initial O fraction	Measured Mn frac. (x)	Estimated O frac.(y)	Lattice const (Å)	Free exciton en. (eV)
Set 1							
1	4135	0.05	0	0.051	0	6.1110	2.4112
2	4481	0.05	0.01	0.041	0	6.1107	2.4021
3	4463	0.05	0.03	0.047	0.0021	6.1073	2.3929
4	4310	0.05	0.05	0.040	0.0018	6.1065	2.3870
5	4462	0.05	0.075	0.031	0.0011	6.1056	2.3866
6	4479	0.05	0.10	0.027	0.0019	6.1035	2.3834
7	4480	0.05	0.15	0.016	0.0008	6.1030	2.3813
Set 2							
8	4487	0	0.05	<0.001	<0.0001	6.1019	2.3785
9	4488	0.03	0.05	0.025	0.0014	6.1038	2.3847
10	4489	0.07	0.05	0.056	0.0023	6.1088	2.3970
Set 3							
11	4506	0.15	0.03	0.187	0.0057	6.1304	2.4550
12	4436	0.03	0.005	0.025	0	6.1065	2.3974

- Despite the fact that the solubility of $MnTe$ in $ZnTe$ is very high ($0 < x < 0.86$) [25], the increase of oxygen concentration in the charge reduces the concentration of manganese in the crystal (see series 1). The manganese is extracted into a reddish compound covering the walls of the ampule.

- If the concentration of oxygen in the charge is less than 1%, the oxygen doping is not effective, even in the presence of manganese (see samples 4481 and 4436).

- To achieve the highest concentration of the oxygen in the crystal, the charge should contain moderate concentration of oxygen ($2-3\%$) and as high as possible concentration of manganese (see sample 4506). Further increase of oxygen content in the charge is not justified since it leads to a considerable decrease of manganese content in the sample.

2.4 Material characterization

2.4.1 Scanning electron microscopy (SEM)

All $ZnMnTe:O$ samples are polycrystalline with the grain size about 0.1-1 mm. The smaller grains were found closer to the tip of the ingot since the tip was cooled in a colder region of the furnace, and hence here the cooling was faster then in the top part of the ingot. A typical example of the SEM image is presented on Figure 7. The image was made for a cross section of the bottom part of the sample 4479 (see table 3) polished mechanically and then chemically in Br-methanol solution.

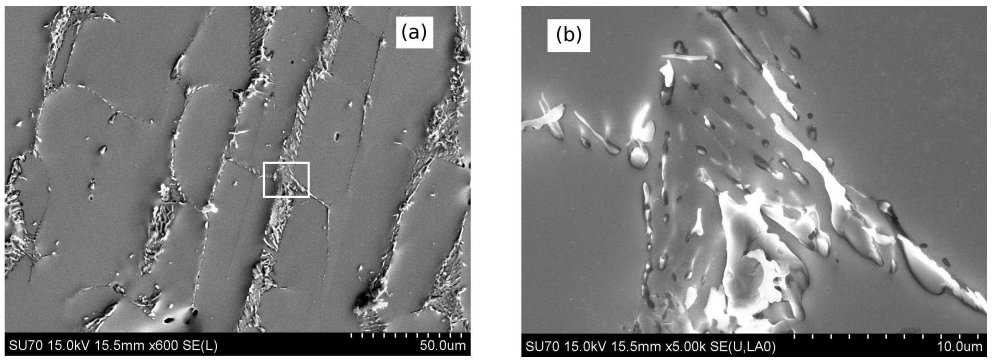

Figure 7: (a) Scanning electron microscope image of the sample 4479. (b) Closer view of the precipitation region.

There are macroscopic precipitations between the grains. Judging from the bright color of the precipitations one may conclude that the precipitations are formed of isolating material, whereas the crystalline blocks covering the majority of the surface are conductive. The composition of both the polycrystalline grains and precipitations was studied by means of micro EDX analysis.

2.4.2 Micro EDX

An example of EDX spectra measured on sample 4479 is shown on Fig. 8. The presented spectra were recorded from a crystalline block (Fig. 8b) and from a precipitation (Fig. 8c). Similar results were observed also on other $ZnMnTeO$ samples.

Micro EDX measurements show that the crystalline grains are composed of Zn, Te and Mn. The estimation of oxygen concentration in the grains was not possible. One of the reasons is that the oxygen concentration in the grains is low. The other reason is that the oxygen peak is masked by a tellurium peak in the EDX spectrum. The oxygen is a light element. The only x-ray emission line $K_{\alpha 1}$ of the oxygen ($0.5249\ keV$) is situated very close to some tellurium emission lines $M_V O_{III}$ at $0.569\ keV$ and $M_{IV} O_{II,III}$ at $0.581\ keV$ [26]. The distance between those lines is about $50-60\ eV$ and the typical width of the emission lines in EDS spectra is $100\ eV$. Thus there

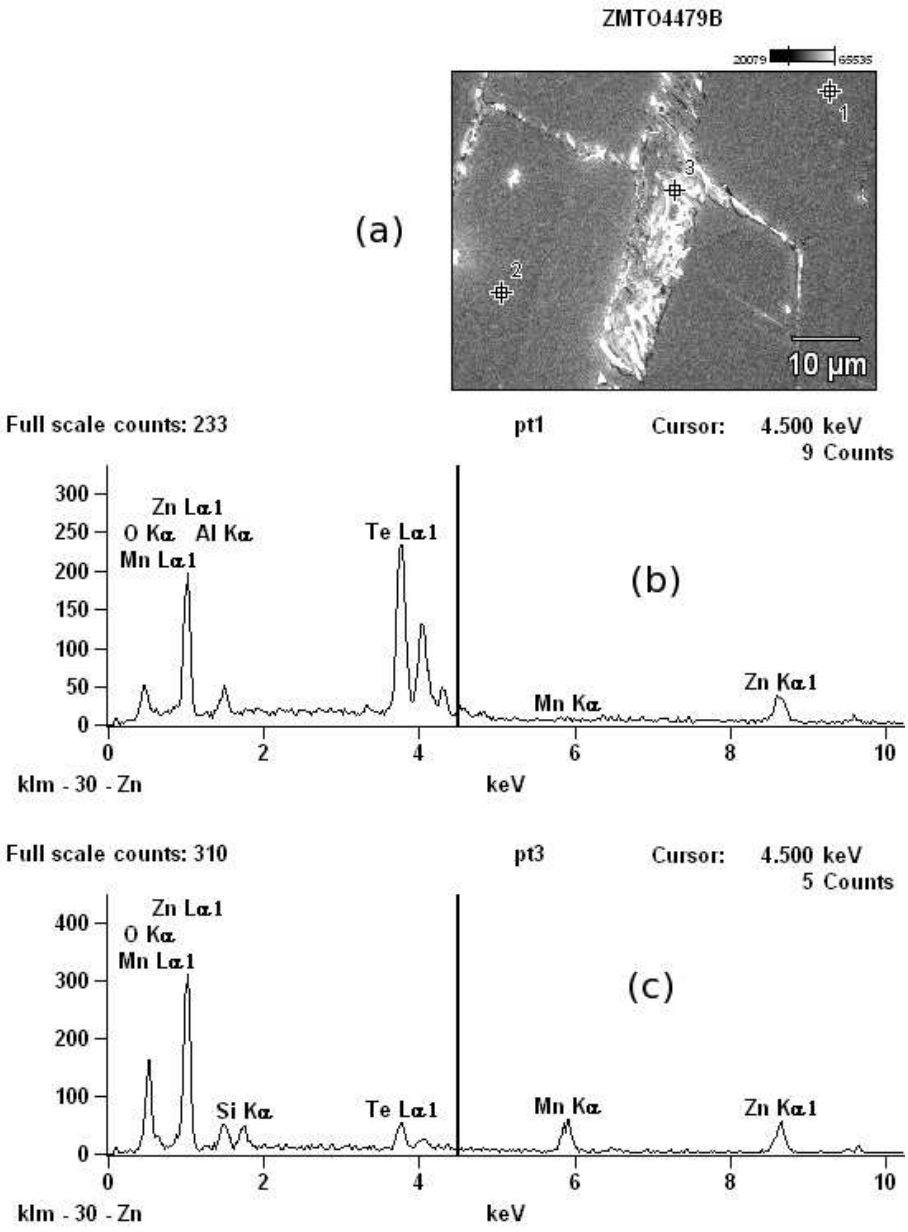

Figure 8: (a) Positions of the spots on the sample surface (marked 1, 2 and 3) were the EDX spectra have been measured. (b, c) EDX spectra measured in the points 1 and 3 respectively.

is a large error in the value of oxygen content determined from the spectra with large tellurium background. For our samples the result of the EDX analysis of the oxygen content was obviously overestimated. This is why the estimation of the substitutional oxygen concentration was made from x-ray diffraction measurements. The whole procedure will be described below.

The material of precipitations which appear between the grains contains mainly Zn, O, Mn, Te and Si. The oxygen concentration here is

higher than the concentration of tellurium. The composition of inter-grain material is not uniform. Since there was no silicon in the ampule charge, it is clear that the silicon originates from the ampule walls corroded by manganese. The aluminum peak, which is visible on both spectra originates from the sample holder.

2.4.3 X-ray diffraction

X-ray powder diffraction was used to study the crystalline structure of the samples and for the estimation of the amount of incorporated oxygen. The measurements were performed on a Siemens "D5000"diffractometer with Cu-K_α (λ=1.54184 Å) radiation. Some of these results were published in [27].

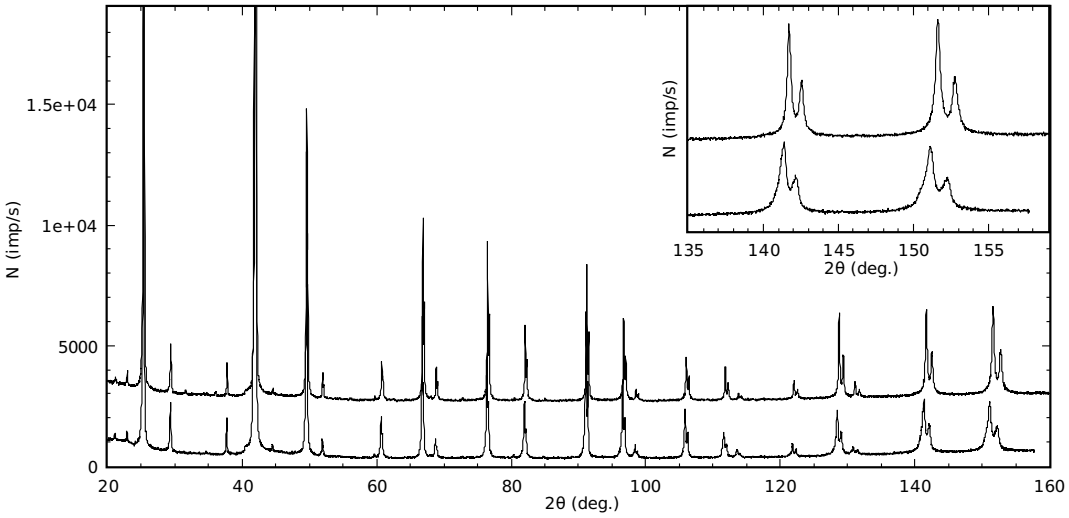

Figure 9: Examples of the powder XRD diagrams for samples 4135 ($ZnMnTe$, lower curve) and 4479 ($ZnMnTeO$, upper curve) (see Table 3). On the inset: a closer look on two diffraction peaks for the same samples.

A comparison of two XRD diagrams measured on samples $ZnMnTe$ (4135) and $ZnMnTeO$ (4479) is presented on Fig. 9. The content of oxygen in the charge for sample 4479 was 10% (see Table 3). However, no additional peaks appear on the upper curve, which could be assigned to oxygen-related precipitations. Other $ZnMnTeO$ samples have similar XRD properties.

The absence of additional peaks due to precipitations is explained in part by the small amount of precipitations in comparison with the material of polycrystalline grains, and in part by the fact that the composition of the precipitations is variable. The position of the diffraction peaks confirms that the material has zinc-blende crystal structure. The value of the lattice constant for each sample is presented in Table 3. The lattice constant varies. As an example, the shift of the XRD lines in the sample doped with

oxygen is illustrated on Fig. 9, on the inset. One can see that the oxygen doped sample (upper curve) has a smaller lattice constant.

2.4.4 Estimation of oxygen concentration

Because other methods could not provide reasonable results, the variation of the lattice constant of the samples was used to estimate the concentration of substitutional oxygen in $ZnMnTe:O$. The advantage of the XRD method is that the lattice constant is sensitive only to oxygen atoms substituted into the $ZnMnTe$ matrix, and it is not sensitive to oxygen located inside even the smallest precipitations. Other methods like SIMS or EDX are sensitive to overall oxygen concentration in the sample.

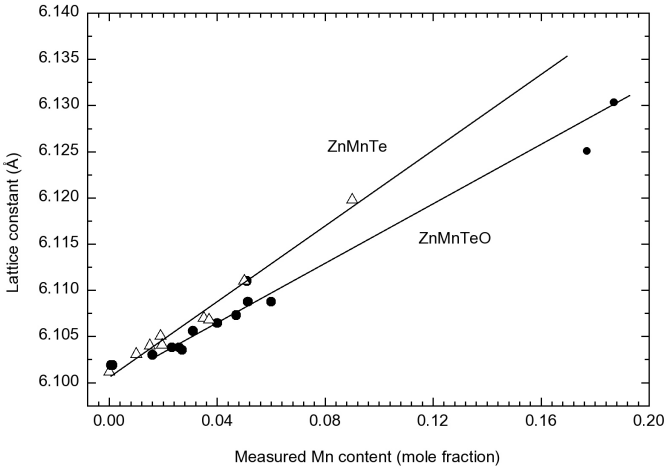

Figure 10: Dependence of the lattice constant on manganese concentration for oxygen-free $ZnMnTe$ (open triangles) and oxygen-doped $ZnMnTe:O$ (filled circles) samples.

The task is complicated by the fact that in our samples both the concentration of oxygen and the concentration of manganese vary. To overcome such difficulty, the dependence of the lattice constant on the manganese concentration for two sets of samples was studied. In one set there were the discussed oxygen-doped samples. In the other set there were oxygen-free $ZnMnTe$ samples. The manganese concentration was measured in both cases by means of bulk EDX analysis.[15] The results are shown on Fig. 10.

The first thing which should be noticed here is that oxygen-doped samples have smaller lattice constant than oxygen-free samples. The decrease of the lattice constant is assigned to the presence of substitutional oxygen

[15]The results of such measurements for $ZnMnTe:O$ samples are presented in Table 3.

in the samples. Such behaviour is expected from the oxygen doped samples, sice oxygen atom has much smaller size than the tellurium atom.

To obtain the substitutional oxygen concentration one needs the dependence of the lattice constant on the oxygen concentration. Since such dependence is not available neither for $ZnTe:O$, nor for $ZnMnTe:O$, it is assumed that the Vegard's law for the lattice constant is valid in this case[16]. According to Vegard's law the lattice constant of the alloy changes linearly with the composition

$$a^{ZMTO} = a^{ZMT}(1-y) + a^{ZMO}y. \tag{4}$$

Hence the oxygen molar fraction may be written as,

$$y = \frac{a^{ZMTO} - a^{ZMT}}{a^{ZMO} - a^{ZMT}}. \tag{5}$$

Here a^{ZMO} is the lattice constant of the $ZnMnO$ alloy with the zinc blend structure. Because the lattice constant dependence of the zinc blend ZMO alloy is not available one can use the value of $(a^{ZnO} - a^{ZnTe})$ as a reasonable approximation of the denominator. Hence the oxygen content fraction was estimated using the formula,

$$y = \frac{a^{ZMTO} - a^{ZMT}}{a^{ZnO} - a^{ZnTe}}. \tag{6}$$

The values of a^{ZMT} were interpolated using the upper curve of the Fig. 10. The value of a^{ZnO} (4.57 Å) having the zinc blend structure was taken from [13]. The value of a^{ZnTe} (6.101 Å) was obtained by measuring XRD of a pure ZnTe crystal. The values calculated using (6) are presented in Table 3.

The dependence of the calculated oxygen content on the measured manganese content in the $ZnMnTe:O$ samples is shown on Fig. 11. The oxygen solubility increases with manganese concentration. The dependence is not linear and tends to saturation. The maximal oxygen content achieved by this method is $y = 0.056$ (or $10^{20}\ cm^{-3}$). It is 300 times higher than the solubility in pure $ZnTe$.

Although oxygen concentration was not obtained by direct measurement, it is confirmed by free exciton reflectivity measurements.

The fact that oxygen solubility increases with maganese concentration suggests that the distribution of the oxygen atoms in the host matrix is non-statistical. It means that in the lattice oxygen atoms are not randomly distributed. To account for increased solubility, the oxygen atoms should be located in vicinity of at least one manganese atom. Manganese probably

[16]Even if the Vegard's law is not applicable for this system, such approximation is reasonable, since the calculations are made for a small region of the composition range near the tellurium reach end. If the dependence of lattice constant on oxygen content is non-linear, the deviation from the Vegard's linear dependence is small in this region.

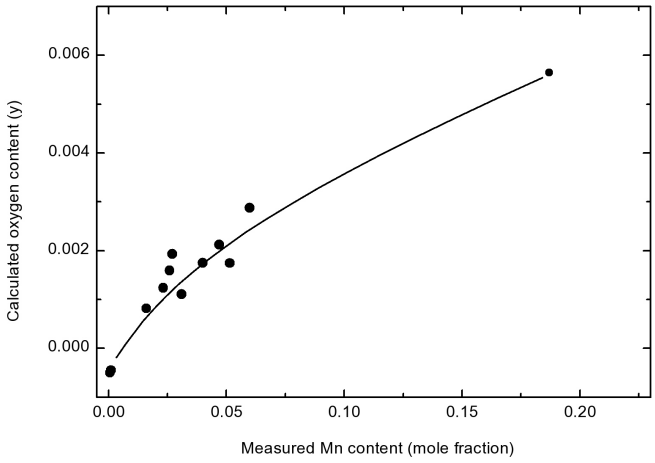

Figure 11: Dependence of substitutional oxygen concentration on manganese concentration in $ZnMnTe : O$.

compensates the difference of properties between oxygen and tellurium. Such conclusion suggests that in the $ZnMnTe$ oxygen creates complex defects of type (Mn_nO), were n is number of manganese atoms surrounding oxygen impurity.

The oxygen concentration was estimated assuming that the Vegard's law is valid in $ZnMnTe : O$. Although there is no information on this subject for $ZnMnTe : O$, there are reports on lattice constant dependence in $ZnTe : O$ [14, 23]. In [14] authors report that lattice constant of $ZnTe : O$ decreases with oxygen, like in our case, however it is not possible to tell whether it follows the Vegard's law. In [23] authors observed an increase of the lattice constant and explain it by presence of interstitial oxygen. Thus the behaviour of the lattice constant depends on the method of synthesis.

Summary: Sample structure and composition

- All $ZnMnTeO$ samples are polycrystalline.
- Polycrystalline grains are composed of $ZnMnTe$ doped with oxygen.
- Precipitations contain mostly Zn, Mn, O and a smaller amount of Si and Te. The composition of the precipitations is non-uniform.
- Oxygen concentration in the polycrystalline grains is estimated from the variation of the lattice constant of $ZnMnTe : O$.
- Maximal oxygen content achieved so far is 0.5%. It is about 300 times higher than in $ZnTe$.
- Oxygen concentration increases with manganese content in $ZnMnTe : O$.

- The increase of oxygen solubility with manganese suggests that oxygen forms in $ZnMnTe$ complex defects of type (Mn_nO).

2.5 Electrical properties

Hall effect

The Hall-effect measurements were performed only at room temperature since the resistance of the samples rapidly increases with cooling. The samples are p-type with hole concentration ranging from $2 \cdot 10^{16} cm^{-3}$ to $2 \cdot 10^{17} cm^{-3}$ (see Fig. 12). The hole concentration decreases with the increasing technological oxygen concentration in the ampule. In $ZnTe$ both manganese and oxygen are isovalent impurities. Hence as well as in $ZnTe$, in $ZnMnTeO$ the holes are produced by native impurities and namely by zinc vacancies (V_{Zn}). In all as-grown samples doped with oxygen the concentration of holes is about 10 times lower then in the pure $ZnMnTe$ samples. One may conclude that there is a lower concentration of zinc vacancies in oxygen doped samples. The other possible reason, the compensation by donor impurities, is ignored, because our impurities should not be electrically active.

The mobility varies between 20 and 40 $cm^2/V \cdot s$. Such low values of mobility are explained by the presence of the barriers between the grains which limit conductivity in the samples.

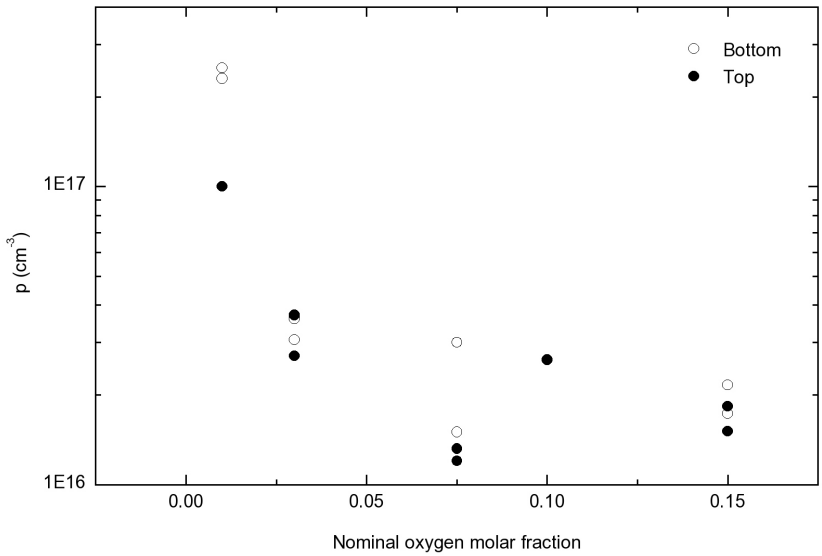

Figure 12: Dependence of hole concentration at room temperature on the content of oxygen in the charge. Samples were taken from the top and the bottom of the ingot.

Deep level transient spectroscopy

Deep level transient spectroscopy (DLTS) measurements were performed on only one sample (4463). The Schottky barrier for the measurement was prepared by making two small contacts to the same poly-crystalline grain. One of the contacts was ohmic, and was prepared using a gold electrode. The other contact which formed Schottky barrier was made of indium.

The measurement revealed three deep levels inside the band gap. Two of them are located about 0.48 eV and 1 eV above the top of the valence band. The third level is located deeper, and its position could not be determined. Since DLTS was not studied systematically, the nature of those levels will not be discussed. It is not known whether those levels are related with the presence of manganese or oxygen in the samples. The reports on DLTS studies in $ZnTe$ show that the spectrum of the observed deep levels in ZnTe is very reach [28, 29]. Deep levels with similar activation energies (0.48 eV and 1 eV) can be also found in $ZnTe$.

2.6 Optical properties

2.6.1 Free exciton reflectance

The measurement of the reflectance in the energy range of the free exciton gives a relatively simple possibility to study the behavior of the semiconductor's band gap. In this work the reflectance was measured as a function of temperature, oxygen concentration and external magnetic field.

The free exciton reflectance was measured on chemically polished polycrystalline samples in temperature range between $6K$ and room temperature. The free exciton structure in reflectance spectra was observed for all samples and occasionally even up to room temperature. As an example the variation of reflectance spectrum (of the sample 4479) with temperature is presented on Fig. 13a. The dependence of the free exciton energy on temperature is shown on Fig. 13b. Fitting the experimental data with a phenomenological dependence $E_g = E_0 - \alpha T^2/(T+\beta)$ [30] gives parameters values of $\alpha = 5.3 \cdot 10^{-4}\ eV/K$, and $\beta = 149\ K$. Here β is a parameter which is proportional to Debye temperature (θ), and α characterizes the variation of the band gap due to temperature-dependent dilatation of the lattice ($\Delta E_g \sim \alpha T$ at $T \gg \theta$).

The width of the exciton structure[17] is about 3.5 meV. The same value was recorded for oxygen-free $ZnMnTe$ samples. The free exciton energy was calculated as the average between energies of the maximum and minimum of the exciton structure. Because of the polaritonic nature of the exciton reflectance [31] the real value of the free exciton energy may be located outside of this region. Thus it is possible that there is a systematical error (about $\pm 2\ meV$) in the presented values of free exciton energy. The values of the free exciton energy for all samples are listed in Table 3.

First of all it should be demonstrated how the free exciton energy (and the band gap) depends on oxygen concentration. However, here appears the same problem we have met during the discussion of XRD results. Since the band gap depends on both manganese and oxygen concentration it is necessary to separate both contributions to the band gap variation. Below follows the explanation of how the band gap of $ZnTeO$ was calculated using free exciton energy of $ZnMnTeO$.

The dependence of the free exciton energy on the manganese concentration in $ZnMnTe$ was studied [32], and can be expressed using the following relation,[18]

$$E_x^{ZnMnTe} = E_x^{ZnTe} + \Delta E_x x, \tag{7}$$

where $\Delta E_x = 0.68\ eV$,[19] E_x denotes the free exciton energy and x denotes

[17] The distance (in energy units) between maximum and minimum of the exciton structure.

[18] It is true only for $x > 0.02$. At smaller x it is nonlinear [32].

[19] This value should be used at low temperatures, around 2 K. A close result $\Delta E_x = 0.75\ eV$ was reported in [38]

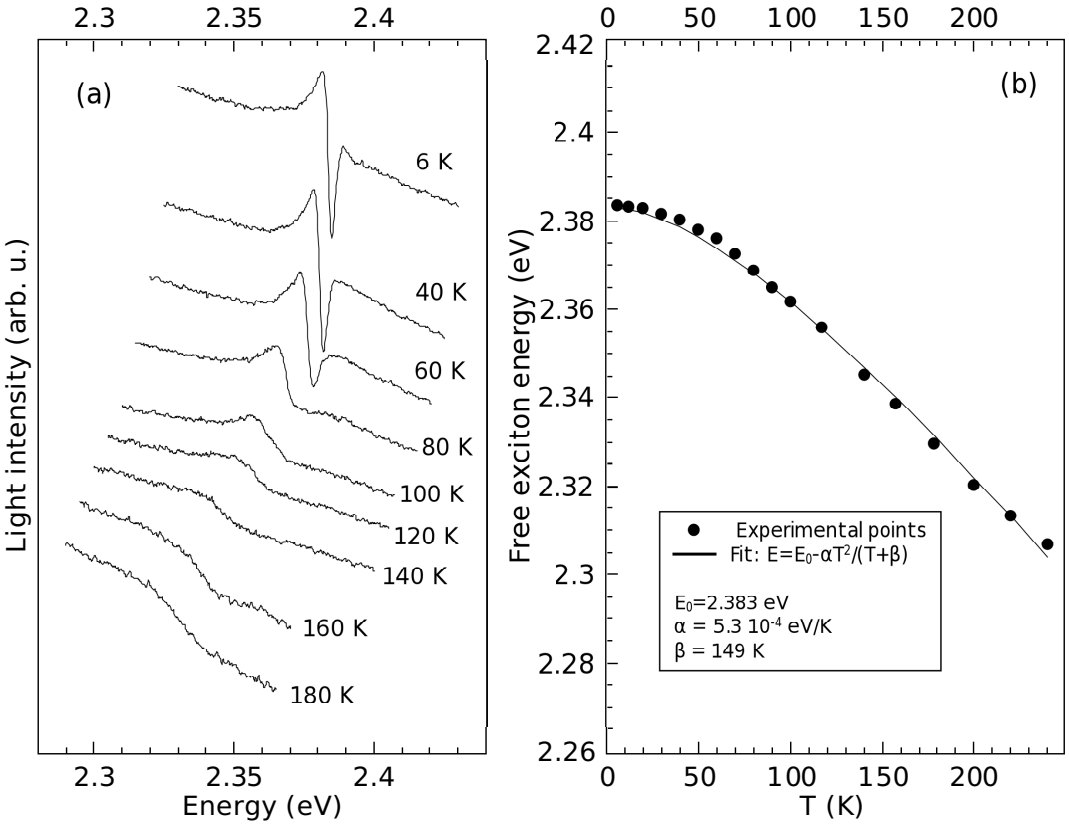

Figure 13: (a) Free exciton reflectance spectra of sample 4479 at different temperatures. (b) The energy of the free exciton as a function of temperature. The solid line represents a nonlinear fit with a phenomenological dependence of the band gap on temperature $E_g = E_0 - \alpha T^2/(T+\beta)$ [30]. The obtained fitting parameters are shown on the figure.

the Mn molar content. Since the oxygen molar content is small the same relation should be applicable in the case of $ZnMnTeO$

$$E_x^{ZnMnTeO} = E_x^{ZnTeO} + \Delta E_x x. \tag{8}$$

To calculate the band gap of the $ZnTeO$ using the free exciton energy one needs also the value of the free exciton binding energy for $ZnTeO$. Since the oxygen molar content is small and the data on the free exciton binding energy in $ZnTeO$ is not available and since the band bowing effect in $ZnMnTeO$ is predicted to be very strong [13], the dependence of the free exciton binding energy on the oxygen molar content will be neglected in the further discussion. Thus the free exciton binding energy in the tellurium-reach region of the alloy will be considered constant and equal to that of the pure $ZnTe$ ($E_{BX}^{ZnTe} = 13.2\ meV$) [33].

Thus the band gap of $ZnTeO$ alloy may be calculated as

$$E_g^{ZnTeO} = E_x^{ZnTeO} + E_{BX}^{ZnTe}. \tag{9}$$

Combination of equations (9) and (8) gives:

$$E_g^{ZnTeO} = E_x^{ZnMnTeO} - \Delta E_x x + E_{BX}^{ZnTe}. \tag{10}$$

The values of E_g^{ZnTeO}, calculated using equation (10) are plotted on Fig. 14 as a function of substitutional oxygen content y.

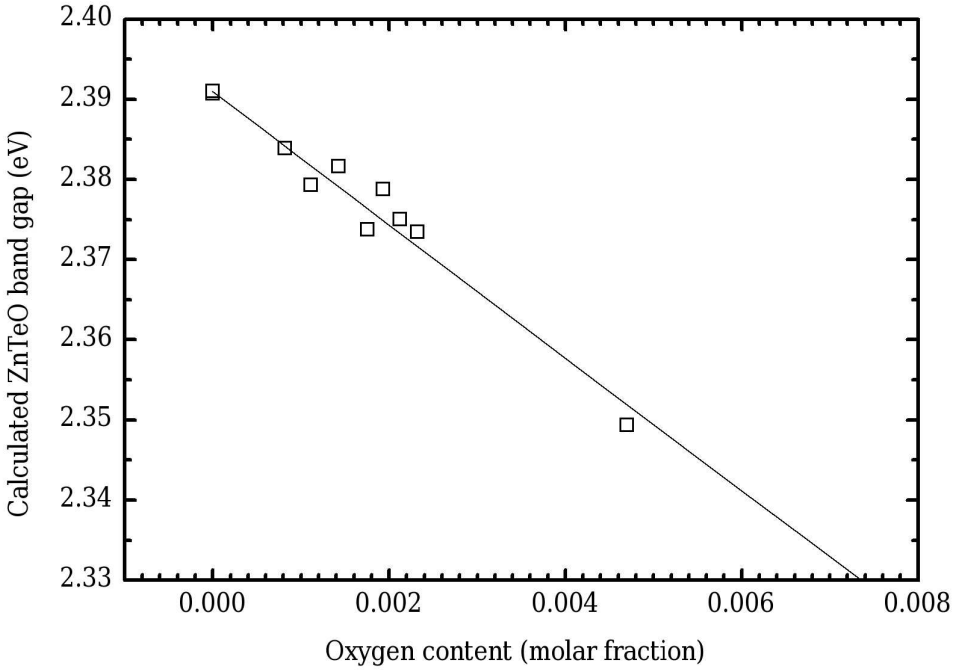

Figure 14: The band gap of $ZnTeO$, calculated using free exciton energy of $ZnMnTeO$, as a function of oxygen content. The solid line was obtained by fitting experimental data with band bowing relation (11).

In accordance with the band bowing theory, the band gap decreases with increasing oxygen concentration. No change of the band gap was observed in manganese free $ZnTe : O$ sample. The points shown on Fig. 14 were fitted by the band bowing relation, analogous to equation (1)

$$E_g^{ZnTeO} = (1-y)E_g^{ZnTe} + yE_g^{ZnO} - by(1-y). \tag{11}$$

The value of $E_g^{ZnO} = 3.3\ eV$ for the zinc blende ZnO was taken from [13]. The value of the ZnTe band gap $E_g^{ZnTe} = 2.391\ eV$ was calculated using the measured free exciton energy and the published value of the free exciton binding energy [33]. The bowing coefficient b served as the fitting parameter. The obtained value of the bowing coefficient is 9.3 eV. It is quite close to the predicted value of 11.6 eV [13], and also to value 8.5 eV discussed on page 12.

The fact that the obtained value of the bowing coefficient is very close to the expected value gives a strong confirmation that the estimated oxygen concentration is reliable. If the concentration of oxygen would be overestimated, the value of the bowing coefficient would be smaller [14]. If the concentration would be underestimated, the bowing coefficient would be larger.

There is a good correlation between oxygen concentration evaluated from XRD data and the band gap behavior of $ZnMnTeO$. Notice, that both methods, XRD and reflectance measurements are not sensitive to other phase precipitations, are collected from large areas of the sample and are sensitive to substitutional oxygen scattered in the host matrix only.

Summary: Free exciton reflectance

- The free exciton reflectance as a function of temperature and oxygen concentration was studied.
- Band gap of $ZnTeO$ was calculated using free exciton energy of $ZnMnTeO$.
- Dependence E_g^{ZnTeO} was plotted as a function of oxygen content x.
- The value of the bowing coefficient b was obtained by fitting of the plot $E_g^{ZnTeO}(x)$ to the band bowing relation.
- The fact that the value of $b = 9.3\ eV$ is close to the expected value confirms that the estimation of oxygen concentration is correct.

2.6.2 Magneto-reflectance

Magneto-reflectance: Introduction

$ZnMnTeO$ is also a semimagnetic semiconductor. This is why an attempt was made to study the influence of the oxygen on the properties related with the presence of magnetic ions in the matrix.

One of the features of semimagnetic alloys like $ZnMnTe$ is the influence of the magnetic ions on the band structure of the alloy [25, 34, 35]. The influence originates from the interaction between the s and p band electrons and $3d^5$ electrons associated with manganese ions, known also as the $sp-d$ interaction. The $sp-d$ interaction results in a giant spin splitting of the electron energy bands under the applied magnetic field. Such splitting in $ZnMnTe$ is much larger then the Landau splitting or the spin splitting, which exist even in the absence of magnetic ions in the lattice[20]. Unlike Landau splitting or the spin splitting where the magnitude of splitting depends on band structure and carrier effective masses, in giant spin splitting the magnitude of splitting depends on special values called exchange integrals (or constants), which describe the strength of exchange interaction

[20]The shift of the free exciton line in $ZnTe$ in magnetic field is about 0.3 meV at 5 T [36].

between free carriers and localized magnetic moments. A schematic diagram of the splitting of the conduction band minimum and the valence band maximum in $ZnMnTe$ is shown on Fig. 15.

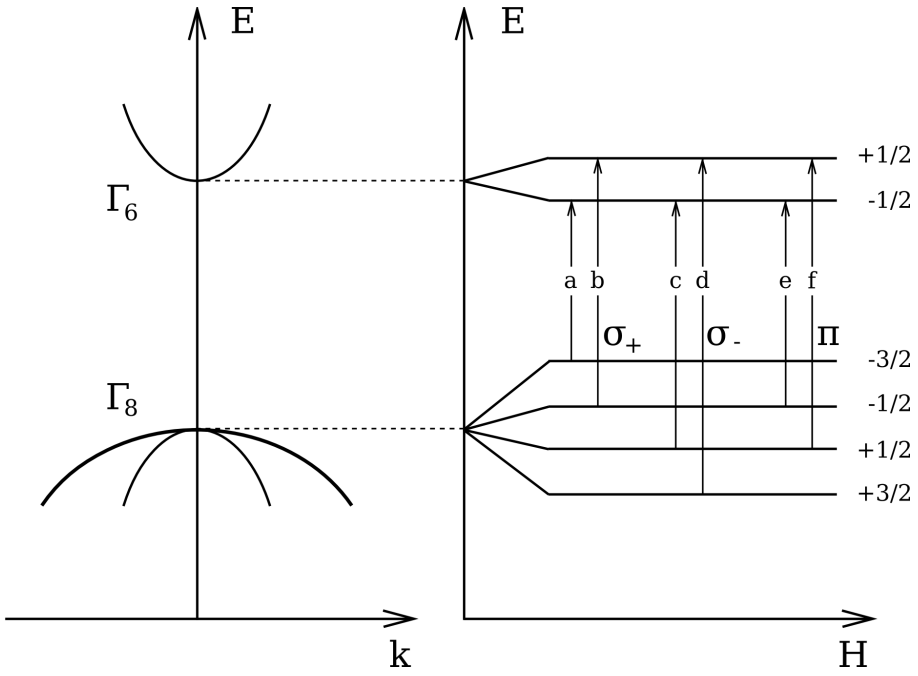

Figure 15: A schematic diagram of the splitting of the conduction band minimum (Γ_6) and valence band maximum (Γ_8) of $ZnMnTe$ in a magnetic field. Arrows indicate electric dipole allowed transitions. σ_+, σ_- and π denote right circular-, left circular- and linear-polarized transitions respectively.

The dependence of the splitting on magnetic field is discussed theoretically in [37, 25] and may me be written as

$$E_{C1,2} = E_C \pm 3A,\ E_{V1,2} = E_V \pm 3B,\ E_{V3,4} = E_V \pm B. \qquad (12)$$

Here C and V denote conduction and valence band respectively, A and B stay for:

$$A = \frac{1}{6} x N_0 \alpha < S_z >_{Mn},\ B = \frac{1}{6} x N_0 \beta < S_z >_{Mn}, \qquad (13)$$

were x denotes manganese mole fraction, N_0 the number of unit cells per unit volume, $< S_z >_{Mn}$ the thermal average of the manganese spin component along the z-direction, and α and β are constants characterizing the strength of interaction between manganese ions and electrons and holes respectively. $\alpha \equiv < S|J^{sp-d}|S >$ and $\beta \equiv < X|J^{sp-d}|X >$ are exchange integrals for conduction and valence bands [37].

Values of the exchange constants α and β in $ZnMnTe$ have been measured experimentally (see Table 4). The obtained values do not depend on manganese concentration.

The discussed exchange integrals are very important parameters of the SMS, which characterize the interaction between free carriers and magnetic ions. **Thus it was tempting to study the influence on them of oxygen doping in** $ZnMnTe:O$.

Table 4: Experimental values of exchange constants.

$N_0\alpha$ (eV)	$N_0\beta$ (eV)	Ref.
0.19	-1.1	[32]
0.20	-1.12	[41]
0.18	-1.05	[38]

Magneto-reflectance: Calculation of exchange integrals

The experimentally observable quantities are not the splittings, but the energy gaps between valence and conduction states, which can be observed through optical effects accompanying electron transitions. The allowed transitions between split valence and conduction band states are shown on Fig. 15. The energies of these transitions (σ_+, σ_- and π) may be derived from equations (12) and are equal [37]:

$$E_a = E_0 + 3B - 3A, \tag{14}$$

$$E_b = E_0 + B + 3A, \tag{15}$$

$$E_c = E_0 - B - 3A, \tag{16}$$

$$E_d = E_0 - 3B + 3A, \tag{17}$$

$$E_e = E_0 + B - 3A, \tag{18}$$

$$E_f = E_0 - B + 3A. \tag{19}$$

Here E_0 is the transition energy in the zero magnetic field.

Two of these equations, which are not linearly dependent, may be used to determine the values of A, B and even the ratio β/α from the energies of inter-band transitions. In this work, the values of A, B were calculated using the method described in [39]. However to determine the exchange integrals α and β one needs to know the values of x and $< S_z >_{Mn}$. These values can be expressed through the measurable value of magnetization, since the volume magnetization $M \sim x < S_z >_{Mn}$, or $M = N_0 x < S_z >_{Mn}$ $g_M n \mu_B$. Here M, μ_B and g_{Mn} are the volume magnetization of the sample, Bohr magneton and the g-factor for manganese ion. Thus:

$$A = -\frac{1}{6}\frac{\alpha M}{g_{Mn}\mu_B},\ B = -\frac{1}{6}\frac{\beta M}{g_{Mn}\mu_B}. \tag{20}$$

In the above consideration an assumption was made that all manganese atoms are separated from each other. However in real samples there are

also small complexes of strongly interacting manganese atoms which also contribute to magnetization. The most numerous are complexes containing two or three manganese atoms. Two-atom complexes are antiferromagnetic and their contribution to magnetization is negligible. The concentration of three-manganese complexes is about 10% of all manganese atoms, at 5% of manganese atoms in the sample [40]. Thus the error introduced by such assumption does not exceed 10%.

Thus to calculate the values of exchange integrals the magnetization of the sample should be also measured in the same conditions of temperature and external magnetic field in which the transition energies were measured.

Measurement of the splitting

In this work the splitting of the conduction and valence bands was investigated by means of free exciton reflectance measurement. On the one hand, the free exciton reflectance is a relatively simple method to measure the splitting. On the other hand, free exciton energy follows the energy of the band gap, and the number of observable free exciton resonances in the spectrum is the same as the number of observable inter-band transitions. Hence the equations (14-19) can be also applied to describe the behavior of free excitons in an external magnetic field[21].

The magneto-reflectance was measured in Faraday configuration (i.e. the wave vector of the reflected light was parallel to the vector of magnetic field induction). In this configuration only σ_+ and σ_- transition are observable. A typical example of measured magneto-reflectance spectra (sample 4479, see Table 2) is presented on Fig. 16. Measurements were performed separately for right-circularly polarized light (σ_+) and left-circularly polarized light (σ_-) in order to distinguish two closely situated and weak free exciton resonances b and c (Fig. 16).

The dependence of the free excitons energies as a function of magnetic field for the same sample is shown on Fig. 17. The measurements were made in magnetic fields ranging between 0 T and 6 T, however the weaker exciton resonances b and c could be distinguished only when the external magnetic field was above 3 T.

The values A and B described above were calculated for each magnetic field when all four exciton resonances were observed.

Calculation of magnetization

The magnetization of the samples as a function of temperature was measured using SQUID magnetometer in magnetic fields of $0.002\ T - 0.004\ T$, and then recalculated to match the conditions of the reflectance measurements according to [39][22]. In a limited range of magnetic field and temperature the magnetization may be described by a phenomenological Brillouin-like function:

[21] With the exception that E_0 here stays for the energy of the free exciton in zero magnetic field.

[22] A more detailed information on magnetization measurements is presented in Chapter 2.7

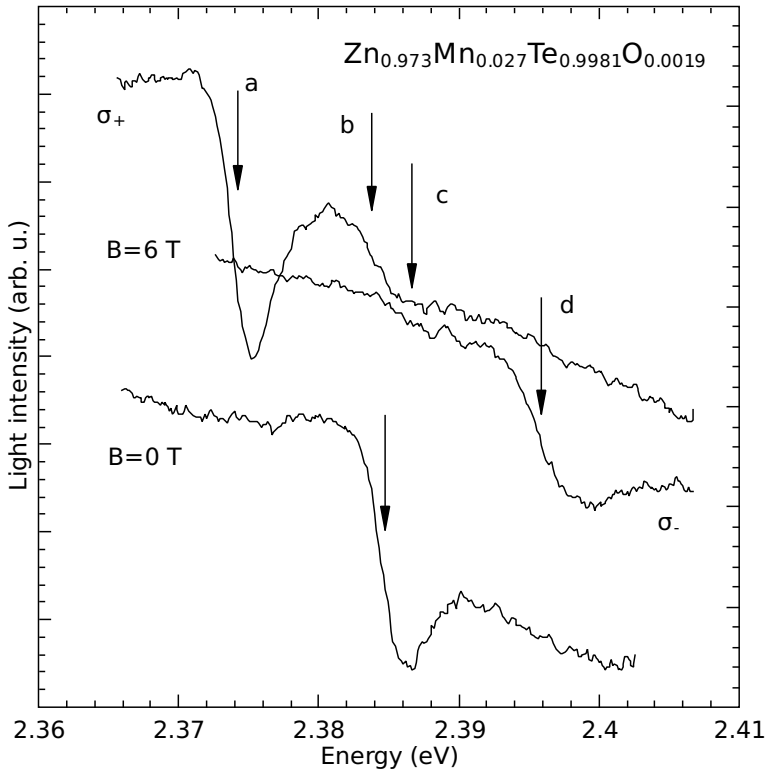

Figure 16: Example of magneto-reflectance spectrum measured on sample 4479B at 5 K, in magnetic field of 6 T in σ^+ and σ^- polarization (two upper curves). The arrows indicate the positions of four exciton resonances. The lower curve represents the reflectance spectrum of the sample measured without external magnetic field.

$$M(T,B) = N_0 x g_{Mn} \mu_B S B_S \left(\frac{S g_{Mn} \mu_B B}{k_B (T + T_0)} \right). \tag{21}$$

Here N_0 is the number of unit cells per unit volume, x is the molar fraction of paramagnetic manganese ions, which contribute to M, g_{Mn} is the g-factor for manganese ion[23], μ_B is Bohr magneton, $S = 5/2$ is the spin of the manganese ion, B_S is the Brillouin function, B is the magnetic induction, k_B is Boltzmann constant, T is the temperature and T_0 is a phenomenological parameter which accounts for weak antiferromagnetic interaction between manganese ions scattered in the crystal matrix.

The experimental points of the $M(T)$ dependence were fitted to equation (21), were x and T_0 were regarded as the fitting parameters. Then, the equation (21) was used to calculate the magnetization at higher magnetic fields which were present during the magneto-reflectance measurement. Finally the calculated magnetization values were used to calculate the exchange integrals from (20). Since a value of exchange integral was obtained for each value of magnetic field, the average value was calculated.

[23] $g_{Mn} = 2.0$ [32].

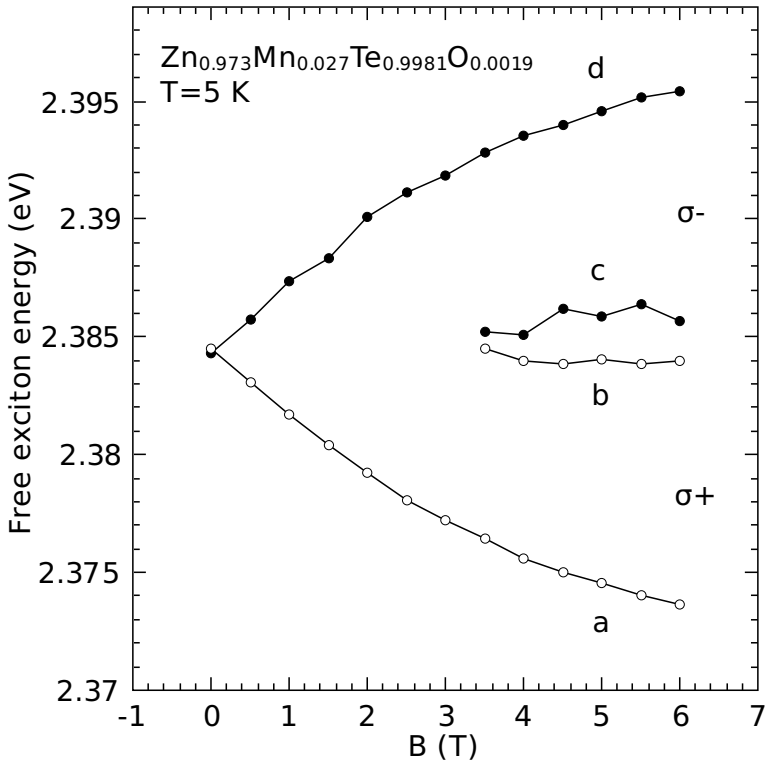

Figure 17: Dependence of the free exciton resonance energies on magnetic field measured at 5 K for sample 4479. Open circles - σ_+ polarization, filled circles - σ_- polarization.

An attempt was made also to measure the magnetization directly. The measurements were performed on a different SQUID magnetometer in an external magnetic field of 5 T. The direct measurement provided greater values of magnetization in comparison with the calculated ones[24]. It is believed that the calculated value provided a better result. Indeed, the discussed samples are polycrystalline with a large amount of inter-grain precipitations (or clusters) containing manganese ions. If the magnetization is measured in low magnetic field, the contribution coming from such precipitations is not observed. If the magnetization is measured in a strong magnetic field, the result contains also the contribution from the magnetized precipitations. Since in equations (13, 20) x stays for content of isolated manganese ions, the magnetization used to calculate the exchange integrals should contain only contribution from paramagnetic ions and not from the clusters with strong interaction between magnetic ions. This is why the magnetization measurements carried out in low magnetic field provide better results.

Additionally a second set of exchange integral values was obtained by a slightly different method. The exchange integral values should be indepen-

[24]As an example the measured magnetization of the sample 4310 at 5 K, 5 T is $M_V = 6.56\ emu/cm^3$, and the value calculated using low-field measurement is $M_V = 6.46\ emu/cm^3$.

Table 5: Summary of magnetization and magneto-reflectance.

Nr.	Sample ID	Single Mn ion content	T_C (K)	$N_0\alpha$ (eV)	$N_0\beta$ (eV)
Set 1					
1	4135	0.030	-2.07	bad	bad
2	4481	0.026	-1.23	0.18	-0.979
3	4463	0.017	-0.70	0.201	-1.098
4	4310	0.011	-0.77	0.155	-0.831
5	4462	0.013	-1.04	0.188	-0.986
6	4479	0.009	-0.30	0.207	-0.955
7	4480	0.007	-0.55	0.118	-0.634
Set 2					
8	4487	-	-	-	-
9	4488	0.010	-0.74	0.205	-1.010
10	4489	0.020	-1.70	0.202	-1.208
Set 3					
11	4506	0.022	-1.90	bad	bad
12	4436	0.021	-1.0	0.141	-0.803
13	4169C21	0.025	-2.2	0.165	-0.985

dent of magnetic field. However generally there is a variation of α and β with magnetic field in the results obtained by the first method (described above). In order to eliminate such variation an additional procedure was applied. Namely, the value T_0 was regarded as a fitting parameter, and varied in a such way, as to obtain a flat dependence $\alpha(B)$ and $\beta(B)$. It was found that the sum of standard deviations of parameters α and β has a minimum at some value T_0^{min}. This value T_0^{min}, which is close to T_0 obtained from magnetization measurements, was used to calculate the exchange integrals in the second (modified) method.

The discussed values of α and β obtained by the modified method, as well as values of x, are summarized in Table 5.

Magneto-reflectance: Results and discussion

A comparison of exchange integral values calculated by both methods is shown on Fig. 18. The values calculated by the first method are shown on Fig. 18a and the values calculated by the modified method are shown on Fig. 18b.

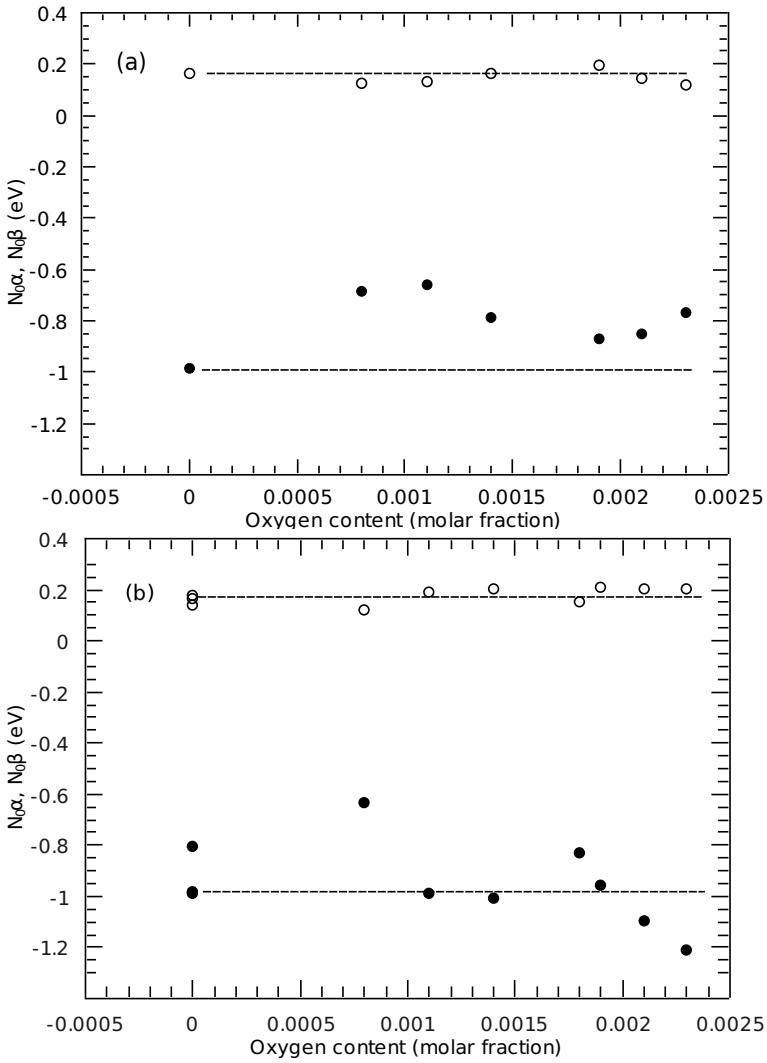

Figure 18: Dependence of the exchange integrals $N_0\alpha$ (open circles) and $N_0\beta$ (filled circles) on oxygen content in $ZnMnTe : O$. (a) Values calculated by method described in [39], (b) values calculated by modified method.

Both methods provide very similar results for $N_0\alpha$ (open circles). There is not any trend in the $N_0\alpha$ dependence on oxygen content. A trend might be expected since the oxygen was shown to influence the conduction band structure due to band anticrossing effect. The lack of a trend may be explained by both, relatively small oxygen content in the samples and large spread of the calculated values, caused by experimental errors.

On the other hand these two methods give different results for $N_0\beta$. In the first method the absolute value of $N_0\beta$ becomes smaller in oxygen

doped samples (Fig. 18a). In the second method $N_0\beta$ remains relatively unchanged and does not depend on oxygen content(Fig. 18a). Since the second method was shown to be more sensible, it is reasonable to conclude that $N_0\beta$ does not depend on oxygen content, or the dependence is very weak. A more careful conclusion would be that the absolute value of $N_0\beta$ does not increase with oxygen content. The influence of oxygen impurity on $N_0\beta$ is also expected, since the wave functions of the valence band are composed mainly of the wave functions of tellurium atoms and the substitutional oxygen atoms.

The large spread of calculated values, and especially of $N_0\beta$, originates mostly from the magneto-reflectance measurement. The largest source of the experimental error are the energies of the "b" and "c" resonances in the magneto-reflectance spectra (see Fig. 16). The intensity of this resonances is three times smaller [37] than the intensity of the components "a" and "b". The splitting of the components "b" and "c" is small and comparable with experimental error (see Fig. 16). Very often the "b" and "c" branches of the free exciton resonances spectra are not symmetrically positioned with respect to the zero-field free exciton line. Since the theory of the giant band splitting in $ZnMnTe$ assumes that the splitting is symmetrical with respect to the zero-field free exciton line, the lack of symmetry in experimental data is also a source of errors.

Magneto-reflectance: Comparison with reported data

The data on exchange constants in $ZnMnTeO$ is not available. However one could take as the reference points the values of exchange constants measured in $ZnMnTe$ and $ZnMnO$. The values of the exchange integrals in $ZnMnTe$ are presented in Table 4. As for the $ZnMnO$, the matter is still being studied and the results are not as conclusive as for $ZnMnTe$.

The configuration-interaction calculations on a MnO_4 cluster model provided p-d exchange constant ($N_0\beta$) of $-2.7\ eV$ [42]. A very close result was reported in [43], where the value $N_0\beta = -3\ eV$ was obtained from x-ray absorption spectroscopy combined with the analysis based on the same configuration-interaction cluster model. A much smaller value ($N_0\beta \approx -0.3\ eV$)[25] was reported in [44]. The value was obtained from the analysis of the magneto-photoluminescence of the neutral-acceptor-bound exciton. Authors suggest that the relatively small value of exchange integral is related with the fact that the carriers are bound, and that it might be larger for free carriers. As another estimation may serve an empirical dependence reported in [45]. According to this dependence, the exchange energy $N_0\beta$ is inversely proportional to the lattice parameter of the crystal, and for $ZnMnO$ $N_0\beta$ should be larger then $2\ eV$. Thus one should expect that the exchange energy $N_0\beta$ of the alloy $ZnMnTeO$ should increase with increasing oxygen content.

The other exchange integral $N_0\alpha$ is considered to be almost independent on both the type of transition metal ion and the host matrix [47, 46]. In all

[25]Reported value $N_0(\alpha - \beta) = -0.1\ eV$. $N_0\alpha$ considered to be approximately $0.2\ eV$.

investigated semimagnetic alloys its value varies somewhere between 2.0 eV and 2.5 eV.

Summary: Magneto-reflectance

- Magneto-reflectance was used to study the evolution of exchange interaction constants (α and β) with oxygen content in $ZnMnTe:O$.
- Because of experimental errors, the studied evolution could not be determined reliably.
- Two methods were used to obtain the values of exchange integrals, which provided slightly different results for $p-d$ exchange integral.
- It is safe to conclude that the $s-d$ exchange integral α remains constant with oxygen concentration and the $p-d$ exchange integral β does not increase in the studied interval of oxygen composition ($< 0.25\%$).

2.6.3 Photoluminescence

The study of photoluminescence (PL) in $ZnMnTe:O$ was not systematic. The PL measurements were performed only on several samples as a function of temperature and magnetic field. However, here will be presented some results typical for the measured samples. The results were published in [27, 49].

The PL spectrum of $ZnMnTe:O$ samples will be conventionally divided into two parts, the near-band-edge emission and long-wavelength emission. The near-band-edge PL spectrum of $ZnMnTe:O$ resembles closely the PL spectrum of ZnMnTe and consist usually of bound exciton line and donor-acceptor pairs line, accompanied by a number of phonon replicas (Fig. 19). However the long-wavelength spectra of $ZnMnTe:O$ samples are completely different from those of $ZnMnTe$ as well as those of $ZnTe:O$. The wide line centered at 1.65 eV (Fig. 19) was not observed neither in $ZnMnTe$ no in $ZnTe:O$ samples.

For comparison the long-wavelength spectra of $ZnMnTe$, $ZnTe:O$ and $ZnMnTe:O$ are presented on Fig. 20. In $ZnMnTe$ there is a PL band located at 1.96 eV, assigned to intra-manganese-ion transitions [48]. In $ZnTe:O$ there is also a wide PL band located at about 1.82 eV. This band is attributed to emission of the localized exciton bound to oxygen impurity and its numerous phonon replicas. The origin of this band was discussed in detail in Chapter 2.1.

In $ZnMnTe:O$ both these lines are barely visible or not visible at all. For example, weak manganese-related band is visible on the high-energy side of the wide band on Fig. 19.

The band centered at 1.65 eV is observed only in samples simultaneously doped with manganese and oxygen. Since this band is the unique

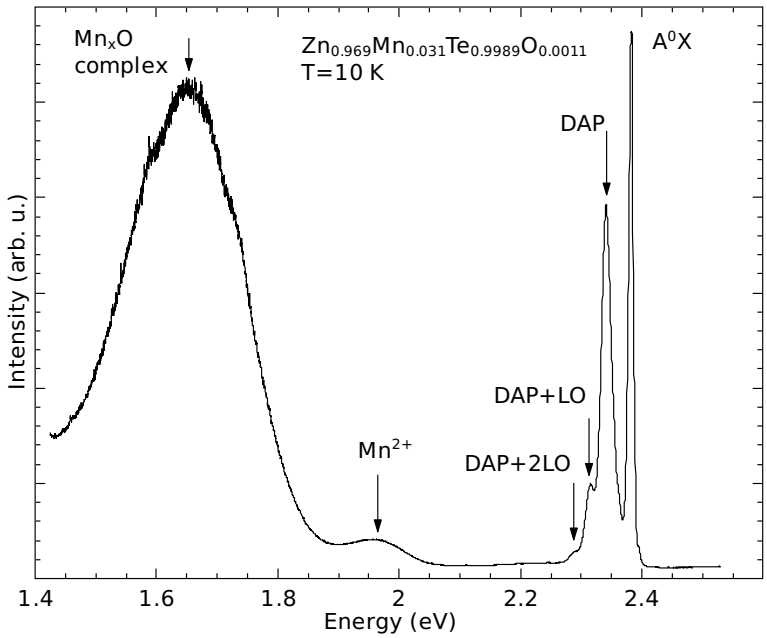

Figure 19: Photoluminescence spectrum of the $ZnMnTe : O$ sample 4462 measured at 10 K.

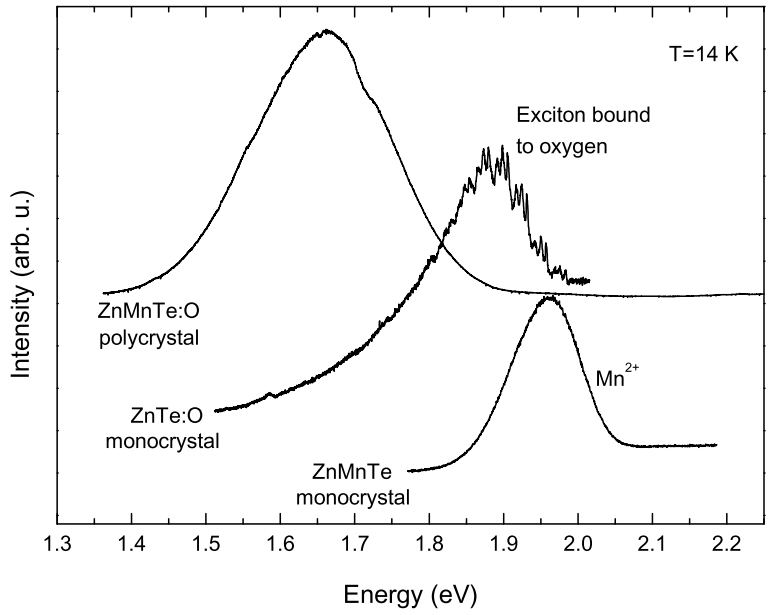

Figure 20: Comparison of the long-wavelength spectra of $ZnMnTe$, $ZnTe : O$ and $ZnMnTe : O$, measured at 14 K.

feature of the $ZnMnTe : O$ samples, only this band will be discussed further.

Because the band at 1.65 eV appears only in samples doped with both manganese and oxygen, it is a fair guess that the centers (microscopic complexes or macroscopic precipitation) responsible for this photoluminescence consist of oxygen and manganese. This conclusion supports another

conclusion made in chapter 2.4, that the oxygen atoms dissolved in the host lattice tend to locate in the vicinity of a manganese atom or several manganese atoms.

Since the samples are polycrystalline with a large number of precipitations between the grains, a question may arise, whether the emission comes from crystal blocks or the inter-grain region. The direct observation shows that the discussed red emission comes from entire sample surface. Thus the emission centers are located inside crystal blocks of $ZnMnTe:O$. Probably the micro-photoluminscence study would provide more information on this subject.

The shape of the band at 1.65 eV suggests that it is formed of a number of narrower bands. The same conclusion may be drawn from the temperature evolution of the band (Fig. 21a). With increasing temperature the band changes its shape and the maximum of the band shifts towards higher energies. Such behavior indicates on the nature of optical transitions producing the emission. The shift toward higher energies means that the transition takes place between two localized states of the same recombination center, and does not involve bands energy states. When the transition involves one of the band (conduction or valence band) the energy of emission decreases with temperature because of both, the decrease of the band gap and the activation of the trapped carriers back into the band states[26]. Thus the discussed PL emission is attributed to emission centers with chemical structure Mn_nO.

The dependence of the intensity of the PL on the temperature for two PL bands centered at 1.65 eV and 1.96 eV is presented on the Fig. 21b. The emission at 1.96 eV, which is attributed to internal transitions of isolated Mn^{2+}-ions, and the emission at 1.65 eV behave differently. The former band decreases and completely disappears[27] at about 47 K, and the latter first increases, passes through a maximum and then slowly decreases.

One of the possible hypotheses [27] is that the band at 1.65 eV has bound-excitonic nature, similar to that in $ZnTe:O$. The deconvolution of the band under consideration provides several bands, the strongest of which are centered at 1.88 eV and 1.73 eV. The oxygen-bound excitons band in $ZnTe:O$ is located at about 1.82 eV (see page 18). This would imply that the Mn_nO complexes form deeper traps then simple substitutional O_{Te} defect. The hypothesis that simultaneous doping with oxygen and manganese should change the binding energy of the oxygen related trap in $ZnMnTe:O$ is supported by *ab initio* calculations [3] of the oxygen trap in $II-VI$ compounds. The authors demonstrated that the energy level of the oxygen trap is strongly influenced by the nearest neighbor cation atoms. Thus when manganese atoms substitute zinc atoms in the first

[26]The charge carriers on the localized states which are located closer to a band, are being activated first. And thus deeper centers with longer PL wavelengths have a greater contribution

[27]This fact will be of some importance in chapter 2.7, were the magnetization measurements will be discussed.

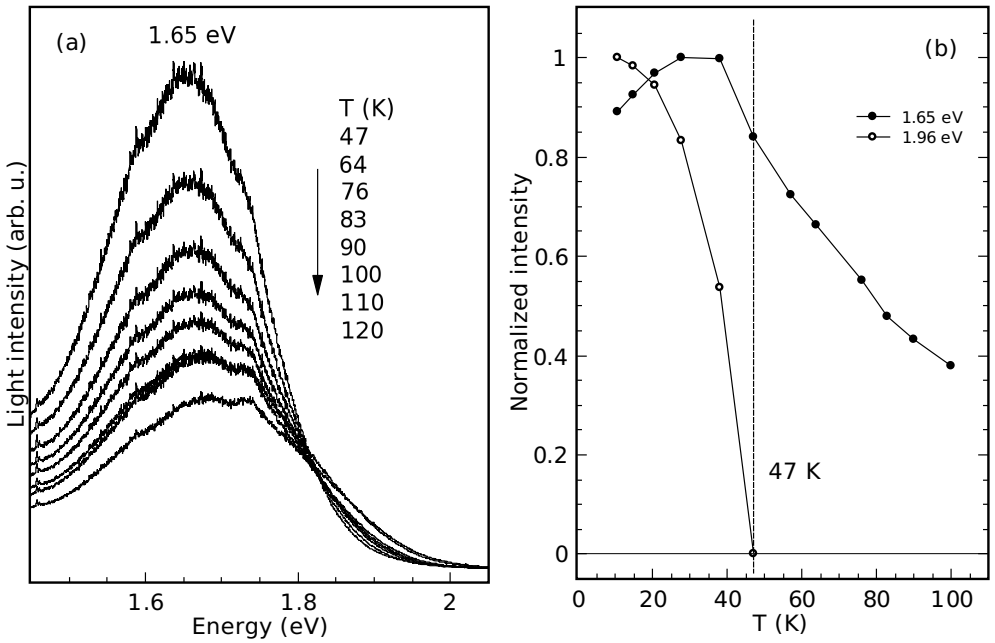

Figure 21: (a) Evolution of the photoluminescence band at 1.65 eV with temperature (sample 4462). (b) Variation of the PL intensity with temperature for two bands centered at 1.65 eV (filled circles) and at 1.96 eV (open circles).

coordination sphere around the substitutional oxygen, the depth of the electron trap can change. Different number of manganese atoms in the nearest neighbor positions would account then for the different sub-bands obtained by deconvolution of the wide band at 1.65 eV.

Photoluminescence: Comparison with MnO

A very similar band (1.66 eV) was reported [50] for MnO crystals. To illustrate the striking similarity between the band at 1.65 eV in $ZnMnTe:O$ and the band reported for MnO, the normalized curves for both spectra are presented on Fig. 22. Although the compared materials have different crystallographic structure[28] and band structure, their red-luminescence bands have similar position and shape. There are two bands in MnO, which are centered at 1.25 eV and 1.66 eV. On the left hand side of the $ZnMnTe:O$ spectrum there is a rising, which suggests that there might be the a second band in $ZnMnTe:O$ also. However, the measurements of the PL in $ZnMnTe:O$ in the range around 1.25 eV have not been carried out.

According to [50] the line at 1.66 eV persists only below 118 K (below the Néel temperature). Above 118 K remains only the line centered at 1.25 eV. Authors attribute both lines to internal transitions between perturbed Mn^{2+} states, assisted by creation/destruction of magnons or short-wavelength collective magnetic excitations. The band centered at

[28] MnO has a $NaCl$ type crystal structure at room temperature, and rhombohedral below 118 K [50]

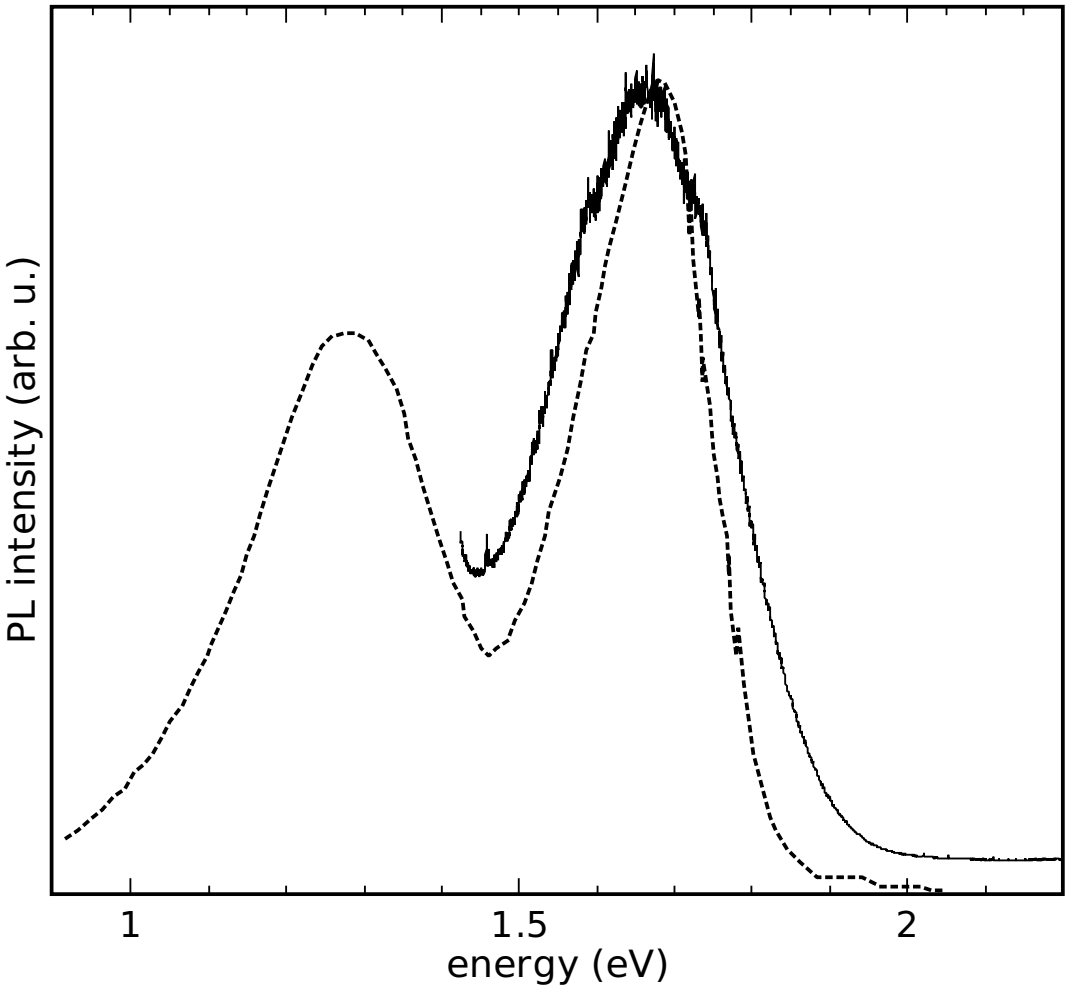

Figure 22: Comparison of the normalized photoluminescence spectra of the $ZnMnTe : O$ (solid line, sample 4463) and MnO (dashed line, digitized from [50]) measured at 77 K.

1.25 eV which remains above antiferromagnetic transition temperature is attributed to Mn_3O_4 perturbed Mn_{2+} states, i.e. to Mn_3O_4 clusters which easily form on the surface of MnO. The other band, centered at 1.66 eV is attributed to Mn_{2+} states in the MnO lattice perturbed by some other (unknown) impurities[29].

If the similarity of those two bands (1.65 eV and 1.66 eV) is not accidental, this observation may also suggest the presence of a large number of small MnO precipitations. The point defects in $ZnMnTe$ with properties similar to those in MnO is difficult to imagine. The symmetry of the first configuration sphere in MnO is octahedral and in $ZnMnTe$ it

[29]The energy of the intra-Mn^{2+} emission in $ZnMnTe$ is less then that of a free atom, because of the tetrahedral crystal field surrounding the manganese ion [35]. Presence of an impurity in the immediate vicinity with the manganese ion will perturb the symmetry and the strength of the crystal field, an thus will change the energy of the internal transition.

is tetrahedral. The only possibility for manganese to form a point defect with octahedral symmetry in $ZnMnTe$ is to be placed in interstices (for example in the center of the unit cell). In such configuration the crystal field around the manganese ion will be similar with that of MnO. Since the atomic radius of oxygen is much smaller than that of tellurium, there is more space in the interstitials surrounding substitutional oxygen O_{Te}, then in the interstitial surrounding tellurium atom.

Summary: Photoluminescence

- A wide band centered at 1.65 eV is observed in the PL spectrum of $ZnMnTe:O$.
- The band appears only in $ZnMnTe:O$ and it was not observed neither in $ZnMnTe$ no in $ZnTe:O$.
- Possible interpretation of the band: exciton bound to Mn_nO complex defect.
- A similar band (1.66 eV) was reported for MnO. Hence it is possible that the band at 1.65 eV in $ZnMnTe:O$ is related with MnO precipitations or interstitial Mn complex defect.
- Temperature dependence of the photoluminescence intensity suggest that some critical phenomenon takes place at about 47 K.

2.6.4 Magneto-photoluminescence

Photoluminescence: Band at 1.65 eV

The magneto-photoluminescence was measured for a limited number of samples, in Faraday configuration, in magnetic fields up to 6 T. The band centered at 1.65 eV in $ZnMnTe:O$ was found to be insensitive to magnetic field. Both the position and intensity of the peak remain constant with magnetic field. There is no difference between spectra measured in σ^+ and σ^- polarization.

The fact that the position of the discussed band does not depend on magnetic field confirms the hypothesis that the emission is produced as a result of internal transitions inside of an emission center. If the initial or final state of the transition would involve band states, the energy position of the band should change, because of the giant band splitting in $ZnMnTe$. The same behavior was observed for manganese-related band at 1.95 eV in $ZnMnTe$.

Photoluminescence: Near-band-edge emission

The near-band-edge emission as well as the band structure of the $ZnMnTe:O$ are sensitive to magnetic field. However the shift of the position of the PL lines (as well as the splitting of the energy states responsible for this emission) is much smaller than the shifts of the conduction and valence bands. As an example the evolution of the bound exciton PL line with

magnetic field (sample 4310) is presented on Fig. 23. The position of the maximum as a function of magnetic field is shown on Fig. 24. The spectra were measured for two circular polarizations, σ^+ and σ^-.

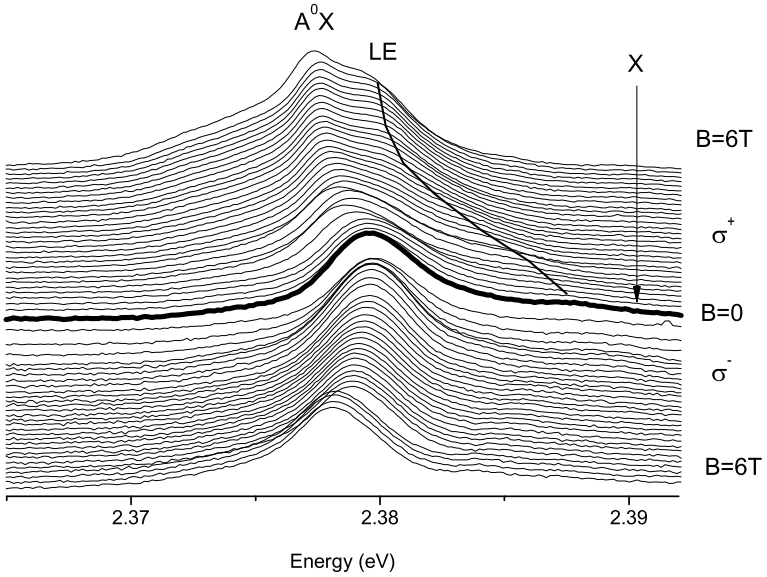

Figure 23: Evolution of the bound exciton PL spectrum of the $ZnMnTe : O$ (sample 4310) with magnetic field measured in σ^+ and σ^- polarization at 1.8 K. Thick spectrum line marks the zero-field spectrum. The thick line, marked as LE, indicates approximately the evolution of disorder localized excitons line with magnetic field. The arrow shows the position of the free exciton at zero field.

As a reference the dependence of the lowest free exciton branch on magnetic field, measured by magneto-reflectance, is presented on Fig. 24. Both, the shift of the bound exciton emission lines with magnetic field and the separation between emission lines with different polarization is much smaller then the shifts and splittings of the extended band states. At magnetic fields stronger then 1.5 T the energy of the PL appears to have higher energy then the energy band gap of the material. On the Fig. 23 there is also another line (marked as LE) which is situated on the right-hand side of the bound exciton PL line (marked as A^0X). This PL line has a stronger dependence on magnetic field, and at zero field its maximum is located only 3 meV below the free exciton energy (marked as X). Taking into account its high energy and strong dependence on magnetic field, this line is attributed to disorder localized excitons.

These phenomena are not characteristic for $ZnMnTe : O$ only. A similar behavior may be observed in $ZnMnTe$.

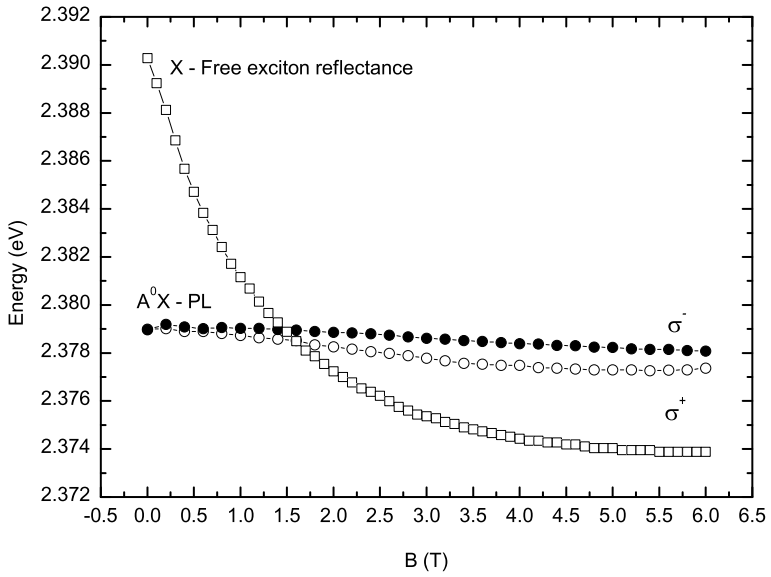

Figure 24: Dependence of the position of the bound exciton (marked as A^0X) PL line on magnetic field measured in σ^+ and σ^- polarization (circles). Dependence of the free exciton position (marked as X) on magnetic field measured in reflectance in σ^+ polarization (squares). Open and filled symbols correspond to σ^+ and σ^- polarization respectively. Measured at 1.8 K.

2.7 Magnetic properties

The magnetization was measured in order to (i) determine the exchange constants in $ZnMnTe:O$ and (ii) study the influence of oxygen doping on magnetic properties of $ZnMnTe$. Most of the measurements were performed on a SQUID magnetometer in a relatively low magnetic field of $200 - 400$ Oe and in the temperature range between 5 K and 200 K in field cooling (FC) and zero field cooling (ZFC) conditions.

Magnetic properties: Zero field cooling

All measured samples are paramagnetic with an admixture of a weak ferromagnetic magnetization. The ferromagnetic magnetization was observed at higher temperatures as a weak background signal.

In order to separate paramagnetic and ferromagnetic signal the dependence of the magnetic susceptibility on temperature was fitted to equation,

$$\chi = \chi_0 + \frac{C}{T - T_C}, \tag{22}$$

where the first term represents the constant ferromagnetic background and the second term is the Curie-Weiss expression, which represents the paramagnetic signal, dependent on temperature. Here χ_0, C and T_C were considered as fitting parameters. The value of the ferromagnetic background signal (χ_0) varies for different samples between $0.5 \cdot 10^{-6}$ emu/g and $7.2 \cdot 10^{-6}$ emu/g. After fitting, the obtained value of χ_0 was subtracted

from the measured susceptibility value in order to obtain the paramagnetic part of the susceptibility.

The validity of such procedure is based on the assumption that χ_0 does not depend (or depends weakly) on temperature. To test this assumption one may plot the calculated paramagnetic susceptibility ($\chi_{para} \equiv \chi - \chi_0$) in the coordinate frame $1/\chi_{para}$ vs. T. If the assumption is correct, the dependence $1/\chi_{para}(T)$ should be linear. An example of the $\chi(T)$ and $1/\chi_{para}(T)$ for sample 4479 is presented on Figure 25.

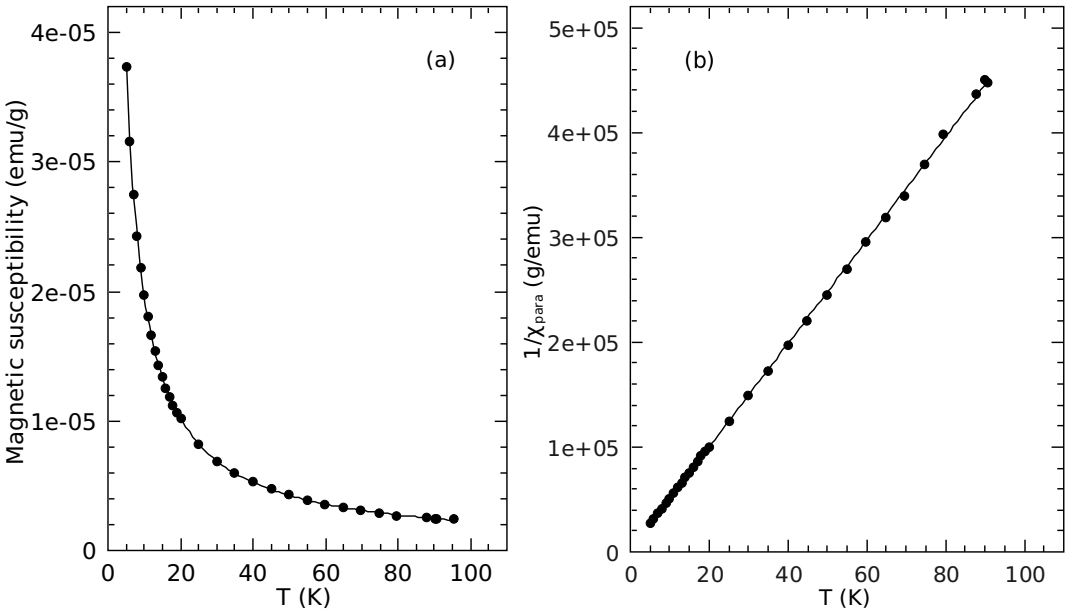

Figure 25: (a) The dependence of the magnetic susceptibility on temperature for sample 4479, measured at 200 Oe. Solid line was obtained by fitting to equation (22). (b) Inverse paramagnetic susceptibility (χ_{para}) as a function of temperature. Solid line reperesents the linear fit of the experimental data.

The dependence of the χ_{para} on temperature was used to determine the concentration of isolated (paramagnetic) manganese atoms (x) and calculate the values of exchange integral, as it was discussed in Chapter 2.6.2. The expression for mass susceptibility was derived from the expression of volume magnetization (21), using equation,

$$\chi_m = \frac{M_V}{\rho H}, \tag{23}$$

where ρ is the material density, M_V is volume magnetization and H is the magnetic field. Since the inverse susceptibility was shown to be linear with temperature the Brillouin function in (21) may be approximated with the first term of its power series. After simple transformations one obtains,

$$\chi_m = \frac{g^2\mu_B^2 S(S+1)x}{3k_B m_c(T-T_C)}, \; or \; \frac{1}{\chi_m} = \frac{3k_B m_c(T-T_C)}{g^2\mu_B^2 S(S+1)x}. \tag{24}$$

Here x is the molar fraction of paramagnetic manganese ions, which contribute to χ_m, g_{Mn} is the g-factor for manganese ion, μ_B is Bohr magneton, $S = 5/2$ is the spin of the manganese ion, k_B is Boltzmann constant, T is the temperature, T_C is Curie temperature and m_c is the mass of the unit cell. Strictly speaking m_c depends on x. However, since concentration of manganese is small and the difference between the atomic masses of manganese and zinc is small, the dependence $m_c(x)$ may be neglected.

In equation (24) parameters x and T_C are unknown. Thus by fitting the experimental data to equation (24) those parameters were obtained. The results are summarized in Table 5.

The negative value of T_C indicates on weak antiferromagnetic interaction between isolated manganese ions[30]. In this respect the situation is very similar with that of $ZnMnTe$. The absolute value of T_C increases linearly with increasing manganese content. The experimental dependence of T_C on manganese content (x) is shown on Fig. 26. As a result of the linear fit of experimental data, a dependence $T_C = -72 \cdot x$ was obtained.

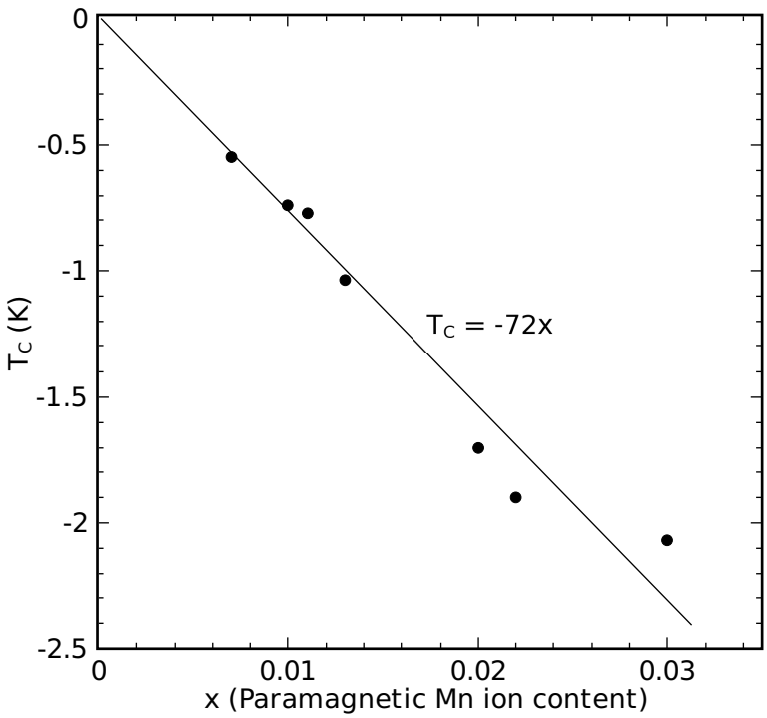

Figure 26: Dependence of the T_C value on isolated manganese-ion content in $ZnMnTe:O$. The dependence $T_C = -72 \cdot x$ was obtained by linear fit of the experimental data.

Such correlation between the T_C and manganese content can be easily explained. When the manganese concentration increases, decreases the average distance between manganese ions, and hence increases the strength of long range antiferromagnetic interaction.

[30]However, since the measurements were carried out above 5 K, the actual antiferromagnetic transition was not achieved.

No correlation between the T_C and oxygen concentration was found. Although oxygen doping might have some influence on manganese-manganese interaction, in this case the concentration of oxygen was at least ten times smaller then the concentration of manganese, and such influence could not be observed.

Magnetic properties: Field cooling

There is a difference between the magnetization measured in field cooling and zero field cooling conditions. The ZFC measurements were carried out as follows: first, the sample was cooled down to 5 K without the external magnetic field, then the field was turned on and the measurements were performed while the sample was warmed up. On the contrary, during the FC measurements the sample was heated up above 150 K, then the magnetic field was turned on and the measurements were performed while the sample was cooled down.

An example of ZFC and FC magnetic susceptibility as a function of temperature for samples 4462 and 4506 is shown on Fig. 27(a, c). As it is the case on the Fig. 27(a, c), in all measured $ZnMnTe:O$ samples under field cooling conditions an additional magnetic susceptibility (magnetization) appears below certain critical temperature. To separate this additional susceptibility from paramagnetic susceptibility signal, the difference between FC and ZFC magnetic susceptibility ($\Delta\chi \equiv \chi_{(FC)} - \chi_{(ZFC)}$) was calculated. As an example two $\Delta\chi(T)$ curves for samples 4462 and 4506 are presented on Fig. 27(b, d). The temperature dependence of $\Delta\chi$ resembles a $\chi(T)$ dependence of a material with ferromagnetic phase transition. The absence of such additional susceptibility during ZFC measurement means that the magnetic moments, responsible for the phenomenon are frozen. For example, changing of the direction of the magnetic field after cooling to opposite, does not change the sign of the additional magnetization. External fields up to 1 kOe do not influence this additional magnetization. It is manifested, for example, in a simple shift of the $M(H)$ curve, measured at FC conditions by an amount of the additional magnetization ($\Delta\chi H$) with respect to $M(H)$ curve measured at ZFC conditions[31].

The difference between FC and ZFC magnetization is a characteristic feature of the spin glass or superparamagnet state [51, 52]. However, in a spin glass material the ZFC magnetization has a distinguishable maximum which appears due to gradual release of the frozen magnetic moments with increasing temperature [51]. In $ZnMnTe:O$ samples the ZFC magnetization does not have such feature and looks like a simple paramagnetic.

Thus, it is concluded that the difference between FC and ZFC magnetization is not related with the spin glass state. It is related rather with the

[31] The $M(H)$ curve has a very narrow hysteresis loop, with remanence comparable with the background magnetization, observed in M(T) measurements. Thus, there are two different sources of ferromagnetic signal: (i) one with small coercivity, which is responsible for the weak hysteresis loop and background signal in M(T) measurement, and (ii) another with high coercivity, which produces additional magnetization in FC M(T) measurements and shifts vertically the hysteresis loop.

presence of small (possibly single domain) ferromagnetic precipitations (or clusters) with strong coercivity. The location of the discussed ferromagnetic precipitations inside the crystal is not clear. They might be located between the crystalline grains as well as inside them.

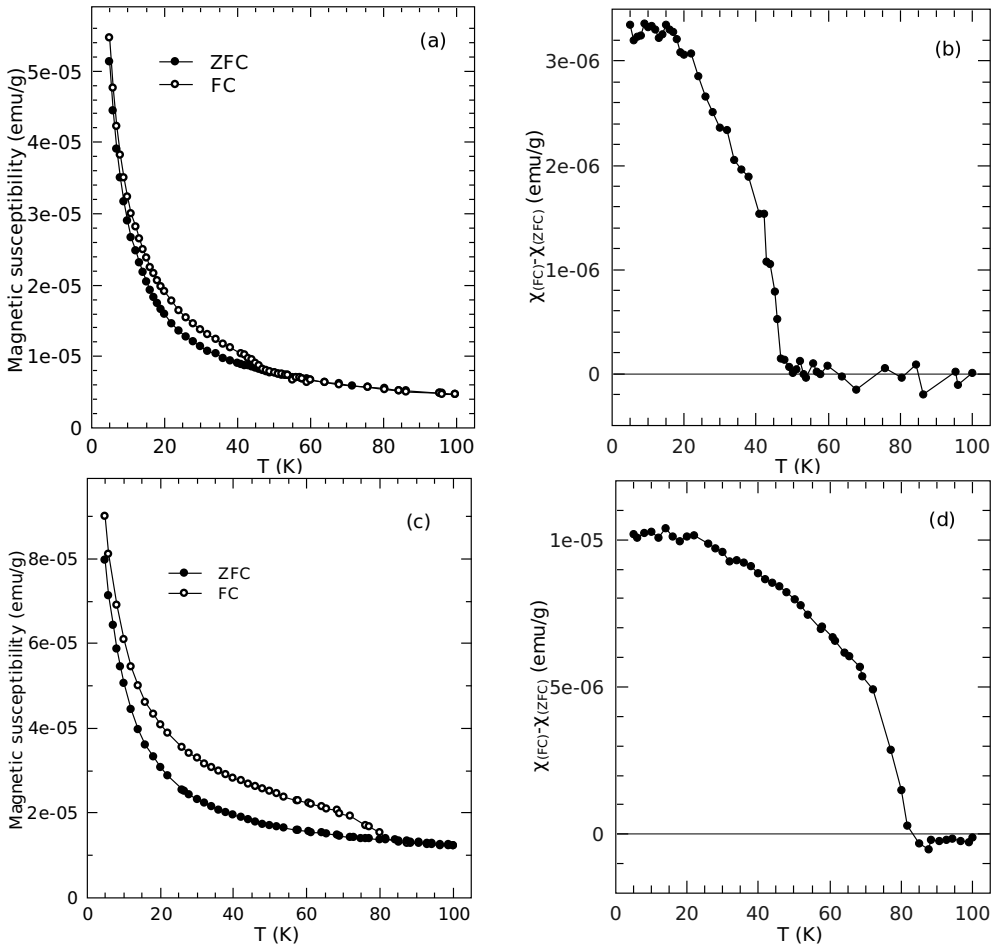

Figure 27: Comparison of the field cooling and zero field cooling susceptibility for sample 4462 (a) and 4506 (c). Open symbols - field cooling, filled symbols - zero field cooling. (b, d) difference between field cooling and zero field cooling susceptibility for samples 4462 and 4506 respectively.

The critical temperature at which the additional magnetization appears in FC measurement, depends on sample, and usually varies between 45 K and 50 K. However critical temperatures of $\sim$ 38 K and 80 K were also observed. Values of critical temperature for all samples are summarized in Table 6. The majority of the samples have critical temperatures around 46 K. Oxygen concentration in those samples is usually below 0.2 $at.\%$. However sample 4506 has a much higher critical temperature of 80 K, and also a higher oxygen concentration (0.56 $at.\%$). It was demonstrated that the increase of critical temperature with oxygen concentration is related with appearance of a new kind of precipitations. Indeed in a sample with intermediate level of oxygen doping, two critical temperatures can be ob-

served simultaneously. As an example the dependence of the magnetic susceptibility on temperature for sample 4697[32] is presented on Figure 28. Here two critical temperatures at about 48 K and 84 K can be distinguished.

Magnetic properties: comparison with photoluminescence

There are some correlations between the results of magnetic properties and photoluminescence measurements. As an example let us consider the temperature dependence of photoluminescence of the sample 4462 presented on page 47. The dependence of the PL intensity on temperature for two PL bands centered at 1.65 eV and 1.96 eV is presented on the Fig. 21b. One can see that the PL intensity is subjected to strong transformations around the critical temperature[33]. The band centered at 1.65 eV, which is attributed to PL from emission centers with Mn_nO structure[34], passes through a maximum and then starts to decrease in the vicinity of the critical temperature. The band centered at 1.96 eV, which is attributed to internal manganese ion transitions, decreases and disappears above the critical temperature.

These magnetic and PL phenomena are related with different objects inside the crystal, and apparently have nothing in common. PL at 1.96 eV is attributed to paramagnetic Mn^{2+} ions, and is observed also in $ZnMnTe$. Whereas additional FC magnetization is attributed to some manganese-reach precipitations and is observed only in $ZnMnTe:O$ samples. Thus there is no direct dependence between these two phenomena.

The correlation may be explained then by some third factor, which has an impact on both phenomena, like, for example, the position of the Fermi energy (or free carriers concentration). The position of the Fermi energy indeed has an impact on the intensity of the emission from Mn^{2+} ions. Such dependence may be described as follows. It is believed that the Mn^{2+} ions in $ZnMnTe$ are excited by an energy transfer process from free excitons to manganese ions [57]. With increasing temperature increases also the concentration of free carriers (the position of the Fermi energy changes) and simultaneously increases the screening of free excitons by the free carriers. The screening of the free excitons by the free carriers is the main reason of free exciton annihilation and thus it is also the reason of the decrease of Mn^{2+} emission.

The influence of the free carrier concentration (Fermi energy) on the ferromagnetic transition in manganese-reach precipitations is not understood. However it could account for the variation of the critical temperature for different samples. As it was mentioned above the critical temperature is not constant and changes from one sample to another. The correlation may also suggest that aggregates that are responsible for the discussed ferromagnetic signal are located inside the $ZnMnTe:O$ crystal grains.

[32]Sample 4697 is not presented in Table 3 since it was not fully investigated. In sample 4697 the nominal manganese and oxygen content was 0.10 and 0.03 respectively.

[33]Which is 47 K for sample 4462, see Table 6

[34]See chapter 2.6.3

Magnetic properties: comparison with manganese oxide

Manganese forms a number of oxides. The most stable solid state oxides are MnO, Mn_2O_3 and Mn_3O_4. MnO is antiferromagnetic with Néel temperature of 118 K. Mn_3O_4 is paramagnetic at room temperature but becomes ferrimagnetic below $41 - 43$ K [54, 55], although the transition temperature was reported to be reduced in nano-crystalline samples to around 39 K [56]. Mn_2O_3 (one of its forms $\gamma - Mn_2O_3$) is ferrimagnetic below 39 K [53].

In discussed $ZnMnTe : O$ samples the critical temperature is slightly higher and varies from sample to sample (see Table 6). Currently the structure of ferromagnetic aggregates and the variation of the critical temperature with sample composition is not understood. Two mechanisms responsible for the variation of the critical temperature may be proposed. (i) First mechanism was already discussed earlier. It is based on the assumption that the critical temperature depends on the free carrier concentration and hence the critical temperature varies for different samples. (ii) Second mechanism may be related with the size of the ferromagnetic precipitations. There are reports demonstrating that in nanoscale ferromagnetic particles the temperature of ferromagnetic phase transition depends on the size of the particles [58, 59].

While critical temperatures with values around $45 - 50$ K still can be explained by appearance of some Mn_3O_4-like aggregates, the critical temperature with values around 80 K cannot be explained by manganese oxide precipitations. Such high critical temperatures were observed only in two samples, having the highest oxygen content. It is possible that the aggregates having such critical temperature include silicon. The silicon gets into the crystal from the walls of the silica ampules. Traces of the silicon were observed in both X-ray diffraction and micro-EDX analysis. The most known compound containing manganese and silicon is probably the manganese silicate (Mn_2SiO_4) or $(ZnMn)_2SiO_4$. However it is antiferromagnetic [60] and cannot account for the observed effects.

Summary: Magnetization

- Both, paramagnetic and ferromagnetic signal were observed in $ZnMnTe : O$.
- Paramagnetic signal is similar to that of $ZnMnTe$. No correlation between antiferromagnetic T_C and oxygen content was observed. The absolute value of T_C linearly increases with manganese content according to $T_C = -72 \cdot x$.
- The ferromagnetic signal is produced by some precipitations located between or inside the $ZnMnTe : O$ crystallites.
- A weak background signal is produced by precipitations which are in ferromagnetic state inside the entire measured interval (5 K-150 K).

Table 6: Summary of FC and ZFC magnetization.

Nr.	Sample ID	Measured Mn frac. (x)	Estimated O frac.(y)	Critical temperature (K)	FM ion concentration (cm^{-3})
Set 1					
1	4135	0.051	0	-	$5.3 \cdot 10^{15}$
2	4481	0.041	0	-	$1.2 \cdot 10^{16}$
3	4463	0.047	0.0021	46	$4.1 \cdot 10^{16}$
4	4310	0.040	0.0018	46	$2.3 \cdot 10^{16}$
5	4462	0.031	0.0011	47	$7.9 \cdot 10^{16}$
6	4479	0.027	0.0019	47	$6.7 \cdot 10^{16}$
7	4480	0.016	0.0008	45	$1.7 \cdot 10^{16}$
Set 2					
8	4487	<0.001	<0.0001	-	-
9	4488	0.025	0.0014	46	$4.4 \cdot 10^{16}$
10	4489	0.056	0.0023	50	$2.3 \cdot 10^{17}$
Set 3					
11	4506	0.187	0.005	80	$4.9 \cdot 10^{17}$
12	4436	0.025	0	$\sim$38	$5.3 \cdot 10^{16}$

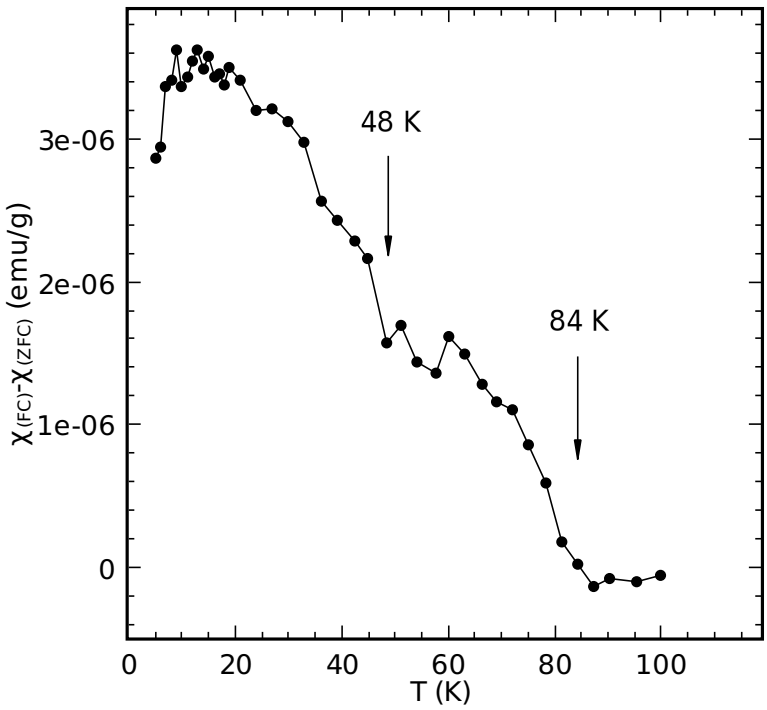

Figure 28: Difference of magnetic susceptibility measured in field cooling and zero field cooling conditions, at 200 Oe for sample 4697.

- Other precipitations are observed only during FC measurement, and appear as a step on $M(T)$ dependence. Such steps of additional magnetization appear at two different (critical) temperatures: $\sim 46\ K$ and $\sim 80\ K$.
- There are two types of aggregates responsible for the additional magnetization. The structure of the aggregates is unknown. The ones with critical temperature at $\sim 46\ K$ are probably manganese oxide precipitations. The once with critical temperature at $\sim 80\ K$ are thought to contain manganese, oxygen and silicon as components.
- The aggregates responsible for the additional magnetization have large coercivity and are frozen.
- There is a correlation between the magnetization and photoluminescence behavior.

2.8 ZnMnTe:O. Conclusions

- Using simultaneous doping of ZnTe with oxygen and manganese the doping level of ZnTe with oxygen was increased by at least two orders of magnitude from 10^{17} cm^{-3} in $ZnTe$ to 10^{19} cm^{-3} in $ZnMnTe$.

- No sign of conduction band splitting was observed, probably because the oxygen concentration in the samples is relatively low. However there is a decrease of the band gap and lattice constant with increasing oxygen content in $ZnMnTe:O$. The value of the bowing parameter obtained for $ZnTeO$ is 9.3 eV. It is in agreement with the expected value.

- The dependence of the exchange constants α and β on oxygen concentration in $ZnMnTe$ was investigated. The results are not convincing. However the preliminary result is that the α does not depend on oxygen concentration, and β (the absolute value) does not increase (i.e. does not change or becomes smaller).

- A new photoluminescence band centered at 1.65 eV was observed in $ZnTe$ doped simultaneously with manganese and oxygen. It is attributed to emission centers having Mn_nO structure.

- Doping with oxygen does not influence the behavior of paramagnetic manganese ions. However appear ferromagnetic aggregates with Curie temperature around ~ 46 K and ~ 80 K. Ferromagnetic aggregates with $Tc \sim 80$ K appear in samples with more than 0.5% of oxygen. Ferromagnetic aggregates with $Tc \sim 46$ K appear in samples with smaller oxygen content. The correlation between magnetization and photoluminescence behavior suggests that the discussed aggregates are not located between the crystal grains, but scattered inside the $ZnMnTe:O$ crystals.

3 ZnMnTe doped with chromium

3.1 Comparison of Mn^{2+} and Cr^{2+} ions in $ZnTe$

Although manganese and chromium are both transition metals and in fact differ by only one electron on their orbitals, their properties in $ZnTe$ matrix are very different. In the zinc blende $II-VI$ lattice both manganese and chromium accord two electrons to create electronic bonds with the surrounding anions. Thus the electronic configuration of Mn^{2+} and Cr^{2+} ions in the undoped $ZnTe$ is $3d^5$ and $3d^4$ respectively.

p-d exchange interaction

The fact that the electronic $3d$ orbital of the chromium ion is less then half filled has a major importance for $p-d$ exchange interaction in $II-VI$ materials doped with chromium. Whereas in manganese doped $II-VI$ SMS there is only possibility for hopping of the spin-down electrons between the valence band p-states and the d-states of the manganese ions, in $II-VI$ SMS doped with chromium both spin-up and spin-down electrons may take part in $p-d$ exchange interaction.

Thus the exchange $p-d$ interaction in chromium doped $II-VI$ SMS was found to be ferromagnetic [47], whereas in manganese doped $II-VI$ SMS it is antiferromagnetic. Since both FM and AFM $p-d$ exchange interaction can result in ferromagnetic ordering of the magnetic ions inside the SMS, an important role has the absolute value of the exchange interaction strength. The experimental value of the $p-d$ exchange integral in $ZnTe:Cr$ is $N_0\beta \approx +4.25\ eV$ [47]. It is quite large in comparison with other $II-VI:Cr$ SMS. In $ZnTe:Mn$ the measured p-d exchange integral value is about $-1.1\ eV$ (see Table 4).

Solubility

Although the solubility of manganese in $ZnTe$ is almost unlimited, the solubility of chromium is very small, probably less than 0.005 parts per mole [61]. In equilibrium growth techniques, like vapor transport, the attempt to grow crystals with higher chromium concentration results in precipitations of $NiAs$-type $CrTe$ [61]. Non-equilibrium growth techniques like MBE allow growth of the samples with much higher concentration of chromium [62].

The low solubility of the chromium in $ZnTe$ and the tendency to create precipitations of a different phase is explained [63] by so called spinodal decomposition effect. According to the theory of spinodal decomposition the energy of creation of a pair of chromium atoms located in the next neighbor positions of the cation sublattice in zinc blende $ZnTe$ crystal is negative and equals $-141\ meV$ [63]. For comparison the energy of formation of a similar pair of manganese atoms is positive $+21\ meV$. Thus chromium doped $ZnTe$ crystal decreases its energy by creation of chromium-reach clusters.

A way to prevent the spinodal decomposition is based on changing of the chromium ion charge state from Cr^{2+} to Cr^{3+} or Cr^{1+}. In this case

Coulomb repulsion between ions carrying an additional charge prevents the creation of chromium-reach aggregates. A decrease of the number and the size of chromium reach clusters was observed in both cases [63]. There are also other reports [64] where a decrease of ferromagnetic signal, caused by chromium-reach precipitations, was observed only in p-doped samples (where chromium is expected to be in Cr^{3+} state), and an increase of ferromagnetic signal was observed in n-doped samples (where chromium is expected to be in Cr^{1+} state).

The fact that chromium can have three different charge states in $ZnTe$ also distinguishes chromium from manganese. Manganese in $ZnTe$ can exist in only one charge state, namely Mn^{2+}. The energy states, corresponding to Mn^{2+}/Mn^{1+} and Mn^{2+}/Mn^{3+} transitions in $ZnTe$ are located deep inside the conduction and valence band respectively [25] and thus charge states Mn^{1+} and Mn^{3+} are not energetically favorable. The energy states corresponding to Cr^{2+}/Cr^{1+} and Cr^{2+}/Cr^{3+} transitions in $ZnTe$ are both located inside the band gap. The Cr^{2+}/Cr^{3+} donor state is located about 200 meV above the valence band maximum, and the Cr^{2+}/Cr^{1+} acceptor state is located about 1.1 eV below the conduction band minimum [63].

Magnetic properties

The magnetic properties of ZnMnTe are defined by the six-fold degenerated ground state of the manganese ion. The closest excited state of the Mn^{2+} ion is located more than 2 eV higher [e.g. 25], and does not influence the magnetic properties (Fig. 29a). In magnetic field the ground state splits in six equidistant levels, and thus undoped $ZnMnTe$ crystal behaves like a Brillouin-type paramagnetic.

The ground state of the chromium ion in $ZnTe$ zinc blende lattice is also a multiplet (five-fold, $L = 0$, $S = 2$) [65], however due to spin-orbit and spin-spin interaction the multiplet is splitted even in the absence of external magnetic field. Thus the lowest state of chromium atom is a singlet ($m_S = 0$), which is followed by the first excited doublet state ($m_s = \pm 1$), separated by 0.26 meV, and second excited doublet state ($m_s = \pm 2$), separated by ~ 1 meV from the lowest state (Fig. 29b).

A singlet ground state is a characteristic feature of a Van-Vleck-type paramagnetic. However since the excited states in $ZnCrTe$ are located very close to ground state, the material behaves also like a Brillouin-type paramagnetic. As an example the $M(H)$ dependence grows slower than a statndard Brillouin function and more rapidly then that of a Van Vleck system.

Ferromagnetism

$ZnMnTe$ is one of the few materials considered as "real" SMS, in which ferromagnetism was observed and has a so called intrinsic nature. The ferromagnetic transition in $ZnMnTe$ occurs at very low (about 2 K) temperatures in highly p-doped samples. It is an example of carrier induced ferromagnetic transition.

$ZnCrTe$ is also often considered as a material with intrinsic nature

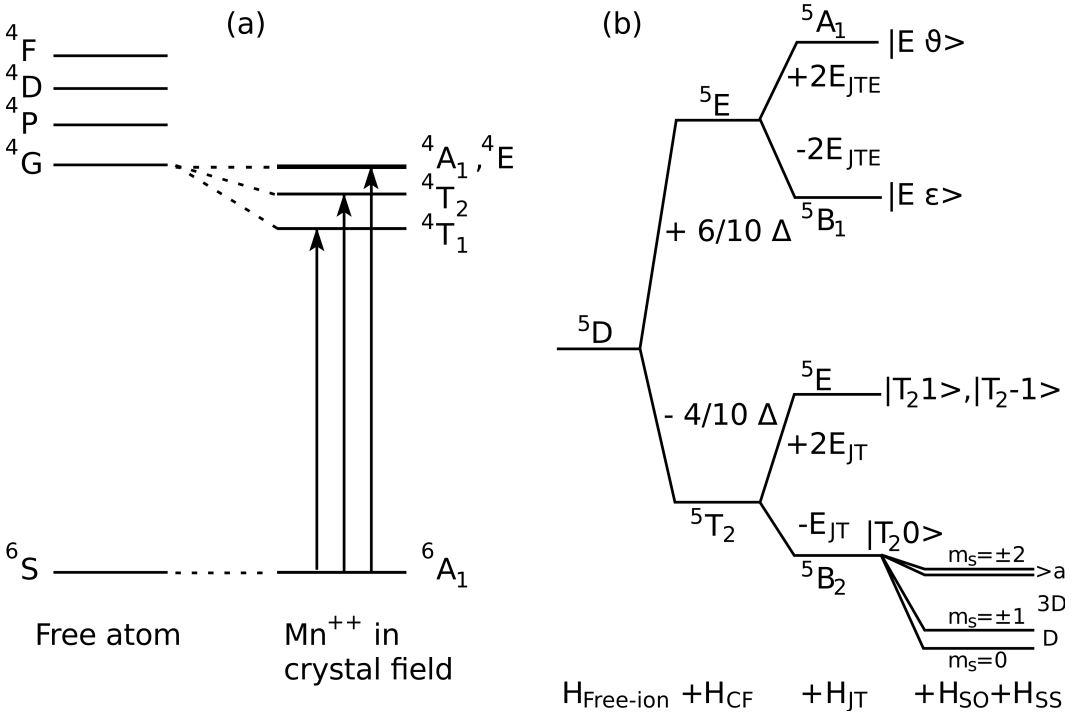

Figure 29: (a) A schematic diagram of the ground state and the splitting of the first excited state of the $3d$ level of Mn^{2+} ion in tetrahedral crystal field [25]. (b) Energy splittings of the $3d$ level of Cr^{2+} ion in $ZnTe$, including crystal field, Jahn-Teller, spin-orbit, and spin-spin effects [65].

[66] of ferromagnetism. However in $ZnCrTe$ ferromagnetism is observed in undoped samples (or n-doped samples), and thus it is definitively not a carrier-induced-type ferromagnetic. The idea of intrinsic nature of ferromagnetism in $ZnCrTe$ stems from the fact that in samples which possess ferromagnetic properties, a giant Zeeman band splitting is usually observed in magnetic circular dichroism (MCD) or reflectance measurements, and the MCD signal displays a hysteresis very similar to that obtained in magnetization measurement [66]. However there are no reports of more direct observations like, for example, observation of crystal-wide ferromagnetic domain structure using magnetic force microscopy (MFM)[35]. The reported temperatures of ferromagnetic transitions in $ZnCrTe$ range between 15 K [67] and 300 K [66, 64, 68] and such discrepancy is explained probably by differences in synthesis technique, chromium concentration and doping.

Ferromagnetism in $ZnCrTe$ is ascribed to short range exchange interaction between chromium ions located in regions with high density of chromium impurity. The distribution of chromium in $ZnCrTe$ with ferromagnetic properties is demonstrated to be nonuniform [63]. Although such regions of high density of chromium may be considered as precipitations,

[35]Obervation of domain structure in polycristalline $ZnCrTe$ was reported in [79]. Authors observed FM grains with size of 45 nm, and very small FM domains having size of ~ 4 nm inside such grains

their crystal structure usually repeats that of the host lattice (e.g. zinc blende in $ZnCrTe$) [63, 68].

In order to explain the ferromagnetic interaction between chromium ions both superexchange [69] and double exchange [70] mechanisms were proposed. Thus both mechanisms, which usually compete in $II-VI$ SMS, stabilize the ferromagnetic state of closely situated chromium ions in $ZnCrTe$. However it is difficult to state which of the two mechanisms prevails. The possibility of double exchange interaction in $ZnCrTe$ is due to the fact that the chromium $3d$ band of spin-up states is not fully occupied, and the remaining empty state is hybridized with the anion 5p states [70]. Thus an electron from a chromium ion can hop to a nearby chromium ion only if the spins of the two ions are oriented ferromagnetically.

The fact that exchange interactions are short-range [71] suggests that in order to achieve dense and uniform distribution of chromium in the sample the concentration of chromium should be rather high. With chromium in $ZnTe$ it is not easy to fulfill, since its solubility is less then 0.5 %. However there are reports [66, 64], where using non-equilibrium techniques (like MBE), much higher concentrations (up to 20 %) were achieved.

In connection with the condition of high chromium concentration should be also mentioned the role of percolation phenomenon [71, 72]. Namely, it was possible to obtain a theoretical T_C value very close to the experimental one, only in conditions when the distribution of chromium atoms reaches the percolation limit (20 % in fcc lattice). Regardless of the approach to chromium distribution, random [71] or in clusters (according to spinodal decomposition) [72], a good agreement with experiment is achieved when separated ferromagnetic clusters connect with each other and form a network which covers an entire crystal. In the experiment however ferromagnetic transition was observed at concentrations lower (e.g. 5 %) than the percolation limit[66, 64].

3.2 Review of reports on simultaneous doping with manganese and chromium

The idea of simultaneous doping with two kinds of magnetic ions is not new. During recent years there was several reports on simultaneous alloying with manganese and chromium [73-77], not to mention other pairs of magnetic ions. The need for such approach stems from the fact that alloying with those magnetic materials separately does not provide the properties which are expected from such alloys. Since different magnetic ions have their unique "good" and "bad" properties, they can complement each other in the alloy. For example, manganese has a very good solubility in $ZnTe$, however the interaction between closely situated manganese ions are antiferromagnetic, and it is rather bad candidate for room-temperature ferromagnetism in $II-VI$ compounds. Chromium, for that matter, was demonstrated to induce ferromagnetic properties in $ZnTe$, however its sol-

ubility is very poor.

A suggestion of simultaneous doping was made for example in [77], where authors predict possibility to create a material which ferromagnetic state may be switched by controlling the electron concentration. Such material is proposed to be made on the basis of ZnO SMS simultaneously doped with an appropriate amount of two transition metals, (Fe, Mn), (Ce, Mn) or (Ni, Mn).

Other benefits, which may result from simultaneous alloying with two kinds of magnetic impurities, are expected from interaction between two different kinds of magnetic ions, and new phenomena which may arise from such interaction.

As an example, in [75] authors studied $CdMnTe : Cr$ as a material for mid-infrared laser development. In such a device the internal transitions of Cr^{2+} ion are expected to produce laser action. An increase of the room temperature lifetime is reported for the $Cd_{0.55}Mn_{0.45}Te : Cr$ in comparison with $Cd_{0.85}Mn_{0.15}Te : Cr$. Besides that, the lifetime became nearly independent of temperature, suggesting an emission efficiency near unity. This is an example of how manganese "improves" the properties of chromium ions.

Another interesting example is alloying $MnTe$ and $CrTe$ [74]. Whereas $MnTe$ is antiferromagnetic with the Néel temperature of $T_N = 310\ K$ and $CrTe$ is ferromagnetic with Curie temperature of $T_C = 342\ K$, the $Mn_{1-x}Cr_xTe$ alloy was found to have a ferromagnetic transition at about 56 K and ferrimagnetic transition at about 305 K. Authors clame that these properties are inherent to $Mn_{1-x}Cr_xTe$ alloy and are not the result of a secondary phase. Although the lattice of the $Mn_{1-x}Cr_xTe$ semiconductor has a structure of NiAs-type, and not fcc like in $ZnTe$, this example demonstrates how new properties may appear due to interaction between different types of magnetic ions.

A study very similar to one, presented in this work, was reported in [73]. It is devoted to magnetization and MCD measurements of $Cd_{1-x-y}Mn_xCr_yTe$ alloy, grown by Bridgman technique. A new band at 1.66 eV was observed in transmission MCD and photoluminescence spectra. The line is assigned to $Cr^+ - Mn$ centers, containing monovalent chromium ion. Such band does not appear neither in $ZnMnTe$ nor in $ZnCrTe$. Hysteresis curves were observed in both magnetization measurements and MCD of the 1.66 eV band, however only paramagnetic signal was observed in the MCD of the absorption edge. Thus the ferromagnetic signal is probably produced by some localized objects and does not induce energy band splitting. The ferromagnetism is explained by creation of bound magnetic polarons around Cr^+ ions. This way the spins of Mn and Cr ions inside the orbit of the polaron form a "ferromagnetic bubble". Authors suggests that the ferromagnetic signal cannot be explained by the presence of the chromium ions alone, and chromium ions are likely to enhance the contribution of manganese magnetic moments to the total magnetization of the material.

3.3 Technological part and structural characterization

The $ZnMnTe : Cr$ crystals were grown by vertical Bridgman method. The charge consisted of a mixture of $ZnTe$, $MnTe$, Cr, Te and Zn_3P_2. The concentration of manganese and chromium in the charge was kept constant, 5 % of manganese and 2 % of chromium. In order to control the concentration of free holes the sample were additionally doped with phosphorus. The concentration of phosphorus in the charge was varied between 0 and $5 \cdot 10^{20}$ cm^{-3}.

The charge was placed in silica ampules coated inside with carbon, the air from the ampules was evacuated and the ampules were sealed. During the growth process inside the the high pressure furnace the ampule was kept in the atmosphere of pure nitrogen, at a pressure of about 12 Bar[36]. The charge was heated up to $1350°C$ and kept at that temperature for 12 hours to achieve better homogenization. During the growth the ampule was moved out of the hot region of the furnace with a speed of 1 mm/h (at the beginning of the process) or 2 mm/h.

Occasionally the ingot consisted of several monocrystalline grains, stretched along the ingot. However the quality of $ZnMnTe : Cr$ crystals was found to be poorer than that of $ZnMnTe$. The increase of the concentration of phosphorus in the charge further decreased the quality of the resulting ingot. The ingots were usually about $10 - 14$ mm in diameter and about 60 mm long. Although the heavily doped ingots were not monocrystalline, a reasonably large piece of monocristalline material for measurements could be easily obtained.

For comparison were used $ZnCrTe$ and $ZnMnTe$ samples, doped with only one type of transition metall atoms. The data on discussed samples is summarized in Table 7.

The X-ray diffraction measurements did not reveal any additional phases, however the microscopic investigation shows that in the samples there are chromium-reach precipitations. The precipitations were observed in all studied samples. Several examples of scanning electron microscope images are presented on Fig. 30. The SEM scans were carried out on chemically polished surfaces. Often, especially in phosphorus doped samples, the precipitations are shaped as microscopic wires with diameter ranging between 500 nm and 2 μm. The largest number of such wires was observed in sample 4516, where almost all precipitations are wire-shaped. The wires are oriented randomly with respect to the growth interface (which was approximately parallel to the scanned surfaces on Fig. 30). Such wires have grown probably while the alloy was in the liquid sate, during the homogenization period, before the growth process started. Later, when the crystallization has begun, such wires were trapped inside the growing crystal. Such model is supported by the fact that the wires have random orientation, and are

[36] pressure at room temperature

Table 7: Summary of ZnMnTe:Cr sample series

Nr.	Sample ID	Nominal Mn content	Nominal Cr content	Nominal P conc. (cm^{-3})	Paramagn. T_C (K)
2	3452	0	0.02	0	-
3	4504	0.05	0.02	0	-2.2
4	4505	0.05	0.02	5e18	+1.36
5	4532	0.05	0.02	5e19	+1.2
6	4516	0.05	0.02	5e20	-0.3
7	4630	0.03	0.01	0	-1.3
8	4631	0.03	0.01	5e18	-0.8

usually oriented parallel to the the growth interface. If the wires would grow during the growth of the bulk crystal, they would be oriented more or less perpendicular to the growth interface of the ingot. The mechanism responsible for the wire-like shape of the precipitations is not known. In MBE method the wires grow on a substrate under a droplet of molten metal, which defines their round cross section and their width. A similar mechanism may be responsible in this case, however there is no clues on what acts as the base and the droplet, needed for the wire growth.

The composition of the precipitations and the surrounding crystal was investigated by means of micro-EDX analysis. Two examples of EDX measurement made on samples 4504 (without phosphorus) and 4532 (doped with phosphorus) are presented on Fig. 31 and Fig. 32 respectively. In the samples which were not intentionally doped with phosphorus, or doped with a smaller amount of phosphorus (samples 4504, 4505) the precipitations consist of chromium and tellurium (Fig. 31). The proportion of the components varies among different precipitations. Judging by quantitative EDX analysis both Cr_2Te_3 and Cr_3Te_4 precipitations are present.

The composition of the precipitation is different in the samples highly doped with phosphorus (samples 4532 and 4516). In such samples the precipitations consist of four chemical elements, zinc, chromium, tellurium and phosphorus (Fig. 32). Although a precise analysis of the composition of such precipitations was not possible, an approximate chemical formula of the compound may be given as $Cr_3Zn_2Te_xP_y$. Here the value of x is found to be between 2 and 3, and the value of y, between 1 and 2.

In the sample containing the highest concentration of phosphorus (4516, $5 \cdot 10^{20}$ of phosphorus in the charge) large precipitations of elementary

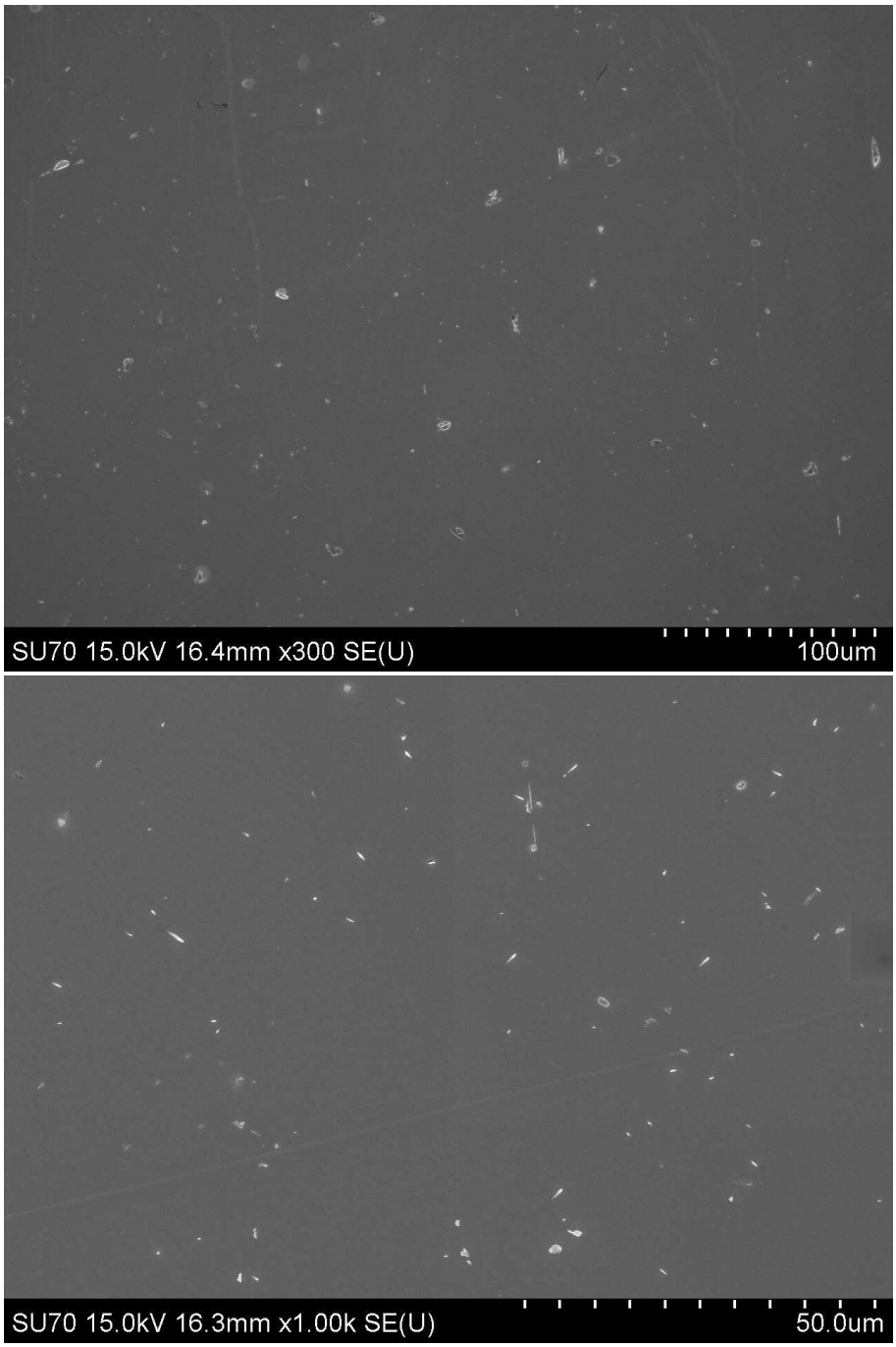

Figure 30: Scanning electron microscope images. (top) sample 4504, (bottom) sample 4532. White spots on both pictures represent precipitations, which are apparently less conductive than the surrounding material. White streaks, which are visible on the second picture, are wire-shaped precipitations. Such wires under stronger magnification are shown on following pictures.

tellurium were found (Fig. 30, large rounded spots on the surface).

Although it might appear that all precipitations are wire-shaped, there

are also irregularly shaped precipitations, which usually prevail. The aluminum peak, which was observed in all EDX spectra originates from the aluminum sample holder, and does not represent the signal from the sample.

The majority phase of the crystal is composed of $ZnMnTe$ alloy (Fig 31, Fig. 32), with a small amount of chromium and phosphorus impurity, undetectable by the used EDX apparatus[37]. Thus the concentration of chromium, diluted in $ZnMnTe$, could not be measured reliably.

The presence of the diluted chromium in the samples may be studied by means of light absorption measurements. It is known that chromium in $ZnTe$ produces an absorption line, centered at 0.69 eV [76]. This line is associated with internal transitions of chromium ion, located in tetrahedral crystal field, between the ground $^5T_2$ state and the first excited ^5E state (see Fig. 29b). As an example, the absorbance spectrum of the $ZnCrTe$ sample 3452 is presented on Fig. 33. Thus, the existence of such absorption peak at 0.69 eV serves as an indicator of the presence of Cr-ions in tetrahedral crystal environment.

It is surprising that this absorption line (0.69 eV) was not observed in the highly phosphorus-doped sample 4532. This observation indicates that the concentration of diluted chromium ions in the highly phosphorus-doped samples is very small, and that the majority of chromium impurity was gathered inside Cr-reach precipitations of type $Cr_3Zn_2Te_xP_y$, which were described above.

Summary: Technological part and structural characterization

- The discussed crystals ($ZnMnTe:Cr,P$, $ZnMnTe$, $ZnCrTe$) were grown by Bridgman technique.
- Structurally the samples consist of two distinguishable systems, the bulk of the grown material consisting of $ZnMnTe:Cr,P$ and chromium-reach precipitations.
- Chromium-reach precipitations were observed in all studied samples, often the precipitations are wire-shaped.
- In samples with low phosphorus content the precipitations having chemical formula Cr_2Te_3 and Cr_3Te_4 were observed.
- In samples with high phosphorus content the precipitations with complicated chemical composition $Cr_3Zn_2Te_xP_y$ were observed.
- The presence of diluted chromium impurity in the $ZnMnTe$ was detected by light absorption measurements. Measurement show that the concentration of diluted chromium in samples highly doped with phosphorus is much lower than in phosphorus-free samples.

[37]The solubility of chromium in $ZnTe$ is reported to be about 0.5 % [61].

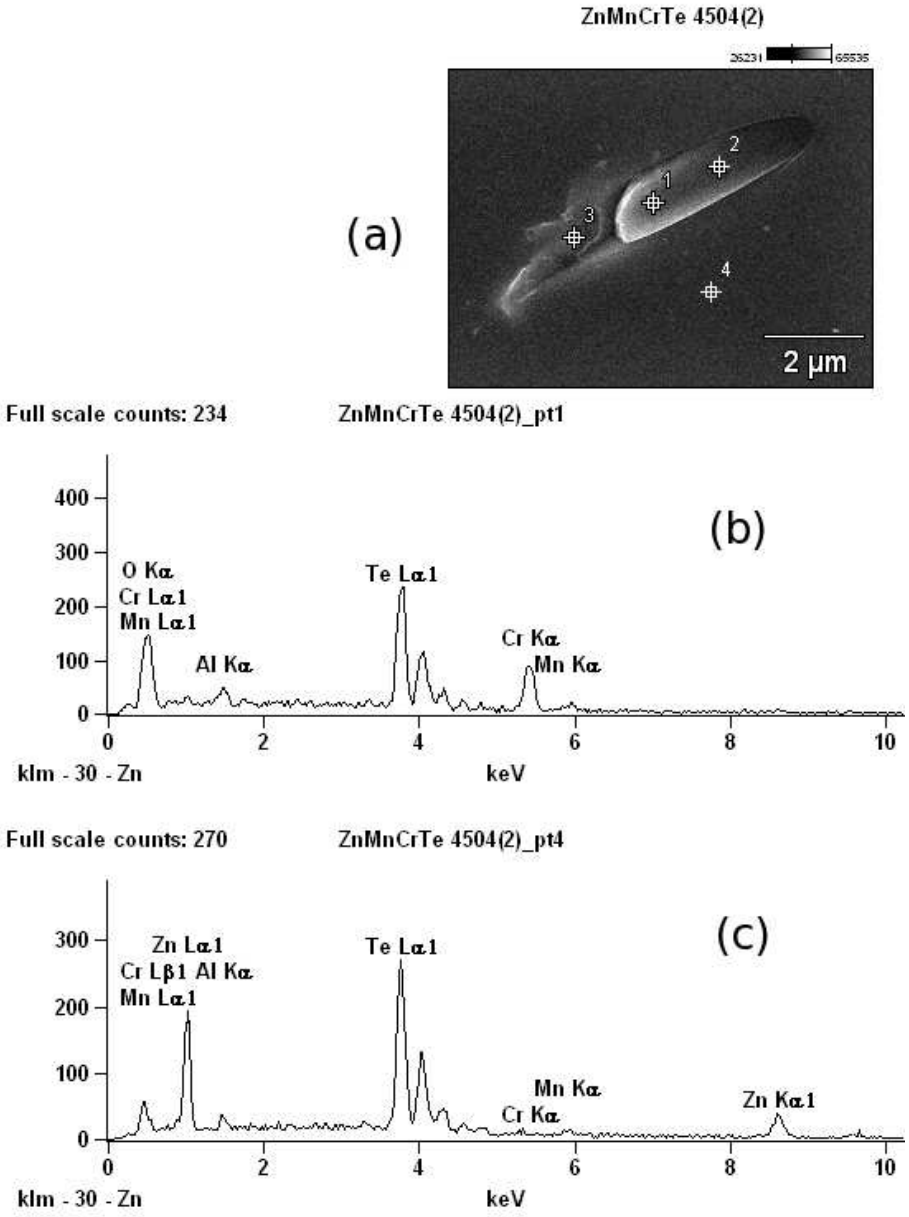

Figure 31: (a) Positions of the spots on the sample 4504 ($ZnMnTe : Cr$) surface (marked 1, 2, 3 and 4) were the EDX spectra have been measured. Spots 1 and 2 are located on a wire-shaped precipitation, and spots 3 and 4 are located on the surface of the bulk $ZnMnTe : Cr$ material. Fig. (b, c) show EDX spectra measured in the points 1 and 4 respectively. The markers above the peaks indicate the position of characteristic peaks for relevant elements. Besides the tellurium-characteristic peaks, both spectra have two additional peaks related with chromium (b) or zinc (c). This shows that the bulk consists mostly of $ZnTe$ and the precipitations of Cr_xTe_y.

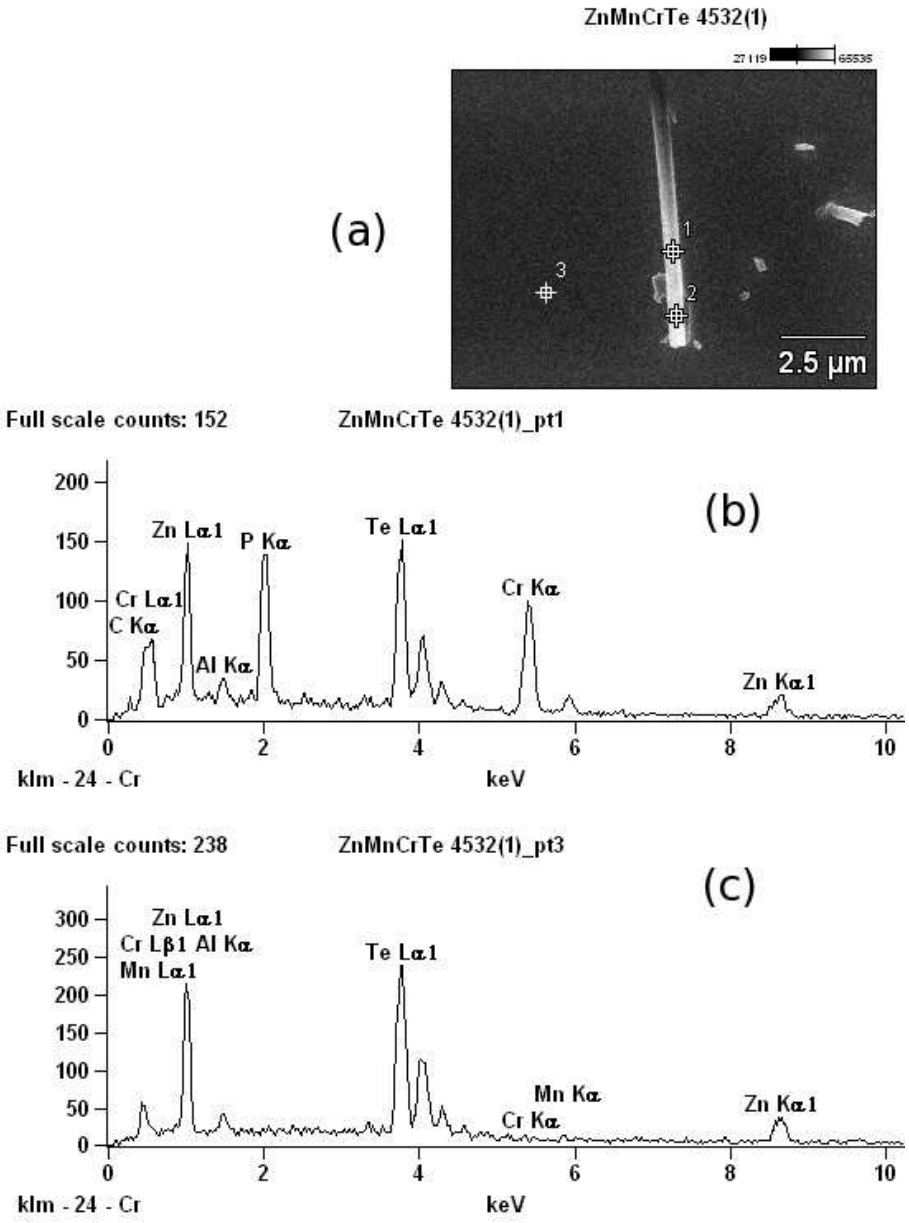

Figure 32: (a) Positions of the spots on the sample 4532 ($ZnMnTe : Cr, P$) surface (marked 1, 2 and 3) were the EDX spectra have been measured. Fig. (b, c) show EDX spectra measured in the points 1 and 3 respectively. Spot 1 is located on a wire-shaped precipitation and spot 3 is located on the surface of bulk material. Comparison with Fig. 31 shows, that composition of the bulk does not change considerably (Compare Fig. c with Fig. 31c). However there is a considerable amount of zinc and phosphorus inside the precipitations besides chromium and tellurium (Compare Fig. b with Fig. 31b).

3.4 Magnetic properties

Comparison of ZnTe:Cr and ZnMnTe:Cr

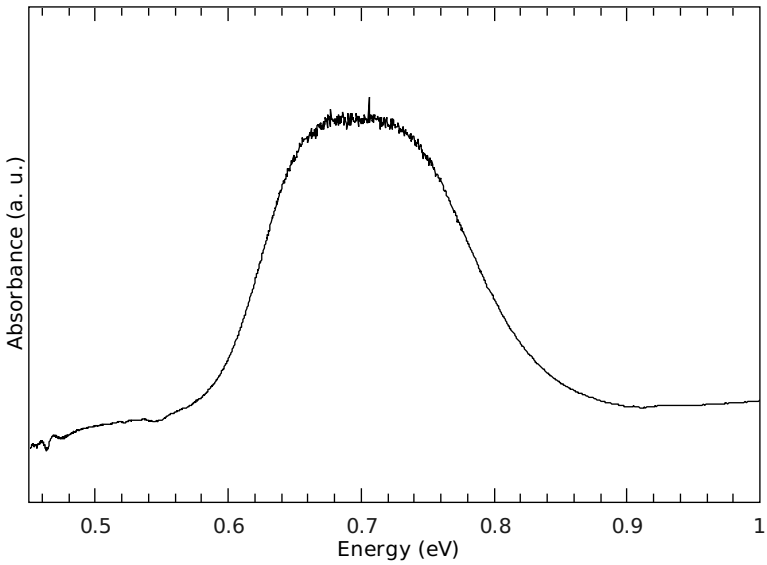

Figure 33: The absorbance spectrum of $ZnCrTe$ sample 3452 measured at room temperature.

In this part the influence of the manganese on the properties of the $ZnTe : Cr$ semiconductor will be considered. As a first example of such influence the dependence of magnetic susceptibility on temperature for two samples, $ZnTe : Cr$ (sample 3452) and $ZnMnTe : Cr$ (sample 4504) is presented on Fig. 34b. The magnetic susceptibility in both cases consists of two contributing parts, ferromagnetic and paramagnetic. The ferromagnetic contribution is manifested as a large background signal with a relatively weak dependence on temperature. It is ascribed to ferromagnetic precipitations, which appear in both samples. The paramagnetic contribution becomes visible at lower temperatures where the magnetic susceptibility strongly increases with decreasing temperature[38]. The paramagnetic signal is produced by isolated chromium and manganese ions diluted in $ZnTe$ lattice. The measurements of the magnetization were made only to 200 K. However the ferromagnetism in the samples was also observed at room temperature.

Although both samples have the same nominal concentration of chromium (2 %), the intensity of the ferromagnetic signal is much higher (five times) in case of $ZnMnTe : Cr$ sample[39]. Since the concentration of chromium in the charge was the same, there might be two possible explanations, (i) doping with manganese increases the amount of ferromagnetic precipitations inside the crystal, (ii) manganese atoms take part in formation of the precipitations and the ferromagnetic signal.

Manganese itself does not form ferromagnetic precipitations in $ZnTe$, and the EDX measurements show that the precipitations in $ZnMnTe : Cr$

[38]For sample $ZnTe : Cr$ such paramagnetic contribution is visible on Fig. 34a

[39]As an example, a considerable piece of such material can be easily picked up by a neodymium magnet

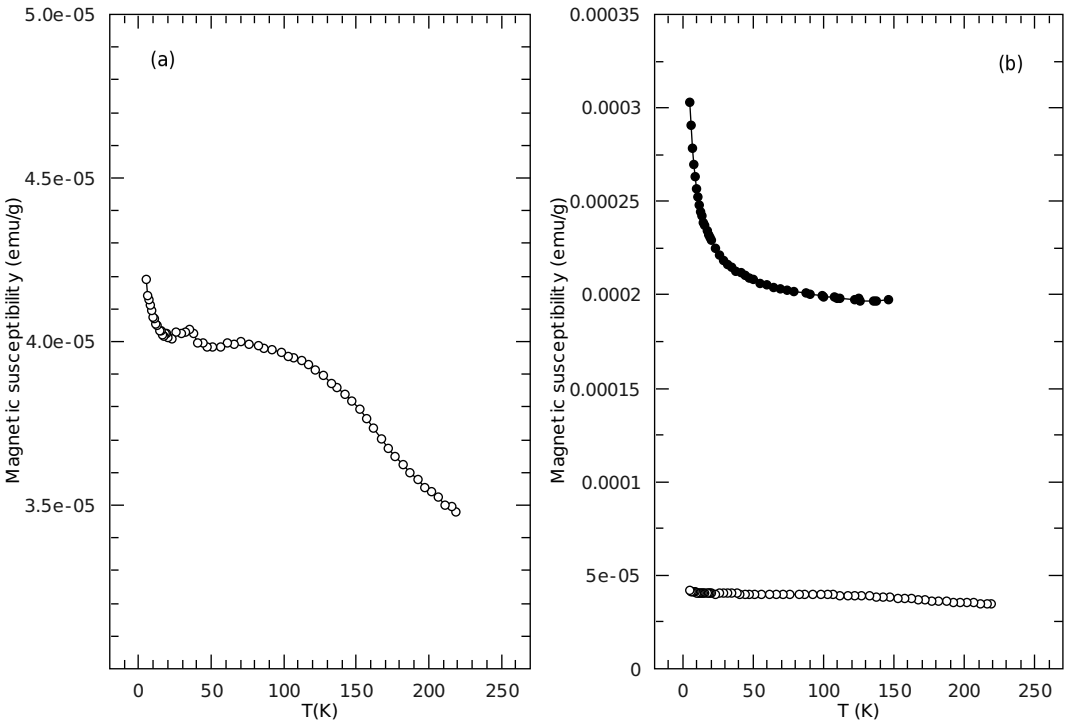

Figure 34: Dependence of the magnetic susceptibility on temperature for $ZnTe : Cr$ (sample 3452, open circles) and $ZnMnTe : Cr$ (sample 4504, filled circles), measured at 200 Oe and 100 Oe respectively. Figure (a) shows the $\chi(T)$ dependence of sample $ZnTe : Cr$ in a smaller scale. Figure (b) shows the $\chi(T)$ dependence for both samples in the same scale.

are composed of chromium and tellurium (Fig. 31), and have a negligible amount of manganese. Thus the latter hypothesis, although it is very attractive, seems to be wrong, unless the ferromagnetic signal is produced by some other objects, which contain both manganese and chromium and do not look like precipitations.

A very similar effect (effect of manganese contribution to FM) was observed in $CdMnCrTe$ alloy and other double-doped alloys (see [73] and reference within). Authors explaine the effect by creation of ferromagnetic "bubbles" around Cr^+ acceptor. A hole weakly bound to such acceptor forms a bound magnetic polaron. The spins of the manganese and chromium ions, located inside the Bohr orbit of such polaron contribute to ferromagnetic signal. Such explanation seems to be unprobable in our case, since the concentration of Cr^+ ions should be very low and cannot account for the ferromagnetic signal. The formation of Cr^+ acceptors should be favorable in n-doped $ZnCrTe$ [63], whereas the presented here samples have p-type conductivity. It is reported [78] that even doping with donors does not always help to create more Cr^+ ions, and the most effective way to create Cr^+ ions is the photogeneration.

The fact that the ferromagnetic signal is produced by precipitations is confirmed by the MFM measurements of one of the $ZnMnTe : Cr$ samples

(4504). The results, together with the atomic force microscope (AFM) image, are presented on Fig. 35. The MFM investigation demonstrated that the ferromagnetic signal is produced by the small (with size around 1 μm) precipitations (see Fig. 35a,c). However, the shape of the magnetic profile usually does not correspond to the shape of topological profile (i.e. the shape of the sample surface). This fact suggests that the observed precipitations are below the surface or cannot be distinguished from the rest of the sample by AFM. The size of magnetic objects observed in MFM measurements corresponds well to the size of the precipitations observed in SEM measurements. However the precipitations observed in SEM images are easily distinguishable from the bulk material. The MFM images were taken on very flat surfaces with surface profile depth of about 10 nm (see Fig. 35a). Thus it is possible that the FM signal is produced not by Cr_xTe_y precipitations only.

A comparison of hysteresis curves measured on $ZnTe:Cr$ and $ZnMnTe:Cr$ samples at different temperatures is presented on Fig. 36. Apart from the large difference of the amplitude of hysteresis curve, there is also a difference of the coercive field, which is 150 Oe in the $ZnMnTe:Cr$ against 400 Oe in the $ZnTe:Cr$ at 5 K. With the increasing temperature the coercive field of the $ZnTe:Cr$ decreases to about 90 Oe at 200 K, while the coercive field of the $ZnMnTe:Cr$ remains constant. The elongated shape of the $ZnMnTe:Cr$ hysteresis curve and the decrease of its amplitude is explained by the large paramagnetic signal originating from single manganese ions.

Since the ferromagnetic objects observed in the samples are of about 1 μm in size, they probably have monodomain structure[40]. The width of hysteresis curve (and the strength of coercive field) is explained by the anisotropy of the magnetization process. Such anisotropy can be related for example with the anisotropy of the crystal structure or the shape of microscopic precipitations.

The mechanism, responsible for difference of the coercive field behavior in $ZnTe:Cr$ and $ZnMnTe:Cr$, is not known. However, the fact that such difference exist confirms the idea that manganese plays an essential role in formation and properties of ferromagnetic precipitations in $ZnMnTe:Cr$.

Magnetoreflectance of ZnTe:Cr and ZnMnTe:Cr

The magnetoreflectance measurements were carried out in order to investigate the influence of simultaneous doping with manganese and chromium on the splitting of the electron bands in the magnetic field. The measurements could be made only on $ZnMnTe:Cr$ sample which was not doped with phosphorus, since in the phosphorus-doped samples the electrical screening by free carriers prevented the observation of the free excitons in reflectance measurements.

[40] In [79] authors report on observation of magnetic domains with size of ~ 4 nm by means of MFM. In the samples discussed in this work such magnetic domains could not be observed.

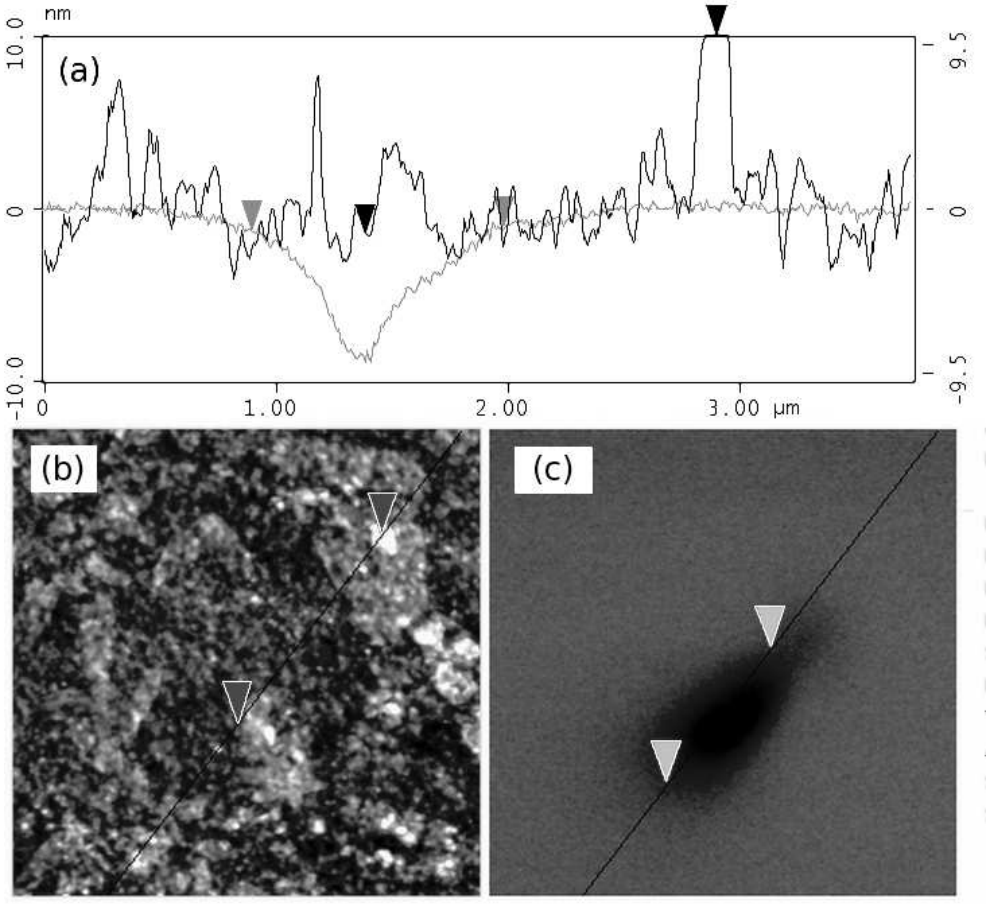

Figure 35: Atomic force microscope image (b) and MFM image (c) of the sample $ZnMnTe : Cr$ (4504) measured at room temperature. Figure (a) represents the topological (surface shape) profile (black line and markers) and magnetic profile (gray line and markers) measured along the lines shown on figures (b) and (c) respectively.

The results are presented on Fig. 37. For comparison, together with the data for $ZnMnTe : Cr$ sample, the figure contains data for $ZnTe : Cr$ and $ZnMnTe$ samples. In all presented samples the concentration of manganese and chromium, where those are applicable, was the same. In case of $ZnMnTe : Cr$ and $ZnMnTe$ this fact is obvious since free excitons in those samples have the same energy at zero magnetic field.

Comparing, first, the magnetoreflectance of $ZnMnTe$ and $ZnTe : Cr$, one notices the opposite splitting of the free excitons in those materials[41]. Unlike it is in $ZnMnTe$, in $ZnTe : Cr$ the σ^+ branch of the free esxciton in

[41]The presence of only two free exciton branches in magnetoreflectance spectra of $ZnTe : Cr$ is explained by the small amplitude of the splitting, which prevents observation of other two, weaker exciton branches. The splitting in this case is small because of the relatively small number of magnetic ions in $ZnTe : Cr$ in comparison with $ZnMnTe$.

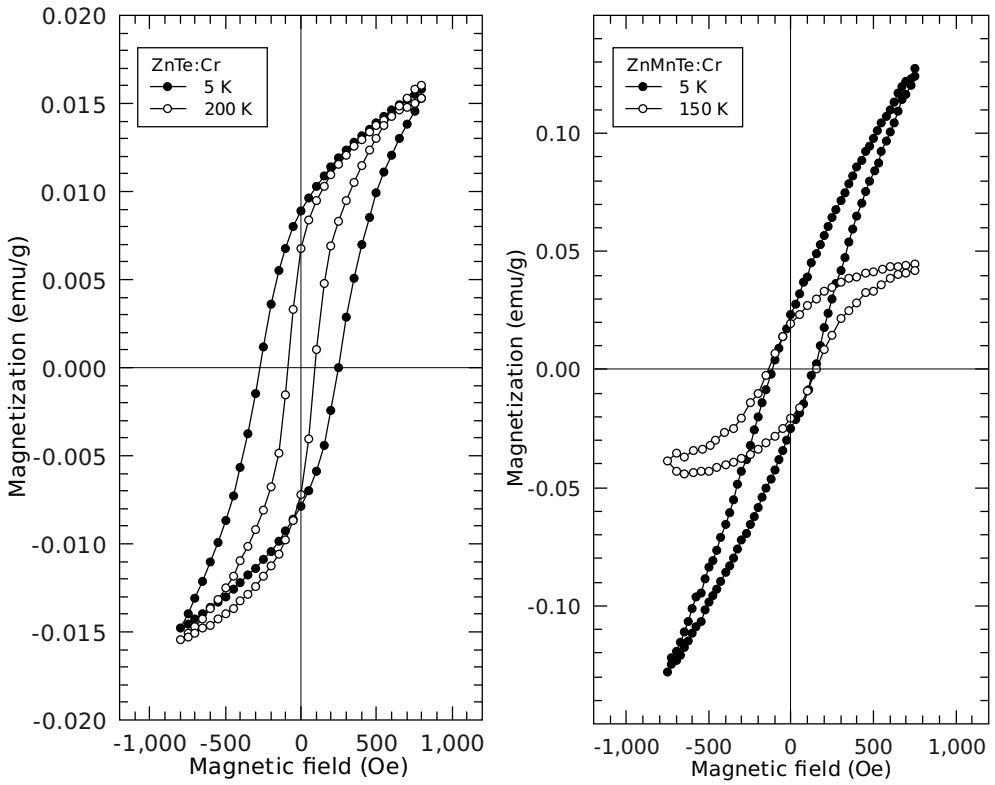

Figure 36: Hysteresis curves measured on $ZnTe : Cr$ (sample 3452, left figure) and $ZnMnTe : Cr$ (sample 4504, right figure) at different temperatures.

magnetic field has higher energy then the σ^- branch. This behavior reflects the fact that the $N_0\beta$ exchange constants in $ZnMnTe$, in $ZnCrTe$ have opposite signs. Hence one could expect, that the simultaneous doping with manganese and chromium would result in a decrease of the free exciton splitting.

A decrease of free exciton splitting in $ZnMnTe : Cr$ in comparison with $ZnMnTe$ was indeed observed (Fig. 37), however it cannot be explained by the opposite influence of the exchange constants of manganese and chromium. The influence of exchange constant should be independent of magnetic field. In Fig. 37 the splitting of free exciton in $ZnMnTe : Cr$ is smaller then that of $ZnMnTe$ at low magnetic fields, however it is almost the same at high magnetic fields. Since the amplitude of free exciton splitting is proportional to magnetization, the magnetization in $ZnMnTe : Cr$, as a function of magnetic field, has a less steep slope and achieves saturation at higher magnetic fields then that of $ZnMnTe$.

The slow growth of magnetization with magnetic field can be explained by the presence of isolated chromium ions in the crystal lattice. Because of the splitting of the lowest multiplet state of Cr^{2+} ion (see Fig. 29b), the magnetization as a function of magnetic field in $ZnTe : Cr$ grows slower than a standard Brillouin function, and approaches the saturation limit at

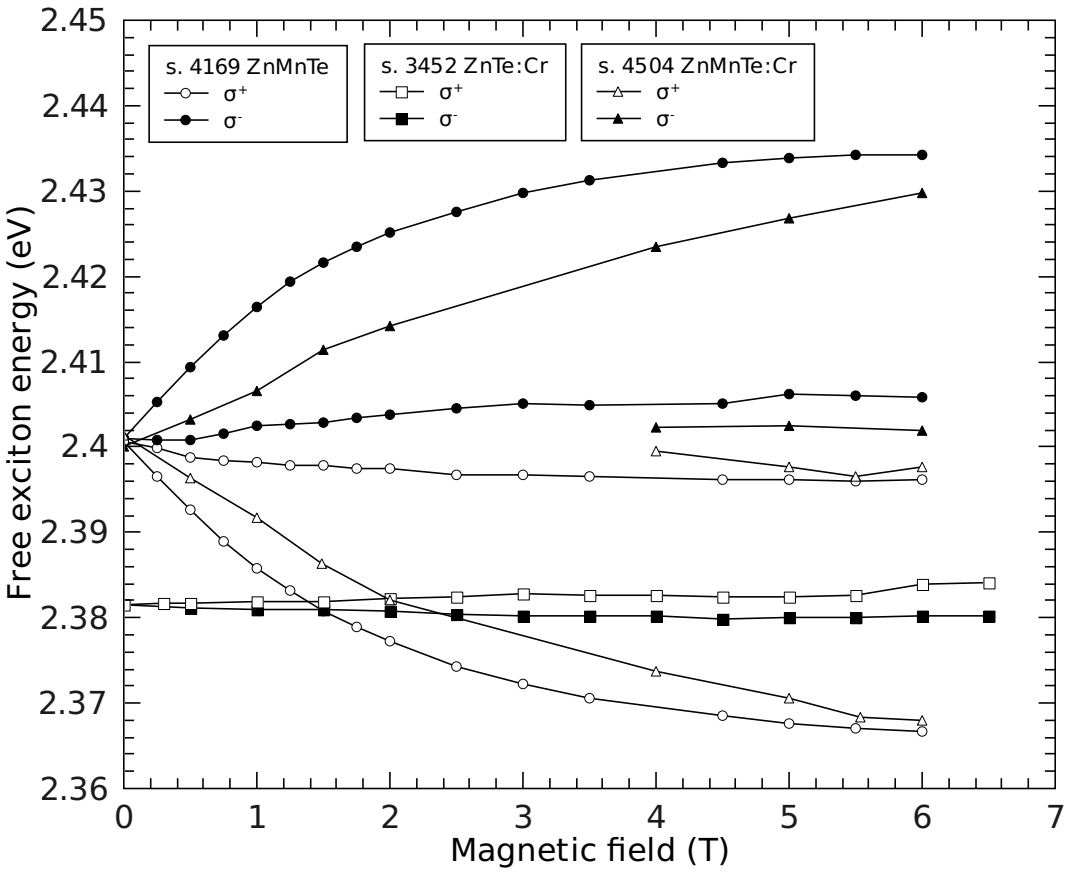

Figure 37: Free exciton energy as a function of magnetic field measured on $ZnMnTe$ (circles), $ZnTe:Cr$ (squares) and $ZnMnTe:Cr$ (triangles) at 5 K. Open symbols and filled symbols represent values measured in σ^+ and σ^- polarization respectively.

about 6 T [65]. The magnetization produced by manganese ions saturates at about $3-4$ T (see Fig. 37).

Thus, if one assumes that there is a superposition of contribution of manganese and chromium system of ions, the splitting of free exciton line[42] should not be monotonic, and should have a maximum at about 4 T. Indeed (see Fig. 38), at lower magnetic fields the contribution of manganese system prevails and the splitting increases. However, at about 4 T, when magnetization of manganese system of ions achieves saturation, the magnetization of chromium system of ions still increases. Since the splitting of free exciton induced by chromium ions has opposite sign, the overall splitting of free excitons should decrease from now on, until the moment when the magnetization of chromium system reaches saturation (at about 6 T).

One could estimate how much the splitting will differ between $ZnMnTe$ and $ZnMnTe:Cr$ in the saturation state. The value of free exciton splitting is proportional to $\Delta E \sim (\beta-\alpha)xS$ (see eq. (14)). Here α and

[42] the difference between the upper and the lower exciton branches

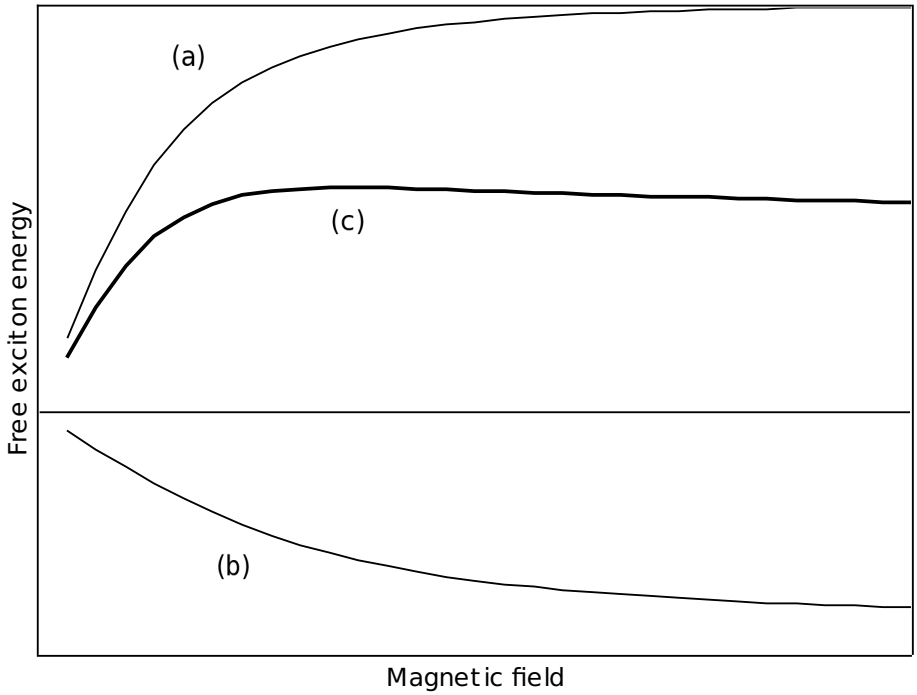

Figure 38: Schematic drawing of the strongest σ^- free exciton line as a function of magnetic field. Line (a) is the contribution of manganese ions, line (b) is the contribution of chromium ions and line (c) is the sum of both contributions.

β are the $sp-d$ exchange integrals, x is the concentration of magnetic ions, and S is the spin of the magnetic ion. Thus, the ratio of free exciton splitting in $ZnMnTe:Cr$ and $ZnMnTe$ can be written as

$$\frac{\Delta E_{Mn,Cr}}{\Delta E_{Mn}} = \frac{(\beta-\alpha)_{Mn} x_{Mn1} S_{Mn} + (\beta-\alpha)_{Cr} x_{Cr} S_{Cr}}{(\beta-\alpha)_{Mn} x_{Mn2} S_{Mn}}. \qquad (25)$$

Here x_{Mn1} and x_{Mn2} denote the concentration of mangenese in both samples.

The concentration of isolated (paramagnetic) manganese ions in $ZnMnTe$, obtained from magnetization measurements is 2.5 %. The concentration of isolated manganese and chromium ions in $ZnMnTe:Cr$ could not be measured, however these values can be estimated. The concentration of chromium does not exceed its solubility limit, which is about $0.5-0.7$ % [61]. The concentration of isolated manganese ions should be close to 2.5 %, since the free exciton energy in both samples has the same value.

Thus, taking into account the discussed above values of exchange integrals, $N_0\alpha_{Mn} = N_0\alpha_{Cr} = 0.2\ eV$, $N_0\beta_{Mn} = -1.1\ eV$, $N_0\beta_{Cr} = +4.25\ eV$, and the values of ion spin as $S_{Mn} = 5/2$, $S_{Cr} = 4/2$, one obtains $\frac{\Delta E_{Mn,Cr}}{\Delta E_{Mn}} = 0.5$. This means, that if one assumes a simple superposition of contribution of manganese and chromium systems to free exciton splitting, the splitting in $ZnMnTe:Cr$ should be two times smaller than that in $ZnMnTe$.

The observed behavior of the free exciton splitting does not correspond

to the described above theory. Hence, in the consideration of $sp-d$ interaction, the effect of manganese and chromium ions should not be calculated separately. Probably one should take into account the interaction between those two magnetic systems.

If, however, the free exciton splitting of the $ZnMnTe : Cr$ sample can be written as $\Delta E \sim (\beta - \alpha)xS$, where all values are considered as specific for this material, then one obtains that the exchange constants have manganese-like character, and the magnetization behavior has chromium-like character. In this respect, the idea proposed in [73] does not look as fantastic as author of this work thought before.

The hypothesis states that the ferromagnetism in $CdMnCrTe$ is explained by formation of bound magnetic polarons around Cr^+ acceptors. The spins of manganese and chromium ions which exist inside the polaron form a "ferromagnetic bubble", which may also be considered as a superparamagnetic particle and which may account for the observed magnetoreflectance effects.

The influence of phosphorus doping on magnetic properties of ZnMnTe:Cr

The high p-type doping promises two effects in $ZnMnTe : Cr$ SMS. On the one hand, the high p-type doping is reported to prevent the formation of chromium-reach precipitations [63, 64], on the other hand, it is thought to be a necessary ingredient for achievement of the carrier mediated ferromagnetism in this semimagnetic semiconductor. Thus the doping of $ZnMnTe : Cr$ samples with phosphorus was carried out to investigate both these effects.

The results of the measurements of magnetic hysteresis of the $ZnMnTe : Cr, P$ samples with different concentration of phosphorus are shown on the Fig. 39. First thing ought to be noticed here is the decrease of the hysteresis loop with increasing concentration of phosphorus (Fig. 39 a,b). In the samples doped with phosphorus to a level higher then $5 \cdot 10^{19}\ cm^{-3}$, the hysteresis loop is no longer observed (Fig. 39 c,d). Such behavior is in agreement with the theory of spinodal decomposition [63]. However, as it was already discussed above, in phosphorus-doped samples still there is a large number of chromium-reach precipitations. The EDX investigation shows that in the samples where the magnetic hysteresis was not observed, appear different type of precipitations with chemical composition $Cr_3Zn_2Te_xP_y$. Whereas in the samples with smaller concentration of phosphorus (samples 4504, 4505), where hysteresis loop was detected, the precipitations of type Cr_2Te_3 and Cr_3Te_4 were observed[43]. It is worth to emphasize that in the sample moderately doped with phosphorus (4505) the observed precipitations are of the same type as in sample not doped with phosphorus (sample 4504). However the ferromagnetism of sample (4505) is weaker than that of sample (4504) which was not doped with phosphorus. Thus the decrease

[43]Both Cr_2Te_3 and Cr_3Te_4 compounds are ferromagnetic, having the transition temperature of 180 K and 360 K respectively [74].

of ferromagnetic signal is not related solely with disappearance of Cr_xTe_y precipitations, and creation of new kind of precipitations.

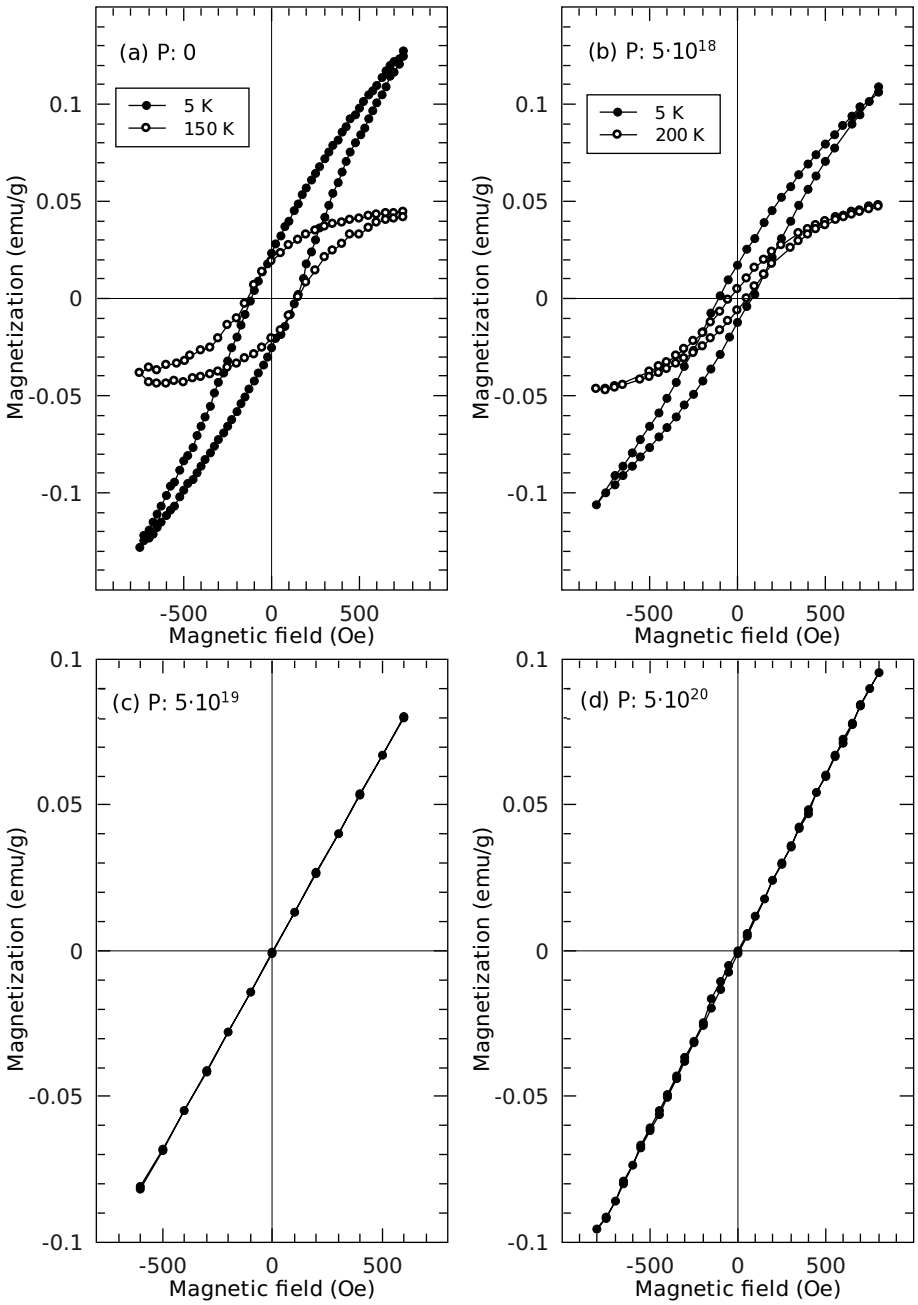

Figure 39: Magnetic hysteresis measured on $ZnMnTe : Cr$ doped with phosphorus. (a) sample without phosphorus (sample 4504), (b) $5{\cdot}10^{18}cm^{-3}$ (sample 4505), (c) $5 \cdot 10^{19}cm^{-3}$ (sample 4532), (d) $5 \cdot 10^{20}cm^{-3}$ (sample 4516).

With increasing phosphorus content decreases the width of the hysteresis loop and the remanent magnetization, however the saturation value does not change (compare the high temperature loops on Fig. 39 a,b). The coercive field becomes dependent on temperature. Thus the moderate

doping with phosphorus (up to $5 \cdot 10^{18}$ cm^{-3}) does not change the amount of magnetic ions which form the ferromagnetic precipitations, however it changes the way in which the magnetic ions interact with each other inside the precipitations. In other words the moderate doping with phosphorus does not change the amount of FM precipitations, but their properties. The fact that the saturation signal has not changed, and the remanence magnetization and coercive field decreased, means that some ferromagnetic domains became more liable to the action of thermal demagnetization. At higher temperatures, when the coercive field further decreases, such isolated ferromagnetic domains act rather like superparamagnetic particles (see Fig. 39b)[44]. Thus the disappearance of ferromagnetism passes through following stages, (i) the ferromagnetic domains turn to superparamagnetic particles at moderate concentration of phosphorus, (ii) at higher concentration of phosphorus the superparamagnetic particles seize to exist. The micro EDX investigation of samples 4504 and 4505 (which are presented on Fig. 39 a,b) does not show any difference of the chemical composition or size of precipitations in both samples. Hence, the decrease of hysteresis loop may be related with transformation of some other ferromagnetic objects in the lattice, which are not visible in SEM or EDX measurements. May be those are some kind of chromium reach regions with zinc blende structure which appear due to spinodal decomposition phenomenon. The disappearance of superparamagnetic particles in heavily phosphorus-doped samples may be explained in this case by the change of the chromium ions charge which prevents spinodal decomposition [63].

Paramagnetic Curie temperature in ZnMnTe:Cr

The paramagnetic Curie temperature was determined as the intersection point of the $1/\chi(T)$ line with the horizontal axis. Although such parameter does not coincide with the real phase transition temperature, it can indicate the trends in the series of samples. The analysis was complicated by the fact that paramagnetic magnetization was sometimes measured on a strong background of ferromagnetic signal, especially in the samples not doped with phosphorus. In all cases the background signal was eliminated by fitting the magnetic susceptibility $\chi(T)$ curve with $\chi = \chi_0 + C/(T - T_C)$ relation. After subtraction of χ_0 background, the function $1/(\chi - \chi_0) = f(T)$ resulted in a linear dependence, and the Curie temperature parameter could be determined. An example of such procedure made for sample 4504 is presented on Fig. 40. The values of paramagnetic T_C, determined in such manner, are presented in Table 7 and on Fig. 41.

Analyzing the series of samples with nominal 5 % of manganese and 2 % of chromium (4504, 4505, 4532, 4516) one can see that in the samples doped with phosphorus the Curie temperature is higher than in undoped sample. The positive value of the Curie temperature suggests the existence of weak

[44] A similar dependence of coercive field on temperature was observed in $ZnTe:Cr$ samles (Fig. 36)

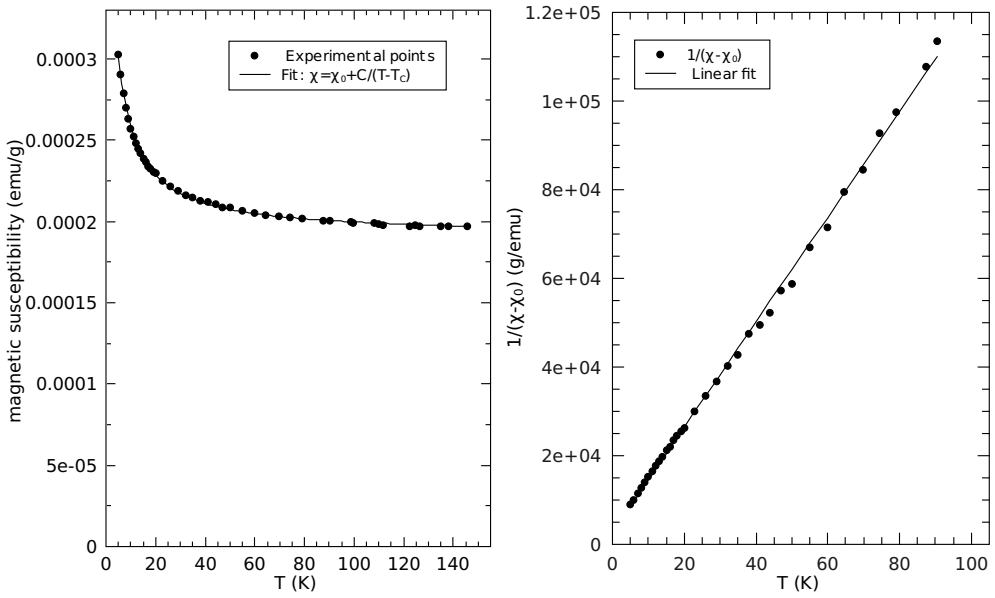

Figure 40: Left figure: Dependence of magnetic susceptibility of the sample 4504 ($ZnMnTe : Cr$) on temperature measured at 100 Oe (filled circles). Solid line represents the result of non-linear fit of the function $\chi = \chi_0 + C/(T - T_C)$, where χ_0, C and T_C were considered as fitting parameters. Right Figure: Paramagnetic susceptibility $1/(\chi - \chi_0)$ as a function of temperature (filled circles). Solid line was obtained by linear fit of the experimental data.

ferromagnetic interaction between isolated manganese ions and gives hope for a bit higher T_C in these samples in comparison with $ZnMnTe : P$. The samples were not measured below 5 K, and the real phase transition could not be observed in the studied samples. It is unknown how big is the influence of chromium on the temperature of phase transition. However, in another series (samples 4630, 4631), were the nominal concentration of chromium was lower (1 %), there is no such large difference between the T_C of phosphorus doped and undoped samples. As a final remark it is worth to note that in $ZnMnTe : P$ samples grown in a similar manner, the ferromagnetic transition was observed only after an annealing process and was not observed in the as-grown samples [80].

Summary: Magnetic properties

- A large increase of FM magnetization is observed in $ZnMnTe : Cr$ samples, in comparison with $ZnTe : Cr$ samples.
- The ferromagnetic signal is produced by small precipitations with about 1 μm size.
- The precipitations of Cr_2Te_3 and Cr_3Te_4 of comparable size were observed in SEM and EDX analysis. However since these precipitations do not contain manganese, it is unclear how the manganese helps to increase the ferromagnetic signal in $ZnMnTe : Cr$.

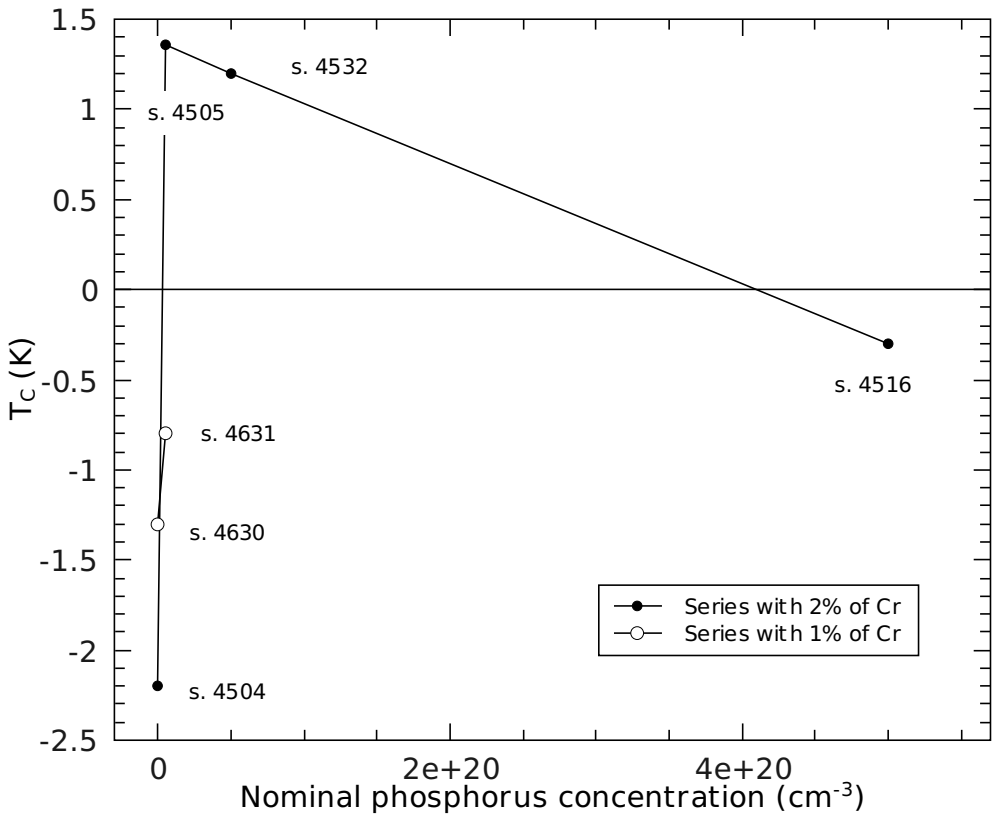

Figure 41: Dependence of the paramagnetic Curie temperature on phosphorus concentration in $ZnMnTe : Cr, P$. The open and filled symbols are used to distinguish two sample series with nominal content of chromium of 1% and 2% respectively.

- The behavior of magnetic hysteresis loop in $ZnMnTe : Cr$ and $ZnTe : Cr$ is different, thus it is concluded that the manganese should be a essential part of ferromagnetic precipitations in $ZnMnTe : Cr$.
- The splitting of free exciton in magnetic field cannot be explained by separate action of manganese and chromium systems of magnetic ions. The exchange constants have manganese-like behavior, and the magnetization has chromium-like behavior. This indicates on some sort of interaction between paramagnetic systems of manganese and chromium ions.
- Doping of the $ZnMnTe : Cr$ samples with phosphorus results in a decrease and (at higher concentrations) disappearance of ferromagnetism.
- Considering the doping with phosphorus, one can distinguish two regions. A region of moderate doping ($< 5 \cdot 10^{18}\ cm^{-3}$) and the region of high doping ($> 5 \cdot 10^{19}\ cm^{-3}$).
- In the region of moderate doping there is no visible change in the size

or composition of Cr_xTe_y precipitations, however a transformation of FM behavior into superparamagnetic one is observed.

- In the region of high doping the FM properties are no longer observed, and appear another type of chromium-reach precipitation with chemical composition $Cr_3Zn_2Te_xP_y$.
- The existence and disappearance of ferromagnetism is not related solely with the Cr_3Te_4 precipitations.
- An increase of paramagnetic Curie temperature was observed in phosphorus-doped $ZnMnTe:Cr$ samples. Occasionally the T_C was found to be positive. It is unknown whether this effect is related with chromium or just a result of high doping with phosphorus.

3.5 ZnMnTe:Cr. Conclusions

It is demonstrated experimentally that simultaneous doping of $ZnTe$ with two kinds of magnetic impurity (manganese and chromium) results in new effects which were not observed in samples where these impurities were introduced separately.

- The studied samples possess both ferromagnetic and paramagnetic components of magnetization signal.
- Although manganese by itself does not produce ferromagnetic precipitations in $ZnTe$, it was found to act as an amplifier of ferromagnetic signal in $ZnMnTe : Cr$ in comparison with $ZnTe : Cr$. The indirect observations lead to a conclusion that most of the ferromagnetic signal comes not from Cr_3Te_4 precipitations, which can be easily observed by microscopic techniques, but rather from some undetected chromium reach formations which structurally do not differ from the rest of the bulk material. These formations, when they subjected to manganese doping account for the observed amplification of ferromagnetic signal and also for the decrease and disappearance of ferromagnetic signal on doping with phosphorus.
- Regarding the properties of paramagnetic system of magnetic ions, the influence of simultaneous doping is also observed. It is manifested in (i) changes in the behavior of the free exciton splitting in magnetic field and (ii) an increase of paramagnetic Curie temperature, which gives hope for a bit higher temperature of carrier mediated ferromagnetic phase transition in $ZnMnTe : Cr, P$.
- Among the experiments which could be done in the future to understand the effects observed in $ZnMnTe : Cr$ are, the measurement of the magnetization at both very low (below 5 K) and high (above room temperature) temperatures in order to observe the ferromagnetic transitions of both the carrier-mediated-type and the transition inside the ferromagnetic precipitations respectively. To separate the effects produced by ferromagnetic precipitations it will be also helpful to produce samples with concentration of chromium below 0.5 %.

4 Summary

This work is dedicated to a study of $ZnMnTe$ doped with oxygen and chromium. Although $ZnMnTe$ is a relatively well studied material, there are very few reports dedicated to $ZnMnTe$ doped with these impurities.

The studied bulk samples were prepared by melt crystallization techniques under high hydrostatic pressure of an inert gas. Namely, the fast crystallization was used in case of $ZnMnTe : O$, and vertical Bridgman method was used in case of $ZnMnTe : Cr$. Two series of samples with different concentrations of oxygen, chromium and manganese were prepared. The chromium doped samples were also additionally doped with phosphorus in order to control the free hole concentration.

Although in both cases obtaining of alloys of type $(Zn, Mn, Cr)Te$ or $(Zn, Mn)(Te, O)$ would be of much interest, the real concentrations of substitutional oxygen and chromium were less then 0.5 %, due to relatively low solubility of these impurities. For the same reason the samples contain precipitations reach in oxygen or chromium. Thus a number of the observed properties are related with the precipitations.

A wide number of experimental techniques was employed for the characterization of the samples. Among those techniques are the x-ray diffraction, energy dispersive x-ray analysis, scanning electron microscopy, atomic and magnetic force microscopy, magneto-reflectance, magneto-photoluminescence, Hall effect and magnetization measurements.

The most significant results are listed below, separately for each of the studied compounds.

In (ZnMnTe:O):

- An increase of the oxygen solubility by two orders of magnitude in $ZnTe$ doped simultaneously with oxygen and manganese was observed. The dependence of oxygen solubility on manganese concentration was obtained.

- The dependence of the band gap energy of the $ZnTe_{1-x}O_x$ alloy on the oxygen content, on the tellurium-reach side of the composition interval was studied. The bowing parameter of the band gap dependence is found to be $b = 9.3\ eV$.

- The dependence of exchange integrals α and β on oxygen concentration was studied. The value of the α exchange integral was found to be insensitive to oxygen concentration in the studied range of concentrations. The result on the dependence of β exchange integral is not conclusive. If author would have to chose, the answer will be that it rather decreases.

- A new photoluminescence band observed in the spectrum of $ZnMnTe : O$ at 1.65 eV is assigned to emission centers which have Mn_nO structure.

- Two kinds of ferromagnetic oxygen-reach precipitations with $T_C \sim 46\ K$ and $T_C \sim 80\ K$ were observed. The latter kind of precipitations appears in heavily oxygen-doped samples (> 0.5 %), and the former, in less doped samples.

In (ZnMnTe:Cr):

- An increase of the ferromagnetic signal is observed (even at room temperature) in $ZnMnTe:Cr$ in comparison with $ZnTe:Cr$. Since manganese by itself does not produce ferromagnetic phase in $ZnTe$ at room temperature, it is concluded that **manganese effectively amplifies the ferromagnetic signal produced by chromium reach clusters**.

- Doping of $ZnMnTe:Cr$ with phosphorus (p-type) results in the decrease and, at higher concentrations ($> 10^{19}\ cm^{-3}$), in disappearance of the ferromagnetic signal. This process involves two steps. First the ferromagnetic clusters turn into superparamagnetic clusters. Then, at higher concentrations of phosphorus, the superparamagnetic particles do not form. Such behavior is in accordance with the theory of spinodal decomposition.

- The influence of simultaneous doping (with manganese and chromium) on paramagnetic system of ions is manifested in (i) changes in the behavior of the free exciton splitting in magnetic field, and (ii) an increase of paramagnetic Curie temperature in phosphorus doped samples.

Although the precipitations sometimes can have a strong influence on the properties of the host material (even on its band structure), and the properties of the described precipitations might have their own practical value, the understanding of the studied phenomena would be much easier if the effects caused by the substitutional defects, and those caused by the precipitations would be separated. Thus for future study in this direction, the preparation of mono-crystalline samples with lower nominal impurity concentrations is required. The question about the microscopic environment of the impurities and their positions with respect to each other in the lattice is important to explain the observed properties. Such question requires a further study.

References

[1] John A. Dean, "Lange's handbook of chemistry", McGraw-hill, Inc., 1291 p., (1999).

[2] K.M. Yu, W. Walukiewicz, W. Shan, J.Wu, J.W. Beeman, M.A. Scarpulla, O.D. Dubon, P. Becla, "Synthesis and optical properties of II-O-VI highly mismatched alloys", J. Appl. Phys., **95**, 6232-6238 (2004).

[3] J. Li, S.-H. Wei, "Alignment of isovalent impurity levels: Oxygen impurity in II-VI semiconductors", Phys. Rev. B, **73**, 041201-041204 (2006).

[4] R.E. Dietz, D.G. Thomas, J.J. Hopfield, "Mirror absorption and fluorescence in ZnTe", Phys. Rev. Lett., **8**, 391-393 (1962).

[5] J.L. Merz, "Isoelectronic oxygen trap in ZnTe", Phys. Rev., **176**, 961-968 (1968).

[6] J.J. Hopfield, D.G. Thomas, R.T. Lynch, "Isoelectronic donors and acceptors", Phys. Rev.Lett., **17**, 312-315 (1966).

[7] J. W. Allen, "Isoelectronic impurities in semiconductors: a survey of binding mechanisms", J. Phys. C: Solid State Physics, **4**, 1936-1944 (1971).

[8] J.D. Cuthbert, D.G. Thomas, "Fluorescent decay times of excitons bound to isoelectronic traps in GaP and ZnTe", Phys. Rev., **154**, 763-771 (1967).

[9] Y. Burki, W. Czaja, V. Capozzi, P. Schwendimann, "The temperature dependence of the photoluminescence and lifetime of ZnTe:O", J. Phys.: Condens. Matter, **5**, 9235-9252 (1993).

[10] H.P. Hjalmarson, C.B. Norris, "A phenomenological modelof the red luminescence kinetics in ZnTe:O", J. Appl. Phys., **61**, 734-737 (1987).

[11] S.H. Sohn, Y.Hamakawa, "Binding energies of simple isoelectronic impurities in II-VI semiconductors", Phys. Rev. B, **46**, 9452-9460 (1992).

[12] M.J. Seong, I. Miotkowski, A.K. Ramdas, "Oxygen isoelectronic impurity in ZnTe: photoluminescence and absorption spectroscopy", Phys. Rev. B, **58**, 7734-7739 (1998).

[13] C.-Y. Moon, S.-H. Wei, Y.Z. Zhu, G.D. Chen, "Band-gap bowing coefficients in large size-mismatched II-VI alloys: first-principles calculations", Phys. Rev. B, **74**, 233202 (2006).

[14] S. Merita, T. Kramer, B. Mogwitz, B. Franz, A. Polity, B.K. Meyer "Oxygen in sputter-deposited ZnTe thin films", phys. stat. sol. (c), **3**, 960-963 (2006).

[15] S.-H. Wei, A. Zunger, "Giant and composition dependent optical bowing coefficient in GaAsN alloys", Phys. Rev. Lett., **76**, 664-667 (1996).

[16] P.R.C. Kent, A. Zunger, "Evolution of III-V Nitride Alloy Electronic Structure: The Localized to Delocalized Transition", Phys. Rev. Lett., **86**, 2613-2616 (2001).

[17] W. Shan, W. Walukiewicz, J.W. Ager III, E.E. Haller, J.F. Geisz, D.J. Friedman, J.M. Olson, S.R. Kurtz, "Band Anticrossing in GaInNAs Alloy", Phys. Rev. Lett., **82**, 1221-1224 (1999).

[18] C. Tablero, A. Martí, A. Luque, "Analyses of the intermediate energy levels in $ZnTe : O$ alloys", Appl. Phys. Lett., **96**, 121104, 1-3 (2010)

[19] W. Walukiewicz, W. Shan, K.M. Yu, J.W. Ager III, E.E. Haller, I. Miotkowski, M.J. Seong, H. Alawadhi, A.K. Ramdas, "Interaction of Localized Electronic States with the Conduction Band: Band Anticrossing in II-VI Semiconductor Ternaries", Phys. Rev. Lett., **85**, 1552-1555 (2000).

[20] K.M. Yu, W. Walukiewicz, J. Wu, J.W. Beeman, J.W. Ager III, E.E. Haller, I. Miotkowski, A.K. Ramdas, P. Becla, "Band anticrossing in group II-O-VI highly mismatched alloys: CdMnOTe quaternaries synthesized by O ion implantation", Appl. Phys. Lett. **80**, 1571-1573 (2002).

[21] K.M. Yu, W. Walukiewicz, J. Wu, W. Shan, J.W. Beeman, M.A. Scarpulla, O.D. Dubon, P. Becla, "Diluted II-VI Oxide Semiconductors with Multiple Band Gaps", Phys. Rev. Lett., **91**, 246403-1 (2003).

[22] Z.T. Kang, C.J. Summers, H. Menkara, B.K. Wagner, R. Durst, Y. Diawara, G. Mednikova, T. Thorson, "ZnTe:O phosphor development for x-ray imaging applications", Appl. Phys. Lett., **88**, 111904-1 (2006).

[23] Y. Nabetani, T. Okuno, K. Aoki, T. Kato, T. Matsumoto, T. Hirai, "Epitaxial growth and optical investigation of ZnTeO alloys", phys. stat. sol. (a), **203**, 2653-2657 (2006).

[24] Y. Nabetani, T. Okuno, K. Aoki, T. Kato, T. Matsumoto, T. Hirai, "Photoluminescence properties of ZnTeO and ZnSeO alloys with dilute O concentrations", phys. stat. sol. (c), **3**, 1078-1081 (2006).

[25] J.K. Furdyna, "Diluted magnetic semiconductors", J. Appl. Phys., **64**, R29-R64 (1988).

[26] J. A. Bearden, "X-Ray Wavelengths", Reviews of Modern Physics, **39**, 78-124 (1967).

[27] A. Avdonin, Le Van Khoi, W. Pacuski, V. Domukhowski, R.R. Gałązka, "Preparation and Optical Properties of $Zn_{1-x}Mn_xTe_{1-y}O_y$ Highly Mismatched Alloy", Acta Physica Polonica A, **112**, 407-414 (2007).

[28] F. El Akkad, "Photo-Induced Current Transient Spectroscopy of Deep Levels in $ZnTe$ and $Mg_{0.21}Zn_{0.79}Te$ Crystals", phys. stat. sol. (b), **201**, 135-141 (1997).

[29] M. Abdel Naby, "Electrical properties of RF sputtered In-ZnTe Schottky diodes", Semicond. Sci. Technol., **10**, 248-352 (1995).

[30] Y.P.Varshni, "Temperature dependence of the energy gap in semiconductors", Physica, **34**, 149-154 (1967).

[31] J.J. Hopfield, D.G. Thomas, "Theoretical and Experimental Effects of Spatial Dispersion on the Optical Properties of Crystals", Phys. Rev., **132**, 563-572 (1963).

[32] A. Twardowski, P. Swiderski, M. von Ortenberg, R. Pauthenet, "Magnetoabsorption and magnetization of $Zn_{1-x}Mn_xTe$ mixed crystals", Solid State Commun., **50**, 509-513 (1984).

[33] H. Venghaus, P. J. Dean, "Shallow-acceptor, donor, free-exciton and bound-exciton states in high-purity zinc telluride", Phys. Rev. B, **21**, 1596-1609 (1980).

[34] J. A. Gaj, "Magnetooptical Properties of Large-Gap Diluted Magnetic Semiconductors" in Semiconductors and Semimetals, vol. 25, ed. by J.K. Furdyna and J. Kossut, 462 (1998).

[35] J. Kossut, W. Dobrowolski, "Diluted Magnetic Semiconductors" in Handbook of Magnetic Materials, vol. 7, ed. by K.H.J. Buschow, 664 (1993).

[36] H. Venghaus, P.E. Simmonds, J. Lagois, P.J. Dean, D. Bimberg, "Magnetoreflectance of the $\Gamma_6 - \Gamma_8$ exciton in $ZnTe$", Solid State Commun., **24**, 5-9 (1977).

[37] J.A. Gaj, J. Ginter, and R.R. Gałązka, "Exchange interaction of Manganese $3d^5$ States with Band Electrons in $Cd_{1-x}Mn_xTe$", phys. stat. sol. (b), **89**, 655-662 (1978).

[38] G. Barilero, C. Rigaux, M. Menant, Nguyen Hy Hau, W. Giriat, "Magnetization and magnetoreflectance in $Zn_{1-x}Mn_xTe$", Phys. Rev. B, **32**, 5144-5148 (1985).

[39] A. Twardowski, T. Dietl, M. Demianiuk, "The study of the s-d type exchange interaction in $Zn_{1-x}Mn_xSe$ mixed crystals", Solid State Commun., **48**, 845-848 (1983).

[40] R.E. Behringer, "Number of Single, Double and Triple Clusters in a System Containing Two Types of Atoms", The J. of Chem. Phys., **29**, 537-539 (1958).

[41] A. Twardowski, "Magneto-optical study of $Zn_{1-x}Mn_xTe$ mixed crystals", Physics Letters A, **94**, 103 (1983).

[42] T. Mizokawa, T. Nambu, A. Fujimori, T. Fukumura, M. Kawasaki, "Electronic structure of the oxide-diluted magnetic semiconductor $Zn_{1-x}Mn_xO$", Phys. Rev. B, **65**, 085209, 1-5 (2002).

[43] J. Okabayashi, K. Ono, M. Mizuguchi, M. Oshima, Subhra Sen Gupta, D. D. Sarma, T. Mizokawa, A. Fujimori, M. Yuri, C.T. Chen, T. Fukumura, M. Kawasaki, H. Koinuma, "X-ray absorption spectroscopy of transition-metal doped diluted magnetic semiconductors $Zn_{1-x}Mn_xO$", J. Appl. Phys., **95**, 3573-3575 (2004).

[44] E. Przeździecka, E. Kamińska, M. Kiecana, M. Sawicki, Ł. Kłopotowski, W. Pacuski, J. Kossut, "Magneto-optical properties of the diluted magnetic semiconductor p-type $ZnMnO$", Solid State Commun., **139**, 541-544 (2006).

[45] T. Dietl, H. Ohno, F. Matsukura, "Hole-mediated ferromagnetism in tetrahedrally coordinated semiconductors", Phys. Rev. B, **63**, 195205, 1-21 (2001).

[46] S.H. Liu, "Exchange Interaction between Conduction Electrons and Magnetic Shell Electrons in Rare-Earth Metals", Phys. Rev., **121**, 451-455 (1961).

[47] W. Mac, A. Twardowski, M. Demianiuk, "s,p-d exchange interaction in Cr-based diluted magnetic semiconductors", Phys. Rev. B, **54**, 5528-5535 (1996).

[48] Y.R. Lee, A.K. Ramdas, R.L. Aggarwal, "Energy gap, excitonic, and "internal" Mn^{2+} optical transition in Mn-based II-VI

diluted magnetic semiconductors", Phys. Rev. B, **38**, 10600-10610 (1988).

[49] A. Avdonin, W. Knoff, R.R. Gałązka, "Magnetic Properties of $Zn_{1-x}Mn_xTe_{1-y}O_y$ Alloys", Acta Physica Polonica A, **116**, 916-917 (2009).

[50] S. Mochizuki, B. Piriou, J. Dexpert-Ghys, "Spin-wave-assisted photoluminescence in MnO crystals", J. Phys.: Condens. Matter, **2**, 5225-5232 (1990).

[51] J. A. Mydosh, "Spin glasses: an experimental introduction", Taylor & Francis, 256 p., (1993).

[52] K. Binder, A.P. Young "Spin glasses: Experimental facts, theoretical concepts, and open questions", Reviews of Modern Physics, **58**, 801-976 (1986).

[53] S.H. Kim, B.J. Choi, G.H. Lee, S.J. Oh, B. Kim, H.C. Choi, J. Park, "Ferrimagnetism in γ-Manganese Sesquioxide ($\gamma - Mn_2O_3$) Nanoparicles", J. of the Korean Physical Society, **46**, 941-944 (2005).

[54] B. Boucher, R. Buhl, M. Perrin, "Magnetic structure of Mn_3O_4 by Neutron Diffraction", J. Appl. Phys., **42**, 1615-1617 (1971).

[55] K. Dwight, N. Menyuk, "Magnetic Properties of Mn_3O_4 and the Canted Spin Problem", Phys. Rev., **119**, 1470-1479 (1960).

[56] I.K. Gopalakrishnan, N. Bagkar, R. Ganguly and S.K. Kulshreshtha, "Synthesis of superparamagnetic Mn_3O_4 nanocrystallites by ultrasonic irradiation", J. of Cryst. Gr. **280**, 436-441 (2005).

[57] U. Stutnbäumer, H.-E. Gumlich, H. Zuber, "The Enrgy Transfer between Free Excitons, Bound Excitons, and the 3d-Shell of Mn^{2+} in $Zn_{1-x}Mn_xSe$ Mixed Crystals and the s-d Type Exchange Interaction", phys. stat. sol. (b), **156**, 561-567 (2006).

[58] Z.X. Tang, C.M. Sorensen, K.J. Klabunde, G. C. Hadjipanayis "Size-dependent Curie temperature in nanoscale $MnFe_2O_4$ particles", Phys. Rev. Lett., **67**, 3602-3605 (1991).

[59] L. Liao, J.C. Li, D.F. Wang, C. Liu, M.Z. Peng, J.M. Zhou "Size dependence of Curie temperature in Co^+ ion implanted ZnO nanowires", Nanotechnology, **17**, 830-833 (2006).

[60] R.P. Santoro, R.E. Newnham, S. Nomura, "Magnetic properties of Mn_2SiO_4 and Fe_2SiO_4", J. of Phys. and Chem. of Solids, **27**, 655-666 (1966).

[61] G. Krishnaiah, N. Madhusudhana Rao, D. Raja Reddy, B.K. Reddy, P. Sreedhara Reddy, "Growth and structural properties of $Zn_{1-x}Cr_xTe$ crystals", J. Cryst. Gr., **310**, 26-30 (2008).

[62] H. Sato, V. Zayets, S. Yamagata, K. Ando, "Room-Temperature Ferromagnetism in II-VI Diluted Magnetic Semiconductor $Zn_{1-x}Cr_xTe$", Phys. Rev. Lett., **90**, 207202, 1-4 (2003).

[63] S. Kuroda, N. Nishizawa, K. Takita, M. Mitome, Y. Bando, K. Osuch, T. Dietl, "Origin and control of high-temperature ferromagnetism in semiconductors", Nature materials, **6**, 440-446 (2007).

[64] N. Ozaki, N. Nishizawa, S. Marcet, S. Kuroda, O. Eryu, K. Takita, "Significant Enhancement of Ferromagnetism in $Zn_{1-x}Cr_xTe$ Doped with Iodine as an n-Type Dopant", Phys. Rev. Lett., **97**, 037201, 1-4 (2006).

[65] T.M. Pekarek, J.E. Luning, I. Miotkowski, B.C. Crooker, "Magnetization and heat-capacity measurements on $Zn_{1-x}Cr_xTe$", Phys. Rev. B, **50**, 16914-16920 (1994).

[66] H. Saito, V. Zayets, S. Yamagata, K. Ando, "Room-Temperature Ferromagnetism in II-VI Diluted Magnetic Semiconductor $Zn_{1-x}Cr_xTe$" Phys. Rev. Lett., **90**, 207202, 1-4 (2003).

[67] H. Saito, V. Zayets, S. Yamagata, Y. Suzuki, K. Ando, "Ferromagnetism in II-VI diluted magnetic semiconductor $Zn_{1-x}Cr_xTe$", J. Appl. Phys., **91**, 8085-8087 (2002).

[68] M.G. Sreenivasan, K.L. Teo, X.Z. Cheng, M.B.A. Jalil, T. Liew, T.C. Chong, A.Y. Du, T.K. Chan, T. Osipowicz, "Structural, magnetic and transport investigations of $CrTe$ Clustering effect in $(Zn, Cr)Te$ system", J. Appl. Phys., **102**, 053702, 1-5 (2007).

[69] J. Blinowski, P. Kacman, J.A. Majewski, "Ferromagnetic superexchange in Cr-based diluted magnetic semiconductors", Phys. Rev. B, **53**, 9524-9527 (1996).

[70] K. Sato, H. Katayama-Yoshida, "First principles material design for semiconductor spintronics", Semicond. Sci. Technol., **17**, 367-376 (2002).

[71] L.Bergqvist, O. Eriksson, J. Kudrnovský, V. Drchal, P.Korzhavyi, I. Turek, "Magnetic percolation in diluted magnetic semiconductors", Phys. Rev. Lett., **93**, 137202, 1-4 (2004).

[72] T. Fukushima, K.Sato, H. Katayama-Yoshida, P.H. Dederichs, "Ab initio study of spinodal decomposition in (Zn,Cr)Te", phys. stat. sol. (a), **203**, 2751-2755 (2006).

[73] S. Shen, X. Liu, Y.J. Cho, J.K. Furdyna, M. Dobrowolska, Y.H. Hwang, Y.H. Um, "Ferromagnetic behavior of $CdMnCrTe$ quaternary system", Appl. Phys. Lett., **94**, 142507, 1-3 (2009).

[74] Y.B. Li, Y.Q. Zhang, N.K. Sun, Q. Zhang, D. Li, J. Li, Z.D. Zhang, "Ferromagnetic semiconducting behavior of $Mn_{1-x}Cr_xTe$ compounds", Phys. Rev. B, **72**, 193308, 1-4 (2005). .

[75] U. Hömmerich, J.T. Seo, A. Bluiett, M. Turner, D. Temple, S.B. Trivedi, H. Zong, S.W. Kutcher, C.C. Wang, R.J. Chen, B. Schumm, "Mid-infrared laser development based on transition metal doped cadmium manganese telluride", J. of Luminescence, **87-89**, 1143-1145 (2000).

[76] J.T. Vallin, G.A. Slack, S. Roberts, A.E. Hughes, "Infrared Absorption in Some II-VI Compounds with Cr", Phys. Rev. B, **2**, 4313 (1970).

[77] K. Sato, H. Katayama-Yoshida, "Stabilization of Ferromagnetic States by Electron Doping in Fe-, Co- or Ni-Doped ZnO", Jpn. J. Appl. Phys., **40**, L334-L336 (2001).

[78] X. Lu, S. Tsoi, I. Miotkowski, S. Rodriguez, A.K. Ramdas, H. Alawadhi, "Raman electron paramagnetic resonance in $Zn_{1-x}Cr_xTe$ and $Cd_{1-x}Cr_xTe$", Phys. Rev. B, **75**, 155206, 1-9 (2007).

[79] D. Soundararajan, D. Mangalaraj, D. Nataraj, L. Dorosinskii, J. Santoyo-Salazar, M.J. Riley, "Magnetic and magneto-optical studies on $Zn_{1-x}Cr_xTe$ ($x = 0.05$) films grown on glass substrate", J. Magn. Magn. Mater., **321**, 4108-4114 (2009).

[80] Le Van Khoi, M. Sawicki, K. Dybko, V. Domukhovski, T. Story, T. Dietl, A. Jędrzejczak, J. Kossut, R. R. Gałązka, "Annealing-Induced Changes in Electrical, Optical and Magnetic Properties of Phosphorus Doped Bulk $Zn_{1-x}Mn_xTe$", phys. stat. sol. (b), **229**, 53-56 (2002).

[81] Tomasz Dietl, "(Diluted) Magnetic Semiconductors" in Handbook on Semiconductors, vol. 3, ed. by S. Mahajan, 2398 (1994).

[82] Joo-Hyoung Lee, Junqiao Wu, J.C. Grossman, "Enhancing the Thermoelectric Power Factor with Highly Mismatched Isoelectronic Doping", Phys. Rev. Lett., **104**, 016602, 1-4 (2010).